

UCLA

UCLA Electronic Theses and Dissertations

Title

Computational Studies of Iridium-Catalyzed Borylation Reactions and Defying
Torquoselectivity in Cyclobutene Ring-Opening via Strain-Induced Thermal Selectivity

Permalink

<https://escholarship.org/uc/item/6fq683n9>

Author

Green, Aaron Gabriel

Publication Date

2013

Peer reviewed|Thesis/dissertation

UNIVERSITY OF CALIFORNIA

Los Angeles

Computational Studies of Iridium-Catalyzed
Borylation Reactions

and

Defying Torquoselectivity in Cyclobutene Ring-
Opening via Strain-Induced Thermal Selectivity

A dissertation submitted in partial satisfaction of the
requirements for the degree Doctor of Philosophy in
Chemistry

by

Aaron Gabriel Green

2013

© Copyright by
Aaron Gabriel Green
2013

ABSTRACT OF THE DISSERTATION

Computational Studies of Iridium-Catalyzed
Borylation Reactions

and

Defying Torquoselectivity in Cyclobutene Ring-
Opening via Strain-Induced Thermal Selectivity

by

Aaron Gabriel Green

Doctor of Philosophy in Chemistry

University of California, Los Angeles, 2013

Professor Craig A. Merlic, Chair

The studies reported in this dissertation illustrate a few selected examples of using density functional theory (DFT) calculations to investigate various aspects of iridium-catalyzed reactions and ring-opening of bicyclic cyclobutene rings. These computational predictions not only reproduce and explain experimental results and offer insights to reaction mechanisms, but also provide theoretical models to predict reactivity, regio- and stereoselectivities.

Chapter 1 is a review surveying the literature of iridium-catalyzed borylation reactions. Emphasis is placed on iridium-catalyzed borylation of alkenes and arenes. In particular, I discuss the history leading up to the current catalyst systems for iridium-catalyzed borylation reactions, and regioselectivity of borylation for a number of different substrates. Despite the

large amount of work on iridium-catalyzed borylation reactions, this review shows that there is still much to be understood regarding the origins of observed regioselectivities.

Chapters 2 and 3 describe theoretical investigations of Ir(III)-catalyzed borylation reactions. The origins of regioselectivities observed in the borylation of pyridine are discussed in Chapter 2. The high selectivity for borylation at the 3- and 4- position of pyridine is attributed to the formation of a Lewis acid-base complex between pyridine and either boron species or iridium species in solution. The origins of regioselectivities for the iridium-catalyzed borylation of substituted arenes and 5-membered heterocycles are discussed in Chapter 3. The distortion/interaction model was employed to understand the origins of the selectivities in these reactions. Computations revealed that regioselectivity is mainly controlled by differences in the interaction energies between the iridium catalyst and arene carbon.

Chapter 4 illustrates a theoretical study of ring-opening in strained, trans-substituted cyclobutenes. The torquoselectively preferred outward ring-opening products are unable to form due to ring strain inherent in 9- and 10-membered macrocyclic (*E,E*)-1,3-dienes. As a result of this study, I propose a general methodology for stereoselective synthesis of macrocyclic (*Z,Z*)-1,3-dienes termed strain-induced thermal selectivity (SITS).

The dissertation of Aaron Gabriel Green is approved.

Xiaofeng Duan

Yunfeng Lu

Craig A. Merlic, Committee Chair

University of California, Los Angeles

2013

DEDICATION

To my family.

TABLE OF CONTENTS

Abstract of the Dissertation	ii
List of Charts.....	vii
List of Figures.....	viii
List of Schemes.....	xii
List of Tables	xiv
Acknowledgements.....	xv
Vita.....	xvii
Chapter 1: On Regioselection in Iridium-Catalyzed Borylation Reactions.....	1
References	46
Chapter 2: Mechanism and Regioselectivity of the Iridium-Catalyzed Borylation of Pyridine Elucidated with Density Functional Theory	51
References	73
Chapter 3: Distortion/Interaction Analysis Reveals the Origins of the Selectivities in Iridium- Catalyzed C–H Borylation of Substituted Arenes and 5-Membered Heteroarenes.....	77
References	108
Chapter 4: Defying Torquoselectivity in Cyclobutene Ring-Opening via Strain-Induced Thermal Selectivity	111
References	135

LIST OF CHARTS

Chart 1.1: Photocatalytic borylation of alkanes and ethers by Cp*Re(CO) ₃ to yield terminal borylated products.....	9
Chart 1.2: Regioselective, catalytic functionalization of alkanes, alkyl ethers and benzene by Cp*Rh(η ⁴ -C ₆ Me ₆).....	11
Chart 1.3: C–H borylation of 1-cycloalkenecarboxylates with B ₂ pin ₂	22
Chart 2.1: Products from the Ir-catalyzed borylation of arene and heteroarene C–H bonds (Bpin = 4,4,5,5-tetramethyl-1,3,2-dioxaborolanyl).....	53

LIST OF FIGURES

Figure 1.1: Regioselectivity for iridium-catalyzed borylation of select monosubstituted benzene rings.....	24
Figure 1.2: Regioselectivity for iridium-catalyzed borylation of 1,2-disubstituted arenes.	24
Figure 1.3: Regioselectivity for iridium-catalyzed borylation of 1,3-disubstituted arenes.	25
Figure 1.4: Regioselectivity for iridium-catalyzed borylation of select 1,4-disubstituted Arenes	26
Figure 1.5: Regioselectivity for iridium-catalyzed borylation of 4-bromo-2-fluorobenzonitrile. 26	
Figure 1.6: Regioselectivities for iridium-catalyzed borylation of unsubstituted 5-membered heteroarenes.	28
Figure 1.7: Regioselectivities for iridium-catalyzed borylation of pyridine and quinoline.....	29
Figure 1.8: Regioselectivities for iridium-catalyzed borylation of substituted 5-membered heterocycles.....	30
Figure 1.9: Regioselectivities for iridium-catalyzed borylation of substituted pyridines.....	30
Figure 1.10: Observed Regioselectivities for bipyridines (Note: mixture of mono and diborylated products was obtained).	31
Figure 1.11: Regioselectivities for iridium-catalyzed diborylation of 2-substituted quinolines...32	
Figure 1.12: Regioselectivities for iridium-catalyzed diborylation of 4,7- and 2,6-disubstituted quinolines.....	32
Figure 1.13: Proton-transfer description for transition state in iridium C–H borylation.	42
Figure 1.14: Proposed transition structure for borylation of pyrrole exhibiting hydrogen bonding between the substrate N–H hydrogen and the oxygen atom of an equatorial boryl ligand.	43

Figure 2.1: Free energy profile for Pathway A with catalyst regeneration by B_2eg_2 . Structures for borylation at the 3-position of pyridine are shown. Results for 2-, 3-, and 4-C–H activation are denoted by red, blue and green lines, respectively.	61
Figure 2.2: Free energy profile for Pathway A with catalyst regeneration by HBeg. Structures for borylation at the 3-position of pyridine are shown. Results for 2-, 3-, and 4-C–H activation are denoted by red, blue and green lines, respectively.	62
Figure 2.3: Free energy profile for Pathway B. Structures for borylation at the 3-position of pyridine are shown. Results for 2-, 3-, and 4-C–H activation are denoted by red, blue and green lines, respectively.	64
Figure 2.4: Transition structures for the oxidative addition step of Pathway B.	66
Figure 2.5: Free energy profile for Pathway C. Structures for borylation at the 3-position of pyridine are shown. Results for 2-, 3-, and 4-C–H activation are denoted by red, blue and green lines, respectively.	67
Figure 2.6: Transition structures for the C–H oxidative addition step of Pathway C.	68
Figure 2.7: Free energy profile for activation of trifluoroborane pyridine complex 2.15 . Structures for borylation at the 3-position of 2.15 are shown. Results for 2-, 3-, and 4-C–H activation are denoted by red, blue and green lines, respectively.	71
Figure 2.8: Transition structures for the C–H oxidative addition step for the borylation of 2.15	72
Figure 3.1: Regioselectivities of various substituted benzene rings.	79
Figure 3.2: Regioselectivities of C–H activation of select 5-membered heterocycles.	80
Figure 3.3: Oxidative addition transition states for the reaction of toluene, 3.1	85
Figure 3.4: Transition state conformer for activation at the 2-position of 3.11 . TS3.11' does not exhibit hydrogen bonding.	89
Figure 3.5: ΔE^\ddagger vs. ΔE_{rxn} for 3.1-3.13	90
Figure 3.6: ΔE^\ddagger vs. ΔE_{rxn} for 3.1-3.10	91

Figure 3.7: Plot for ΔE^\ddagger vs. Ir–C BDE for substrates 3.1-3.13 .	92
Figure 3.8: Plot of substrate distortion energy ($\Delta E^\ddagger_{\text{dist}}(\text{arene})$) versus the C–H bond length in the transition state for 3.1-3.13 .	96
Figure 3.9: ΔE^\ddagger vs. $\Delta E^\ddagger_{\text{dist}}(\text{arene})$ for 3.1-3.13 .	97
Figure 3.10: ΔE^\ddagger vs. C–H BDE for 3.1-3.13 .	98
Figure 3.11: Energy (ΔE^\ddagger), distortion energy ($\Delta E^\ddagger_{\text{dist}}(\text{thiophene})$) and interaction energy of toluene ($\Delta E^\ddagger_{\text{int}}$) with the iridium complex as a function of the breaking C–H bond length in the reaction of 3.7 .	101
Figure 3.12: Energy (ΔE^\ddagger), distortion energy ($\Delta E^\ddagger_{\text{dist}}(\text{toluene})$) and interaction energy of toluene ($\Delta E^\ddagger_{\text{int}}$) with the iridium complex as a function of the breaking C–H bond length in the reaction of 3.1 .	102
Figure 3.13: Energy (ΔE^\ddagger), distortion energy ($\Delta E^\ddagger_{\text{dist}}(\text{acetanisole})$) and interaction energy of toluene ($\Delta E^\ddagger_{\text{int}}$) with the iridium complex as a function of the breaking C–H bond length in the reaction of 3.6 .	103
Figure 3.14: Fragment orbital analysis of the transition structure of 3.7 activated at the 2-position.	104
Figure 3.15: Plot of activation energy ΔE^\ddagger versus transition state Ir–C bond energy ΔE_{tbe} for reactions with 3.1-3.13 .	106
Figure 3.16: C–H BDE (B3LYP) vs. ΔE^\ddagger for 3.1-3.13 .	107
Figure 4.1: Computed free-energy surface for electrocyclic ring-opening of 4.1 to give either 4.13 or 4.14 .	118
Figure 4.2: Predicted strain enthalpies (kcal/mol) of 4.15-4.23 relative to the parent acyclic diene (calculated at the B3LYP/6-31G(d) level of theory).	120
Figure 4.3: Structure of 10-membered (<i>E,Z</i>)-1,3-diene 4.24 .	121
Figure 4.4: Attempted synthesis of a 10-membered (<i>E,Z</i>)-1,3-diene from a bisvinylboronate and the resulting possible cyclobutene products.	121

Figure 4.5: Structures of the desmethoxy model compounds 4.29 and 4.30	122
Figure 4.6: Predicted lowest energy structures, dihedral angles and relevant coupling constants for 4.29 and 4.30	124
Figure 4.7: Structures and free energies for 4.29-4.34	125
Figure 4.8: Computed free-energy surface for electrocyclic ring-closure of (<i>E,E</i>)-1,3-diene 4.31 to give the trans-cyclobutene product 4.30 and ring-opening of 4.30 to yield (<i>Z,Z</i>)-1,3-diene 4.34	126
Figure 4.9: Structures and selected C–C bond lengths of 4.30 , 4.31 , 4.34 , TS4.3 and TS4.4 ..	128
Figure 4.10: Structure of bisvinylboronate sulfide 4.36	129
Figure 4.11: Computed free-energy surface for electrocyclic ring-closure of (<i>E,E</i>)-1,3-diene sulfide 4.38 to give the trans-cyclobutene product 4.37 and ring-opening of 4.37 to yield (<i>Z,Z</i>)-1,3-diene sulfide 4.39	130
Figure 4.12: Structures and selected C–C bond lengths of 4.37 , 4.38 , 4.39 , TS4.5 and TS4.6	131
Figure 4.13: Computed free-energy surface for electrocyclic ring-closure of (<i>E,E</i>)-1,3-diene sulfone 4.41 to give the trans-cyclobutene product 4.40 and ring-opening of 4.40 to yield (<i>Z,Z</i>)-1,3-diene sulfone 4.42	133
Figure 4.14: Structures and selected C–C bond lengths of 4.40 , 4.41 , 4.42 , TS4.7 and TS4.8	134

LIST OF SCHEMES

Scheme 1.1: Halogenation route versus direct C–H activation method for borylation of unactivated substrates	2
Scheme 1.2: Formation of tris(boryl)iridium(III) piano stool complexes by reaction of $[(\eta^6\text{-Ind})\text{Ir}(\text{COD})]$ with HBcat in an arene solvent	5
Scheme 1.3: Stoichiometric irradiation of benzene in the presence of monoboryl metal carbonyls to form PhBcat	6
Scheme 1.4: Stoichiometric borylation of alkanes by metal carbonyl complexes	7
Scheme 1.5: Equation for the first formal catalytic borylation reaction	8
Scheme 1.6: Catalytic cycle for the photocatalytic borylation of alkanes and ethers by $\text{Cp}^*\text{Re}(\text{CO})_3$	10
Scheme 1.7: Selected example highlighting the preference for selective arene C–H borylation of iridium versus rhodium in the reaction of <i>m</i> -xylene	12
Scheme 1.8: Proposed catalytic cycle for borylation of benzene by $(\text{PMe}_3)_n\text{Ir}(\text{Bpin})_3$	13
Scheme 1.9: Catalytic borylation of arenes using $[\text{IrCl}(\text{COD})]_2/\text{bpy}$ catalyst system and the structure of an isolated Ir(III) active intermediate	14
Scheme 1.10: Iridium-catalyzed borylation of cyclic alkenes with subsequent transformation ...	17
Scheme 1.11: Mechanism for iridium-catalyzed borylation of alkenes to produce allyl Products	18
Scheme 1.12: Relay-directed <i>ortho</i> -borylation with a siloxy group	27
Scheme 1.13: Outer-sphere directed borylation	28
Scheme 1.14: Steric effect of methyl substituents on reactivity in 1,3-dimethylbenzene and 1,4-dimethylbenzene	34

Scheme 1.15: Steric effect of chloro substituents on reactivity in 1,3-dichlorobenzene and 1,4-dichlorobenzene	35
Scheme 1.16: Competition experiments between electron rich and electron poor arenes and between benzene and electron rich 5-membered heterocycles	36
Scheme 1.17: Proposed catalytic cycle for the catalytic borylation of benzene by Ir(dtpby)(Bpin) ₃	39
Scheme 1.18: Possible C–H activation mechanisms for the iridium catalyzed borylation of arenes: Oxidative addition (Path A), sigma bond metathesis with the formation of the C-B bond in a single step (Path B), and sigma bond metathesis with formation of a borane σ complex prior to the formation of the C-B bond (Path C)	41
Scheme 2.1: Ir-catalyzed borylation of pyridine and quinoline	54
Scheme 2.2: Proposed catalytic cycle for the Ir-catalyzed borylation of benzene	55
Scheme 2.3: The three reaction pathways studied for pyridine borylation by the model system Ir(bpy)(Beg) ₃ , illustrated for 3-functionalization	57
Scheme 2.4: Structures and free energies of 2.7 and 2.8	59
Scheme 3.1: Catalytic cycle for the iridium-catalyzed borylation of aromatic rings	78
Scheme 4.1: Outward (favored) and inward (disfavored) ring-opening	112
Scheme 4.2: Thermal isomerization of trans-3,4-dimethylcyclobutene	112
Scheme 4.3: Formation of tetrahydronaphthalene products via outward ring-opening of trans-cyclobutene 4.3	113
Scheme 4.4: Stereoselective ring-opening of bicyclic cyclobutene 4.5 to give torquoselectively disfavored “in” product 4.6	114
Scheme 4.5: Isolated product 4.9 upon ring-opening of cyclobutene triester 4.8	114
Scheme 4.6: Pd(II) cyclization of terminal bis-vinylboronate to give the TADA product 4.12	115

LIST OF TABLES

Table 1.1: Effect of anionic ligands on borylation of benzene by B ₂ pin ₂	15
Table 1.2: Iridium-catalyzed borylation of linear alkenes followed by palladium-catalyzed cross-coupling by Szabó and coworkers.	19
Table 1.3: Borylation of vinylic C–H bond of five- and six-membered cyclic vinyl ethers.....	21
Table 1.4: Iridium-catalyzed borylation of 2,7-disubstituted quinolines.	33
Table 2.1: Activation free energies for 2-, 3-, and 4-borylation of pyridine by Pathways A–C.....	70
Table 3.1: Activation energies and C–H/Ir–C distances in the oxidative addition transition states in the C–H borylation reaction with monosubstituted benzenes and the BDE of C–H bonds in the substrates.....	84
Table 3.2: Activation energies and C–H/Ir–C distances for the oxidative addition transition states in the C–H borylation reaction with 1,2-disubstituted benzenes and the BDE of C–H bonds in the substrates.....	86
Table 3.3: Activation energies and C–H/Ir–C distances for the oxidative addition transition states in the C–H borylation reaction with 5-membered heterocycles and the BDE of C–H bonds in the substrates.....	88
Table 3.4: Ir-Aryl BDEs and transition state energies for 3.1-3.13	93
Table 3.5: Distortion/Interaction analysis for the oxidative addition transition states of 3.1-3.13 . The activation energies, ΔE^\ddagger , the distortion energies of the iridium catalyst, $\Delta E^\ddagger_{\text{dist}}(\text{Ir cat.})$, the distortion energies of the substrate, $\Delta E^\ddagger_{\text{dist}}(\text{arene})$, and the interaction energies, $\Delta E^\ddagger_{\text{int}}$, are given in kcal/mol.	95
Table 4.1: Free energies and weighted Boltzmann average contributions for conformers of the cis isomer 4.29 calculated using the B3LYP/6-31G(d) level of theory at 298.15 K.	123
Table 4.2: Free energies and weighted Boltzmann average contributions for conformers of the trans isomer 4.30 calculated using the B3LYP/6-31G(d) level of theory at 298.15 K.	123

ACKNOWLEDGEMENTS

First and foremost, I would like to express my sincere gratitude to my supervisor, Professor Craig Merlic. Ever since I joined his group in 2012, Prof. Merlic has given me incredible support. His guidance has been invaluable to my growth as a scientist and his trust in me has enabled me to grow as an independent researcher. I would like to thank him for not only being a great mentor, but also a great friend.

I would also like to thank Prof. K. N. Houk for his continuous insight, especially with regards to the iridium-catalyzed borylation sections of this dissertation. Collaborating with Prof. Houk has been a real dream come true. Working with Prof. Merlic and Prof. Houk has been very enjoyable and has reminded me of what brought me to chemistry in the first place—the people.

Acknowledgement must also be given to my collaborator and friend Dr. Peng Liu, whose expertise in computational chemistry and excellent explanations accelerated my understanding and learning of this field.

Some additional thanks are also in order:

- To my high school teacher, Richard Roosa, who inspired me to enter chemistry
- To Prof. Charles Walsby, who took me on as one of his first undergraduate researchers at Simon Fraser University. Prof. Walsby was a joy to work with and supported me a great deal in my applications to graduate school
- To Prof. Roland Pomeroy, whose love of chemistry was infectious and who was one of the drivers behind my passion for organometallic chemistry
- To Dr. Craig Cooke and Richard Gafney, pirates of the H.M.S. Pomeroy

- To Prof. Dr. Jürgen Heck, who let me work and publish in his lab in Germany (even after setting a corner of it on fire)
- To Paula Diaconescu, who was my adviser for my first three years at UCLA
- To Colin Carver, Erin Broderick and Marissa Monreal who helped me with glove box techniques and organometallic synthesis
- To my good friend Kevin Miller, who is one of the finest chemists I have ever met
- To my coworker Andrew Elliott, who is also an excellent chemist and at least twice as intelligent as I am
- To my collaborators and coworkers Matthew Kiesz, Andrew Buechler, Bryon Lydon, Jeremy Oria, Johannes Hohenberger, Byron Boon, Prof. Jeffrey Zink and Prof. Karsten Meyer
- To Eric Chen who helped me get started on Gaussian 09 and Unix commands
- To the National Science Foundation (Graduate Research Fellowship under Grant No. DGE-0707424)
- To the members of the Merlic group, past and present. It has been a great two years!

Finally, I would like to thank my parents and my family, whose love and support has made all of this possible. I wouldn't be here without you.

Chapter 3 is a version of a manuscript submitted to *Journal of the American Chemical Society*. The co-authors of the manuscript are A. G. Green, P. Liu, C. A. Merlic and K. N. Houk. This is a collaborative theoretical study with Prof. K. N. Houk's group at University of California, Los Angeles.

VITA

- 2007 B.Sc. Chemistry
Simon Fraser University
Burnaby, BC Canada
- 2008 M.Sc. Chemistry UCLA
Los Angeles, CA

AWARDS AND HONORS

- 2010-2013 National Science Foundation Graduate Research Fellowship
- 2010 Department of Energy Office of Science Graduate Fellowship - finalist
- 2009 Chemistry Department Graduate Fellowship, UCLA
- 2008 RISE-pro scholarship, DAAD, Germany
- 2008 Chancellor's Distinguished Student Award, UCLA
- 2007 RISE scholarship, DAAD, Germany
- 2006 Canadian Society of Chemistry Silver Medal for academic excellence
- 2006 Canadian Institute of Chemistry 3rd Year Academic Achievement Award
- 2005 CanTest Ltd. Life Sciences Award

PUBLICATIONS AND PRESENTATIONS

Trtica, S., Prosenc, M.H., Schmidt, M., Heck, J., Albrecht, O., Gorlitz, D., Reuter, F., Rentschler, E. **Stacked Nickelocenes: Synthesis, Structural Characterization, and Magnetic Properties.** *Inorg. Chem.* **2010**, *49*, 1667-1673. *Acknowledged for significant experimental work.*

Green, A.G., Diaconescu, P.L.D. **A General Method for the Synthesis of Heterobimetallic 1,1'-Diamidometallocene Complexes.** Paper presented at: Southern California Organometallics Meeting. Jan. 8, 2011. Los Angeles, CA.

Green, A.G., Elliott, A.G., Buechler, A.K., Kiesz, M.D., Hohenberger, J., Meyer, K., Zink, J.I., Diaconescu, P.L. **Characterization of an Iron-Ruthenium Interaction in a Ferrocene Diamide Complex.** Poster session presented at: Spring 2012 San Diego ACS National Meeting. Mar. 26, 2012. San Diego, CA.

Elliot, A.G., Green, A.G., Diaconescu, P.L. **Transfer Hydrogenation with a Ferrocene Diamide Ruthenium Complex.** *Dalton Trans.* **2012**, *41*, 7852-7854.

Green, A.G., Houk, K.N., Merlic, C.A., **A Density Functional Theory Study on the Borylation of Pyridines Using an Iridium Catalyst.** Poster session presented at: The 2012 Winstein Symposium. Oct. 6, 2012. Los Angeles, CA.

Green, A.G., Oria, J., Elliott, A.G., Buechler, A.K., Kiesz, M.D., Hohenberger, J., Meyer, K., Zink, J.I., Diaconescu, P.L. **Characterization of an Iron-Ruthenium Interaction in a Ferrocene Diamide Complex.** *Inorg. Chem.* **2013**, *52*, 5603.

Green, A.G., Liu, P., Houk, K.N., Merlic, C.A. **Origins of Selectivities in Iridium-Catalyzed Borylation of Substituted Arenes and Heteroarenes.** *Submitted to JACS November 2013.*

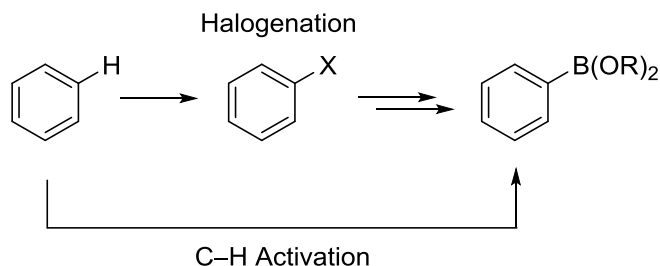
CHAPTER 1: On Regioselection in Iridium-Catalyzed Borylation Reactions

INTRODUCTION:

Organoboronate esters are well-established building blocks in synthetic organic chemistry. From these reagents, a wide variety of coupling products and functionalized molecules can be accessed in a single step.^{1,2} Reactions involving organoboronate esters are often catalytic, amenable to functional groups, and have been utilized in numerous syntheses of small molecules.³⁻¹⁰ Thus, new methodologies for syntheses of organoboronate esters are an important area of research which can lead to valuable products for synthetic and medicinal chemistry.

Traditional methodologies for the formation of aryl C–B bonds have relied on borylation of arylhalides. The synthesis of arylhalides, however, often requires harsh reaction conditions with low tolerance for functional groups. A more efficient synthesis of arylboronate esters is through C–H activation of the parent organic compound (Scheme 1.1). Direct C–H borylation allows for synthesis of arylboronate products in fewer steps while obviating the need for halogenation protocols. Over the past decade, iridium-catalyzed C–H borylation of alkene and aromatic substrates has shown great promise and utility for the synthesis of a wide range of arylboronate esters. Notably, these reactions occur under mild conditions exhibiting high regioselectivity and good yields.

Scheme 1.1: Halogenation route versus direct C–H activation method for borylation of unactivated substrates



Despite many recent advances in iridium-catalyzed borylation reactions, the origins of regioselectivities observed in these reactions are not well understood. For many substrates, such as monosubstituted arenes, steric effects appear to be the driving factor for observed regioselectivities. However, when the substrate is not sterically demanding, as in the case of unsubstituted 5-membered heterocycles, reaction occurs at the electron-rich carbon alpha to the heteroatom. Interestingly, when pyridine is used as the borylation substrate, the reaction furnishes statistical distribution of *meta*- and *para*-borylation without any *ortho*-borylation, suggesting either strong steric or electronic influences in the regioselectivity-determining step. Though there has been recent headway made towards a theoretical understanding of the regioselectivity in these reactions,^{11,12} there is still no clear model which explains the regioselectivity preferences across all of these substrates. This dilemma of explaining regioselectivities observed in iridium-catalyzed borylation reactions has been alluded to in multiple papers and reviews.¹³⁻¹⁷

Several excellent review articles for iridium-catalyzed borylation have been published. Ishiyama and Miyaura initially reviewed transition metal-catalyzed borylation reactions in 2003.¹⁸ A subsequent review by the same authors focused specifically on iridium-catalyzed borylation reactions.¹⁴ Since then, an excellent comprehensive review of borylation reactions utilizing transition metals was published in 2010.¹⁵ Hartwig specifically reviewed the regioselectivity of borylation reactions in 2011¹⁶ and published a 2012 account of his laboratory's research highlighting borylation reactions.¹⁷ Coupling products arising from one-pot syntheses involving an iridium-catalyzed organoboronate ester intermediate, which was not isolated, are not reviewed. This review focuses only on reports where borylated products are isolated. The purpose of this review article is to provide an overview of iridium-catalyzed borylation reactions of alkenes and arenes through the lens of regioselectivity with hopes to highlight the ongoing disparities between experiment and theory.

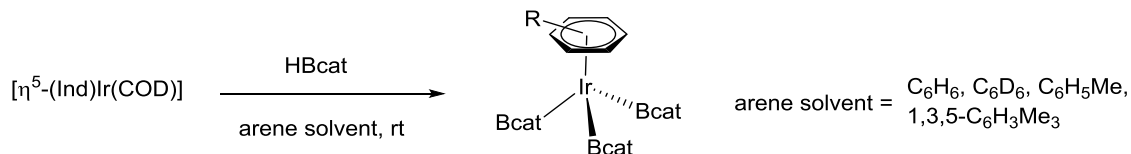
BACKGROUND:

Alkyl-, alkenyl-, and aryl-boranes, boronic acids and boronates are common synthetic intermediates in organic chemistry. Their utility can be illustrated in a couple examples: (1) alkylboranes can be converted to functionalized molecules including amines, alcohols and alkenes as well as other functionalities in a single step;^{1,2} and (2) Suzuki-Miyaura cross-coupling methods allow for efficient coupling of organoboranes, organoboronic acids, and organoboronate esters with alkyl-, alkenyl- and arylhalides. While Suzuki-Miyaura cross-couplings for alkylboranes¹⁹ and alkylboronates²⁰⁻²³ have been reported, they are far less developed than the Suzuki-Miyaura coupling of sp^2 and sp hybridized carbon centers.^{3,24}

While these valuable reagents were originally prepared via stoichiometric reactions, as the utility of these synthetic intermediates became recognized, catalytic methods for incorporating boron into organic molecules became highly sought after. Many metal catalysts have been found that are suitable for catalytic borylation reactions. In the past decade, however, iridium-catalyzed borylation reactions have emerged as one of the most valuable methodologies for the synthesis of organoboronate esters. The development of methods for iridium-catalyzed borylation of alkanes, alkenes and arenes occurred almost simultaneously.

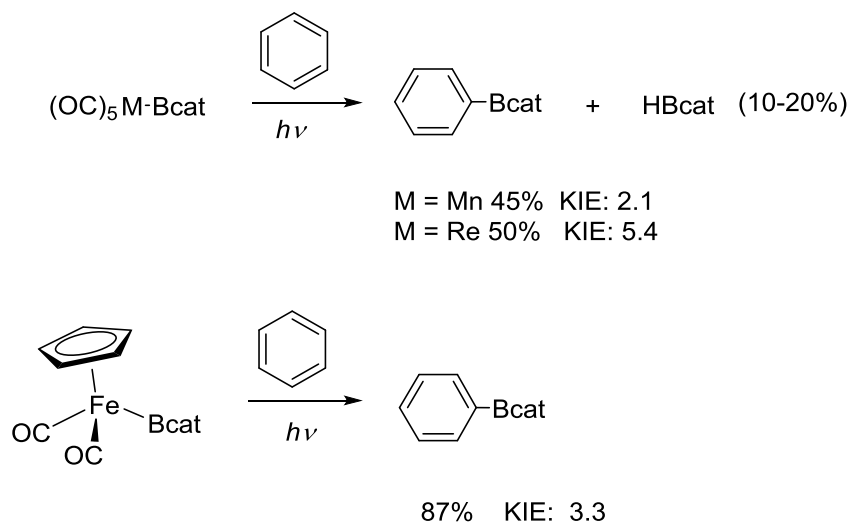
Initial investigations on transition metal-mediated borylation began with the work of Hartwig and Marder, who established stoichiometric conversions of alkanes, alkenes and arenes into boronate esters. Marder initially published a study in 1993, detailing the synthesis of a series of tris(boryl)iridium complexes $[(\eta^6\text{-arene})\text{Ir}(\text{Bcat})_3]$ (arene = C_6H_6 , C_6D_6 , $\text{C}_6\text{H}_5\text{Me}$, 1,3,5- $\text{C}_6\text{H}_3\text{Me}_3$; Bcat = catecholboron) from $(\text{Ind})\text{Ir}(\text{COD})$ (Ind = indenyl; COD = 1,5-cyclooctadiene) shown in Scheme 1.2.²⁵ The complexes were found to adopt three-legged piano stool structures as verified by X-ray crystallography. While the authors did not specifically mention catalysis in the article, they did report in the supplementary material the formation of borylated toluene species as detected by GC/MS, products which were indicative of catalytic borylation.

Scheme 1.2: Formation of tris(boryl)iridium(III) piano stool complexes by reaction of $[(\eta^6\text{-Ind})\text{Ir}(\text{COD})]$ with HBcat in an arene solvent



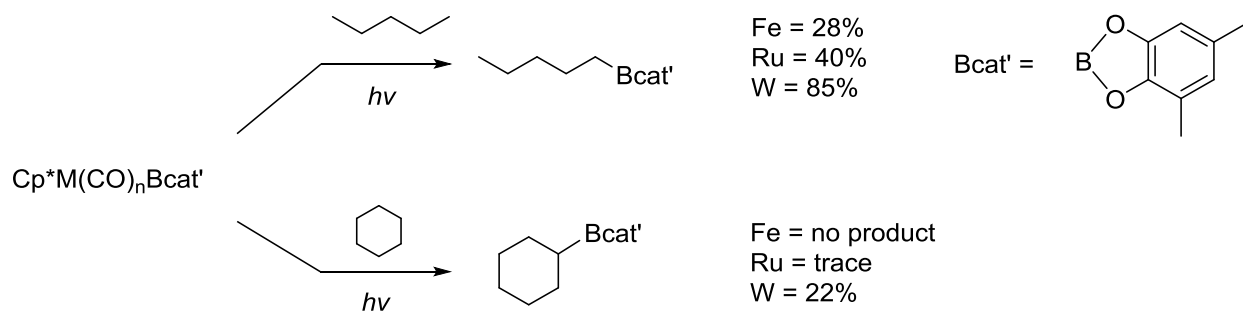
In 1995, Hartwig and coworkers examined the irradiation of several transition metal boryl complexes in the presence of arenes and alkenes (Scheme 1.3).²⁶ The selectivities they observed were different for each metal. Upon irradiation of the carbonyl complexes $\text{M}(\text{CO})_5(\text{Bcat})$ ($\text{M} = \text{Mn}$ or Re) in benzene, PhBcat and HBcat were formed competitively, whereas irradiation of $\text{CpFe}(\text{CO})_2\text{Bcat}$ ($\text{Cp} = \text{C}_5\text{H}_5$) in benzene led to PhBcat being formed exclusively. Kinetic isotope effect (KIE) studies ruled out a radical mechanism but did not allow for discrimination between reaction of an unsaturated 16-electron metal intermediate or a photochemically-generated excited state.

Scheme 1.3: Stoichiometric irradiation of benzene in the presence of monoboryl metal carbonyls to form PhBcat



In a subsequent study, Hartwig reported the stoichiometric functionalization of primary C–H bonds of alkanes (Scheme 1.4).²⁷ Under UV irradiation, the Cp* (Cp* = C₅Me₅) complexes Cp*M(CO)_nBcat (M = Fe, Ru, W) exhibited high selectivity for the primary position of pentane, ethylcyclohexane and isopentane. Reaction with cyclohexane resulted in only 20% conversion for the tungsten complex and trace conversion for the ruthenium complex. No cyclohexane conversion products were observed for the iron complex. KIE studies again ruled out a boryl radical mechanism and, based on product distributions when different ratios of PMe₃ were added, the authors suggested that the reaction proceeds through a 16-electron unsaturated intermediate formed by the loss of CO. Several steps and external reagents were required in order to regenerate the boryl complex from the resulting metal hydride and dimeric metal carbonyl products, limiting this system to stoichiometric transformations.

Scheme 1.4: Stoichiometric borylation of alkanes by metal carbonyl complexes



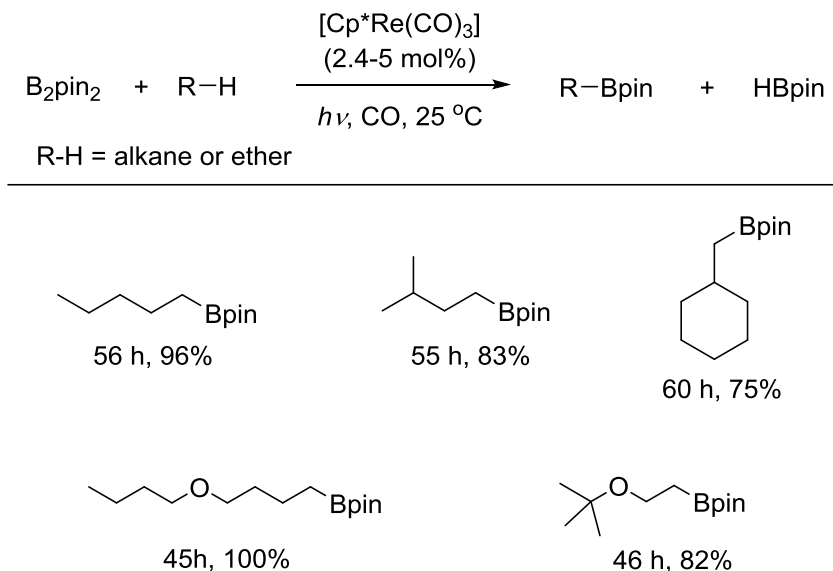
Iverson and Smith reported the first formal catalytic borylation in 1999 (Scheme 1.5).²⁸ Initially, the authors investigated a catalytic cycle consisting of thermal B–C and photochemical Ir–C bond forming steps. Starting with the iridium dihydride complex $\text{Cp}^*\text{Ir}(\text{PMe}_3)(\text{H})_2$ and a C_6H_6 solution of 5 equivalents of HBpin, they first photolyzed the reaction mixture to form the aryl intermediate $\text{Cp}^*\text{Ir}(\text{PMe}_3)(\text{H})(\text{Ph})$. Heating this intermediate yielded PhBpin and the monoboryl species $\text{Cp}^*(\text{Ir})(\text{PMe}_3)(\text{H})(\text{Bpin})$. Subsequent photolysis to regenerate the dihydride species completed the thermal/photolytic cycle. However, the authors noted that all of the borane was consumed after just three cycles, implicating a thermal catalytic process. Thermolysis of $\text{Cp}^*(\text{Ir})(\text{PMe}_3)(\text{H})(\text{Bpin})$ (17 mol%) in the presence of C_6H_6 and HBpin at 150 °C resulted in the formation of PhBpin in 53% yield with an effective turnover number of 3, thus establishing the first thermal catalytic borylation.

Scheme 1.5: Equation for the first formal catalytic borylation reaction



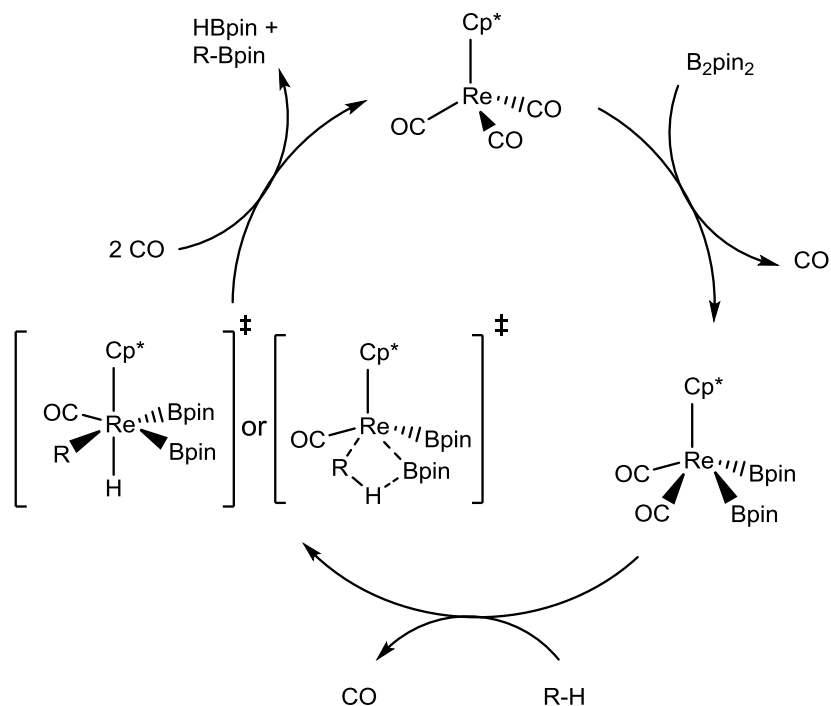
Soon after Smith's report, Hartwig reported the photocatalytic borylation of alkanes and ethers (Chart 1.1).²⁹ Having studied the stoichiometric borylation of pentane with bis(pinacolato)diboron (B_2pin_2) using $\text{Cp}'\text{M}(\text{CO})_3$ ($\text{Cp}' = \text{C}_5\text{H}_4\text{Me}$, $\text{M} = \text{Mn}$; $\text{Cp}' = \text{C}_5\text{H}_5$, $\text{M} = \text{Re}$; $\text{Cp}' = \text{C}_5\text{Me}_5$ (Cp^*), $\text{M} = \text{Re}$) under irradiation conditions, the authors found that the rhenium complex $\text{Cp}^*\text{Re}(\text{CO})_3$ converted pentane to borylated product in quantitative yield based on yield. By performing the reaction under a CO atmosphere the authors were able to make the reaction catalytic, presumably by regenerating the active $\text{Cp}^*\text{Re}(\text{CO})_3$ complex instead of forming catalytically inactive bridging carbonyl dimers. The reaction showed broad substrate scope for alkanes and ethers and exhibited high regioselectivity for the primary position. Less than 1% of other regioisomeric products were observed. In addition, the reaction was shown to be active for transformation of $\text{C}(\text{sp}^2)\text{-H}$ bonds, as benzene was borylated in 76% yield.

Chart 1.1: Photocatalytic borylation of alkanes and ethers by $\text{Cp}^*\text{Re}(\text{CO})_3$ to yield terminal borylated products.



In the catalytic cycle, the authors proposed that first $\text{Re}(\text{I})$ oxidatively adds to B_2pin_2 to give the $\text{Re}(\text{III})$ bisboryl complex (Scheme 1.6). This reactive intermediate then undergoes reaction with the alkane via either oxidative addition to give a $\text{Re}(\text{V})$ species or sigma bond metathesis involving $\text{Re}(\text{III})$. Reductive elimination then yields HBpin and the borylated alkane. An alternative catalytic cycle involving initial oxidative addition of the alkane followed by reaction of the alkylrhenium hydride was unable to be ruled out by the authors, but was disfavored because of their ability to isolate the bisboryl complex $\text{Cp}^*\text{Re}(\text{CO})_2(\text{Bpin})_2$ by reaction of B_2pin_2 with $\text{Cp}^*\text{Re}(\text{CO})_3$. Additionally, the alternative catalytic cycle is disfavored because the hydride intermediate $\text{Cp}^*\text{Re}(\text{CO})_2(\text{H})(\text{CH}_3)$ is known to be unstable.³⁰

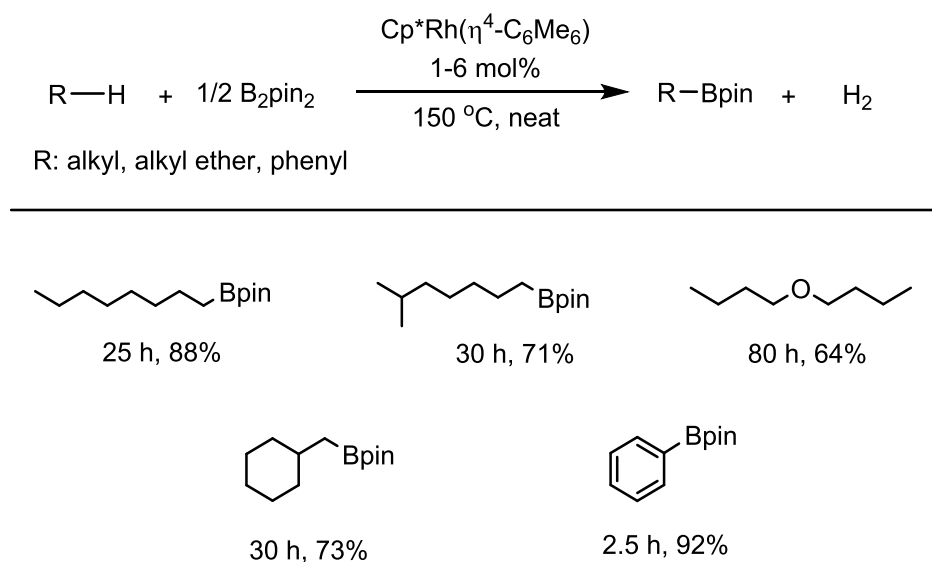
Scheme 1.6: Catalytic cycle for the photocatalytic borylation of alkanes and ethers by $\text{Cp}^*\text{Re}(\text{CO})_3$



Hartwig and coworkers disclosed a much more active rhodium catalyst for the borylation of alkanes in 2000.³¹ Initial screenings were performed on Cp^*IrH_4 and $\text{Cp}^*\text{Ir}(\text{C}_2\text{H}_4)_2$, since these compounds are known to extrude H_2 or dissociate alkene, respectively, under thermal conditions. However, reaction yields with these complexes never exceeded 20%, so, the authors chose to use the more reactive rhodium analog, $\text{Cp}^*\text{Rh}(\text{C}_2\text{H}_4)_2$. Borylation of *n*-octane to give *n*-octylBpin in 84% yield required 5 h at 150 °C (Chart 1.2). After optimization, the authors found the rhodium arene complex $\text{Cp}^*\text{Rh}(\eta^4\text{-C}_6\text{Me}_6)$ provided the best balance of activity and stability. Good to moderate yields were obtained for borylation of *n*-octane, 2-methylheptane,

methylcyclohexane, *n*-butyl ether and benzene, and exclusive regioselectivity for the terminal position of the alkane was observed.

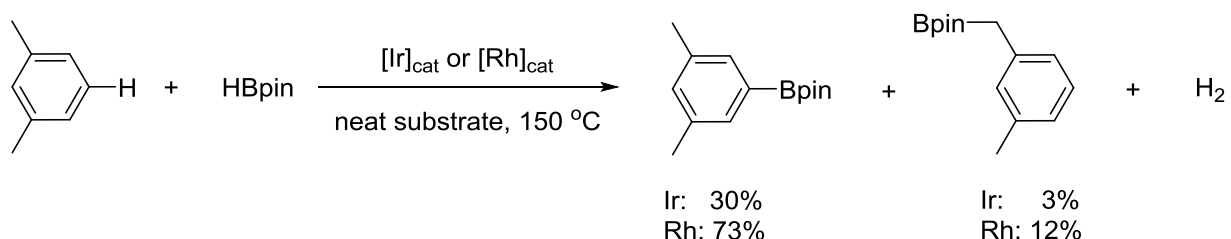
Chart 1.2: Regioselective, catalytic functionalization of alkanes, alkyl ethers and benzene by $\text{Cp}^*\text{Rh}(\eta^4\text{-C}_6\text{Me}_6)$.



This work was soon followed by a study by Smith comparing the regioselectivities of the catalysts $\text{Cp}^*\text{Ir}(\text{PMe}_3)(\text{H})\text{Bpin}$ and $\text{Cp}^*\text{Rh}(\eta^4\text{-C}_6\text{Me}_6)$ with respect to arene borylation (Scheme 1.7).³² Regioselectivity was found to be sterically controlled for most arenes. This is in contrast to traditional aromatic substitutions which are dominated by electronic effects. Interestingly, iridium was found to be more selective for arene borylation than rhodium which yielded higher amounts of borylation products arising from benzylic activation. In an ensuing study that

supported Smith's findings, Marder and coworkers reported a rhodium catalyst that exhibited high selectivity for the benzylic position of substituted arenes.³³

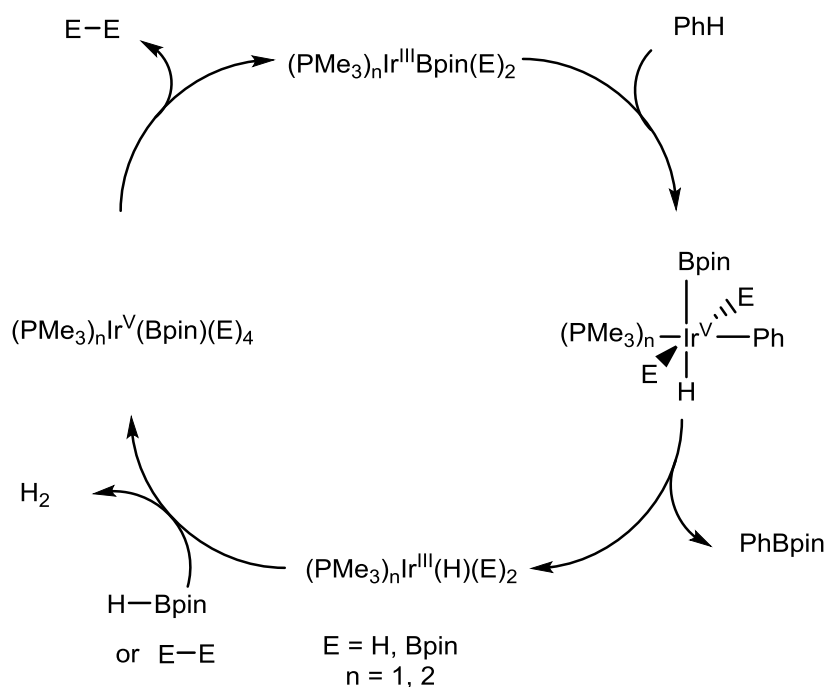
Scheme 1.7: Selected example highlighting the preference for selective arene C–H borylation of iridium versus rhodium in the reaction of *m*-xylene



In 2002, Smith, Maleczka and coworkers published a landmark paper on iridium-catalyzed borylation of arenes.³⁴ Starting from (Ind)Ir(COD), the authors prepared (η^6 -mesitylene)Ir(Bpin)₃ in a procedure analogous to the previously reported synthesis by Marder for the synthesis of iridium trisboryl complexes.²⁵ The authors noted that the complex (η^6 -mesitylene)Ir(Bpin)₃ becomes catalytic towards arene borylation in the presence of phosphine. Their proposed catalytic cycle is shown in Scheme 1.8. Because the synthesis and isolation of (η^6 -mesitylene)Ir(Bpin)₃ proved difficult, the authors opted for the generation of an active catalyst by addition of phosphine ligand to (Ind)Ir(COD). Particularly high turnover numbers were obtained when bidentate phosphines were used as ligands. Smith postulated that the complex (PMe₃)_nIrBpin₃ was the key reactive intermediate in this transformation. The authors favored a mechanism involving Ir(III) and Ir(V) intermediates over Ir(I) complexes for several

reasons: (1) No borylation products were observed for iodobenzene when iridium(I) sources were used; (2) Improved catalytic activity was observed with bisphosphine complexes, favoring a bisphosphine intermediate formed from reductive elimination of H₂, HBpin or B₂pin₂; and (3) Ir(PMe₃)₂H₅ was an effective borylation precatalyst.

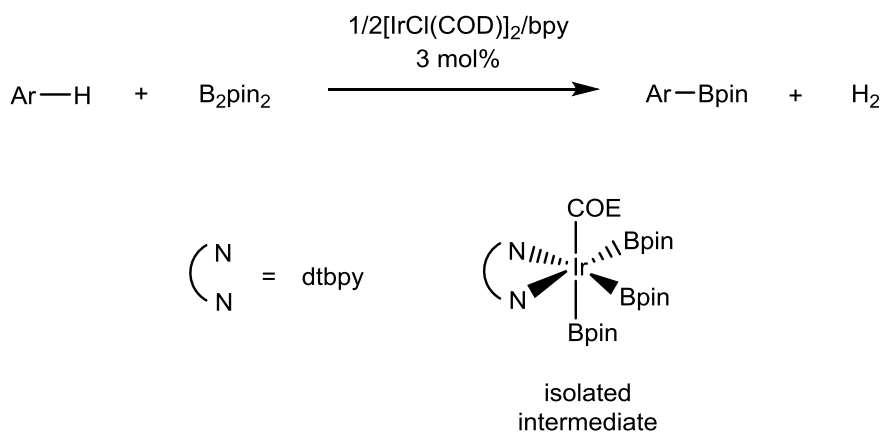
Scheme 1.8: Proposed catalytic cycle for borylation of benzene by (PMe₃)_nIr(Bpin)₃



A simultaneous report by Ishiyama, Miyaura and Hartwig established a mild iridium-catalyzed borylation procedure with high turnover numbers and isolation of an active Ir(III) intermediate (Scheme 1.9).³⁵ The precatalyst comprised an iridium(I) species [IrCl(COD)]₂ with 2,2'-bipyridine (bpy) as a ligand. Complexes generated from 1,10'-phenanthroline as a ligand

were also effective, but led to lower yields. Other ligands, such as pyridine, TMEDA, PPh₃ and dppe were ineffective. Pt(dba)₂ did not produce any borylated products and the rhodium(I) analog [RhCl(COD)]₂ with bpy only, produced PhBpin from benzene in 20% yield at 150 °C. A broad substrate scope of mono- and disubstituted arenes was investigated with the iridium(I) system. Ultimately, with 4,4'-di-tert-butyl-2,2'-bipyridine (dtbpy) as a ligand, an active iridium(III) intermediate [Ir(dtbpy)(Bpin)₃(COE)] (COE = cyclooctaethylene) was able to be structurally characterized lending credence to an Ir(III)/Ir(V) mechanism.³⁵

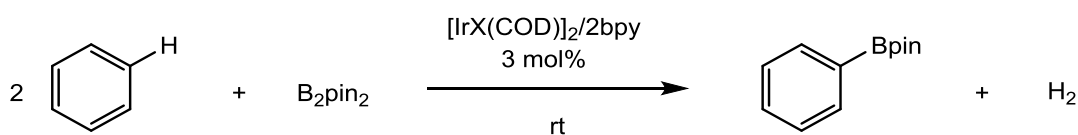
Scheme 1.9: Catalytic borylation of arenes using [IrCl(COD)]₂/bpy catalyst system and the structure of an isolated Ir(III) active intermediate



Shortly thereafter, a follow-up report by the same group disclosed the catalytic, room-temperature borylation of arenes.³⁶ Key to this discovery was increasing catalytic activity by varying the anionic ligand (Table 1.1). Halide and cationic complexes did not catalyze the reaction at room temperature. Employing the more basic alkoxo complexes possessing OH, OPh

or OMe ligands, however, enabled room temperature catalysis. Methoxide was found to be the best anionic ligand for borylation of a variety of substrates in excellent yields. Thorough screening of combinations of anionic ligands with substituted bpy ligands yielded $[\text{Ir}(\text{OMe})(\text{COD})]_2/\text{dtbpy}$ in nonpolar solvent as the catalyst system of choice. The dtbpy ligand was less amenable to degradation via C–H activation and made the catalyst system more soluble. The $[\text{Ir}(\text{OMe})(\text{COD})]_2/\text{dtbpy}$ catalyst system is currently the most active for arene borylation and has been utilized in numerous studies which will be reviewed in subsequent sections.

Table 1.1: Effect of anionic ligands on borylation of benzene by B_2pin_2 .



Ir(I) precursor	Time (h)	Conversion (%) ^a	Yield (%) ^b
$[\text{IrCl}(\text{COD})]_2$	24	0	0
$[\text{Ir}(\text{COD})_2]\text{BF}_4$	24	3	0
$[\text{Ir}(\text{OH})(\text{COD})]_2$	4	100	88
$[\text{Ir}(\text{OPh})(\text{COD})]_2$	4	100	84
$[\text{Ir}(\text{OMe})(\text{COD})]_2$	4	100	90
$[\text{IrCl}(\text{COD})]_2/4\text{NaOMe}$	4	100	73
$[\text{Ir}(\text{OAc})(\text{COD})]_2$	24	19	1

(a) Conversions of B_2pin_2

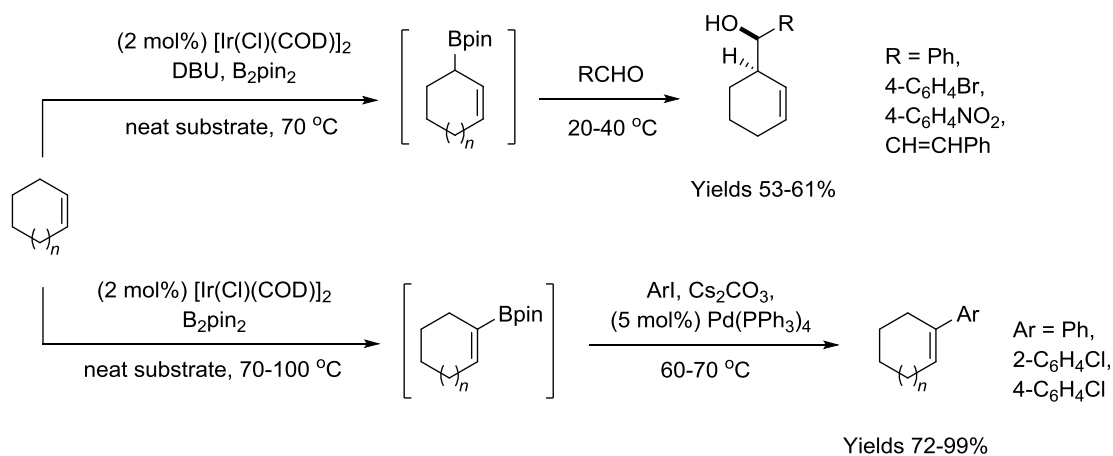
(b) GC yields based on boron atom in B_2pin_2

ALKENES:

Borylation of alkenes poses an interesting challenge with regards to selectivity since both $C(sp^2)$ -H and $C(sp^3)$ -H bonds are often available for functionalization. Additionally, preference for allylic borylation versus vinylic borylation must be considered. Furthermore, preference for borylation of an alkene C-H bond versus borylation of an aromatic C-H bond should be taken into account. Iridium has demonstrated a preference for $C(sp^2)$ -H borylation in contrast to rhodium catalyst systems, which have a preference for $C(sp^3)$ -H borylation.^{32,33} Borylation of alkenes by iridium catalysts is much less developed than borylation of arenes; however, several examples of iridium-catalyzed borylation of alkenes exist in the literature.

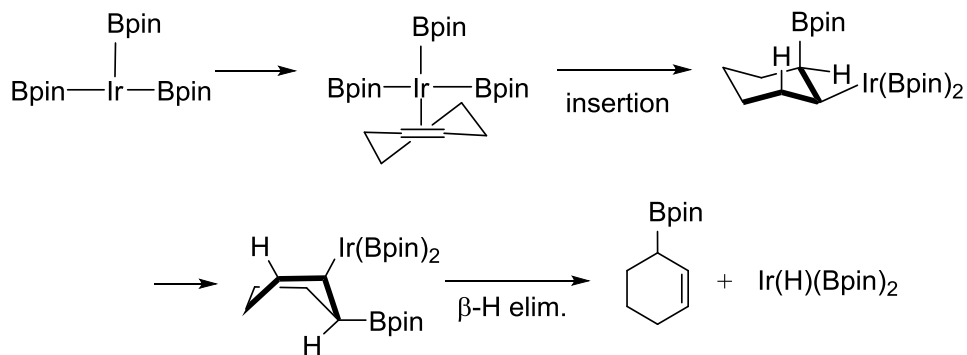
In 2007, Szabó and coworkers achieved selective C-C bond formation for a range of cyclic alkenes via a one-pot synthesis involving a C-H borylation step (Scheme 1.10).³⁷ While the organoboronate esters were not isolated, ¹H NMR studies conducted on borylation of cyclohexene revealed initial formation of a 1:1 mixture of allylic and vinylic borylation products after 3 h at 70 °C. After 16 h, only vinylic borylation products were observed. Addition of 0.5 equiv of 1,8-diazabicyclo[5.4.0]undecane (DBU) to the initial reaction mixture retarded formation of the vinylic product producing allylic and vinylic borylated products in a 5:1 ratio. The authors utilized these findings to generate a series of allylic and vinyl boronate esters in moderate yields.

Scheme 1.10: Iridium-catalyzed borylation of cyclic alkenes with subsequent transformation



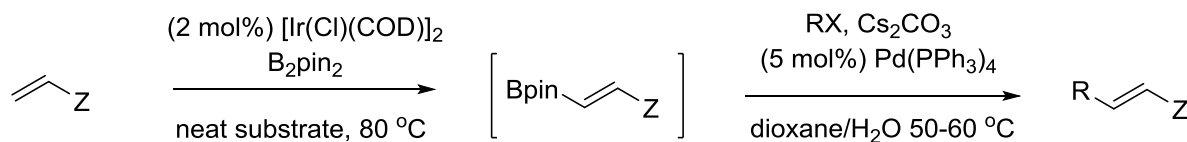
The authors propose a mechanism originally reported by Lloyd-Jones and Brown,³⁸ and by Marder,^{39,40} for Rh(I) catalyzed C–H activation reactions, which involves insertion of the metal complex into the double bond followed by β -hydride elimination (Scheme 1.11).³⁷ Regioselectivity of the reaction is initially determined by the kinetic preference for *syn* insertion rather than C–H oxidative addition. After insertion, only the allylic C–H bond is able to adopt the *syn* conformation required for β -hydride elimination. The kinetic product is then the allyl boronate ester. In the absence of DBU, however, borylation leads to the thermodynamically favored vinyl boronate ester.

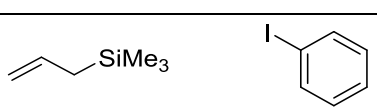
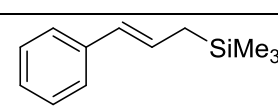
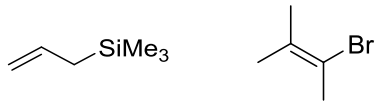
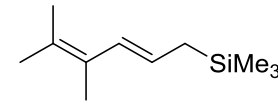
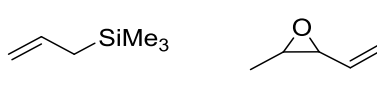
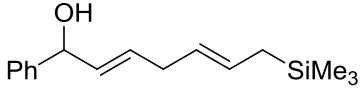
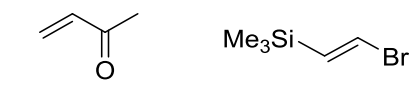
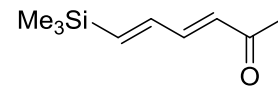
Scheme 1.11: Mechanism for iridium-catalyzed borylation of alkenes to produce allyl products

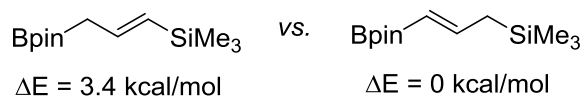


In another example of a highly regioselective borylation of alkenes, Szabó and coworkers reported the borylation of allylsilane and various linear terminal olefins at 80 °C with [Ir(Cl)(COD)]₂ and B₂pin₂ (Table 1.2).⁴¹ The borylation products were not isolated, but were further coupled with aryl and vinyl halides in a one-pot sequence. The authors propose the reaction mechanism proceeds through the dehydrogenative borylation mechanism shown previously for cycloalkenes (Scheme 1.11). The reaction was selective for the terminal alkene C–H bond and there was no observed cis-trans isomerization of the vinyl boronate ester formed *in situ*. DFT studies suggested that the regioselectivity is thermodynamically controlled favoring borylation at the terminal position.⁴¹

Table 1.2: Iridium-catalyzed borylation of linear alkenes followed by palladium-catalyzed cross-coupling by Szabó and coworkers.

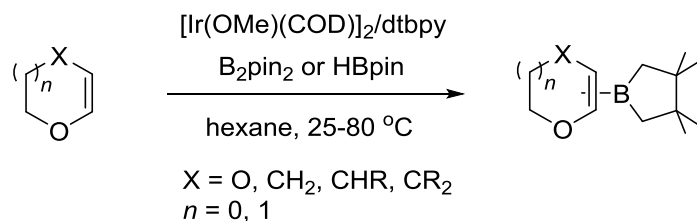


Entry	Substrates	Products	Yield (%)
1			56
2			73
3			55
4			87



Ishiyama, Miyaura and coworkers reported vinylic C–H borylation of cyclic vinyl ethers by B_2pin_2 using $[\text{Ir}(\text{OMe})(\text{COD})]_2/\text{dtbpy}$ as the catalyst system (Table 1.3). Reactions with 1,4-dioxene occurred at room temperature whereas reactions with dihydropyran and dihydrofuran derivatives required elevated temperatures.^{42,43} Dihydropyran and dihydrofuran produced alpha-

and β -borylated products in ratios of 75:25 and 49:51, respectively. The lack of regioselectivity is somewhat surprising given significant difference in polarization of the two positions and the preference for furan to borylate at the 2-position. Addition of substituents to the 3-position of dihydropyran led to improved alpha selectivity. Addition of substituents to the 3-position of dihydrofuran favored alpha borylation, but still yielded small amounts of beta-borylated products. Substrates containing both vinylic and aromatic C–H bonds selectively formed vinyl boron compounds.

Table 1.3: Borylation of vinylic C–H bond of five- and six-membered cyclic vinyl ethers.

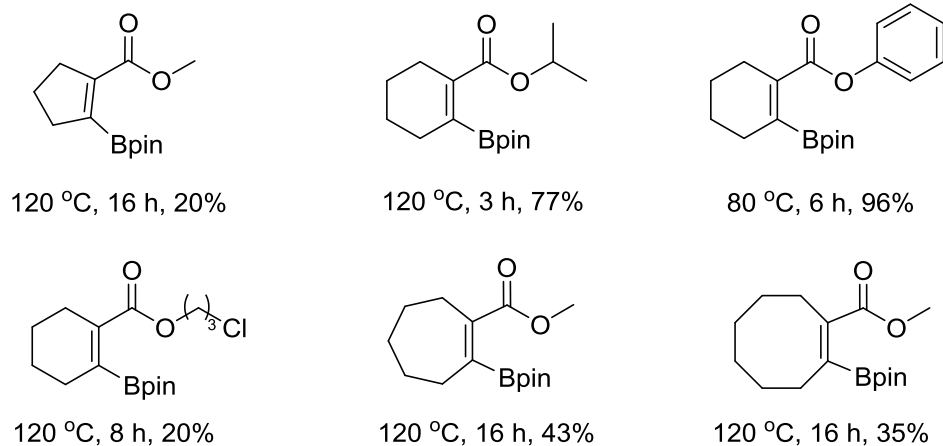
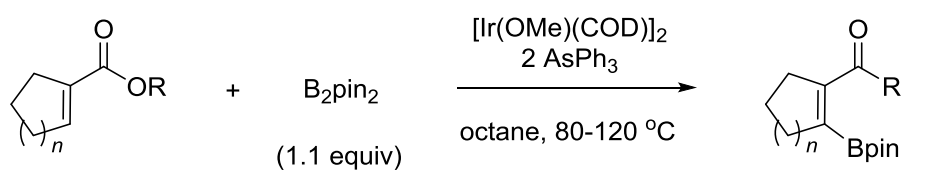
Entry	Substrate	Products	Yield (%) ^a
1		+	64 (75:25)
2			61
3			81
4		+	75 (49:51)
5		+	73 (95:5)

(a) GC yields based on boron atom in B_2pin_2

Recently, Ito, Ishiyama and coworkers reported vinylic C–H borylation of 1-cycloalkenecarboxylate derivatives with B_2pin_2 (Chart 1.3).⁴⁴ Using an iridium complex consisting of $[\text{Ir}(\text{OMe})(\text{COD})]_2$ and AsPh_3 as a ligand—a protocol that the authors developed

previously for the C–H borylation of aryl ketones⁴⁵—they found that the carbonyl oxygen directed borylation to yield the vinylic boronate ester preferentially. The protocol tolerated a broad substrate scope with functional groups such as halogen, acyl, alkoxy, carbamoyl, and epoxy.

Chart 1.3: C–H borylation of 1-cycloalkenecarboxylates with B₂pin₂.



ARENES:

In the absence of directing groups, the borylation of aromatic ring systems is dominated by steric effects. These effects are so important that a simple rule of reactivity for borylation of aromatic rings exists: except in rare cases, reaction does not occur *ortho* to a substituent when a C–H bond lacking an *ortho* substituent is available.¹⁶ In substrates where *ortho*-borylation is unavoidable, reactivity is greatly diminished. When steric effects are negligible, as in the case of symmetrical disubstituted arenes or unsubstituted heteroarenes, electronic effects influence the selectivity of borylation. The origins of regioselectivity based on electronic effects have been debated, but a definitive and encompassing model remains elusive.

Ortho-borylation is always disfavored for monosubstituted benzene rings lacking directing groups. When the size of the substituents is similar, slight electronic effects can be observed. For example, using an iridium complex consisting of $[\text{Ir}(\text{OMe})(\text{COD})]_2$ and dtbpy as a ligand, toluene borylates in a 0:69:31 ratio (*ortho:meta:para*), whereas trifluorotoluene and anisole borylate in a 0:70:30 and 1:74:25 ratio, respectively (Figure 1.1).³⁵ The regioselectivity of the more electron rich anisole differs slightly from toluene and trifluorotoluene.

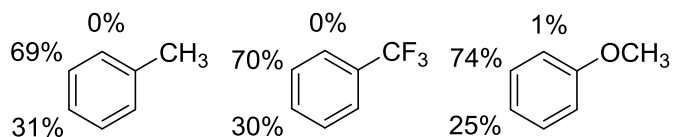


Figure 1.1: Regioselectivity for iridium-catalyzed borylation of select monosubstituted benzene rings.

Reaction regioselectivities for select 1,2-disubstituted arenes are shown in Figure 1.2. In most cases, symmetrical 1,2-disubstituted benzene rings borylate exclusively at the 4-position.^{35,36,46} The notable exception is benzo[d][1,3]dioxole which borylates primarily at the *ortho* position, which the authors attribute to the greater acidity of the *ortho* hydrogen.¹¹ When there are two different substituents, a mixture of products tends to form.¹² Marder et al. recently showed that for unsymmetrical 1,2-disubstituted benzene rings, π -electron acceptors favor borylation at the *para* position while π -donors and σ -electron withdrawing groups direct borylation to *meta* positions.¹²

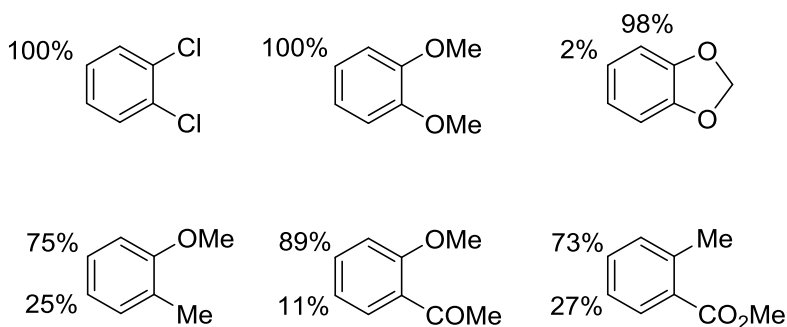


Figure 1.2: Regioselectivity for iridium-catalyzed borylation of 1,2-disubstituted arenes.

Steric effects control regioselectivity for borylations of 1,3-disubstituted and 1,2,3-trisubstituted arenes such that 1,3,5-trisubstituted and 1,2,3,5-tetrasubstituted products are generally formed regardless of the substituents (Figure 1.3).^{35,36,47} Two notable exceptions are 3-cyanobenzonitrile, which gives borylation at both the 5- and 4-positions, and 1,3-difluorobenzene, which yields a mixture of products borylated at the 5-, 4-, and 2-positions.⁴⁸ Borylation at the *ortho* position of 1,3,5-trisubstituted arenes will occur, however, we are unaware of any reports describing borylation of unsymmetrical 1,3,5-trisubstituted arenes.

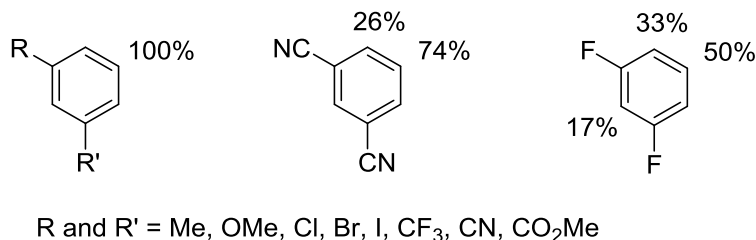


Figure 1.3: Regioselectivity for iridium-catalyzed borylation of 1,3-disubstituted arenes.

Borylation of 1,4-disubstituted benzene derivatives yield *ortho*-borylated products (Figure 1.4). Symmetrical 1,4-disubstituted arenes can only yield one product, whereas borylation of unsymmetrical 1,4-disubstituted arenes yields two 1,2,4-trisubstituted products.^{35,36,46-48} While it is difficult to separate steric and electronic effects, Smith argues that steric factors control regioselectivity in the borylation of 1,4-disubstituted arenes.⁴⁸

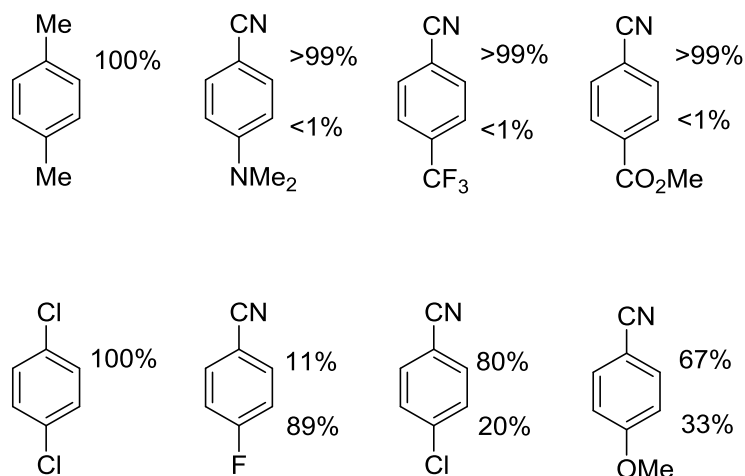


Figure 1.4: Regioselectivity for iridium-catalyzed borylation of select 1,4-disubstituted arenes.

One example exists of borylation of a 1,2,4-trisubstituted compound, namely, 4-bromo-2-fluorobenzonitrile, which borylates primarily at the position *ortho* to the cyano group, in a similar fashion to *para* substituted benzonitriles (Figure 1.5).⁴⁸

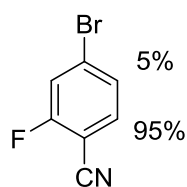
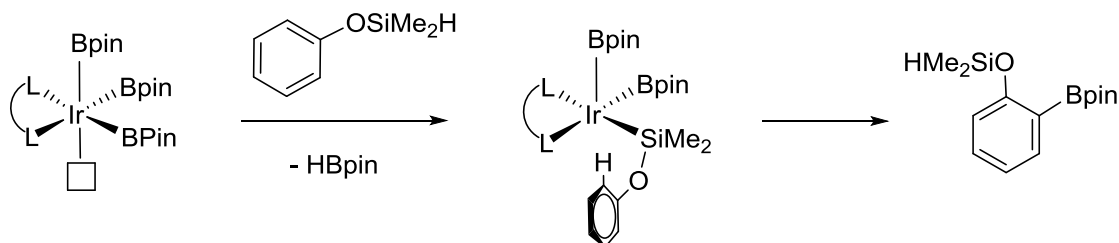


Figure 1.5: Regioselectivity for iridium-catalyzed borylation of 4-bromo-2-fluorobenzonitrile.

Borylation *ortho* to a substituent can occur when the substituent also functions as a directing group. Thus, borylation occurs exclusively at the position *ortho* to a silylmethyl or

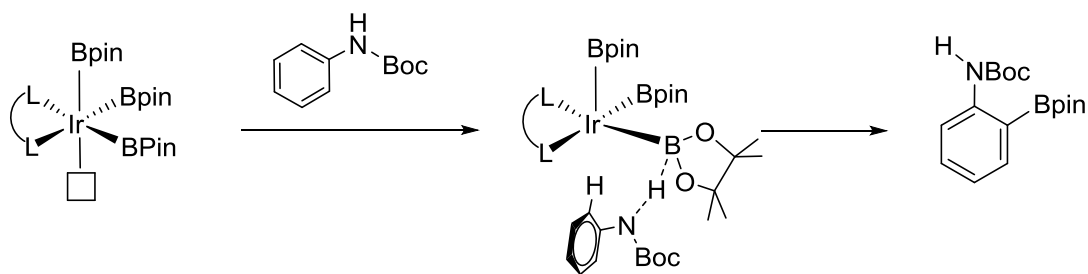
siloxo group.⁴⁹ This so-called relay-directed *ortho*-borylation developed by Hartwig and coworkers has been studied extensively for arenes containing phenolic or N-methyl functionalities and also for arenes that have alkyl substituents where a benzylic silylmethyl group can be inserted (Scheme 1.12). In the case of indole, silylation of the nitrogen leads to exclusive reactivity at the 7-position whereas reaction at the 2-position is normally preferred.⁵⁰

Scheme 1.12: Relay-directed *ortho*-borylation with a siloxy group



In another example of directed *ortho*-borylation, Smith et al. recently developed use of N-Boc as a directing group.⁵¹ Whereas the Hartwig methodology utilizes an inner-sphere mechanism, borylation with an N-Boc directing group proceeds through an outer-sphere mechanism whereby a proton on the nitrogen interacts with one of the boryl ligands (Scheme 1.13). *Ortho*-borylation was favored in all N-(boc)-aniline substrates studied. In the case of 3-substituted N-(boc)-anilines, minor products due to borylation at the 5-position were observed. In general, direction will occur for the least hindered *ortho* position though borylation can still occur if the adjacent substituent is small, such as fluorine.

Scheme 1.13: Outer-sphere directed borylation



While borylation of arenes is largely controlled by steric factors, borylation of unsubstituted heterocycles is dominated by electronic effects. The 5-membered heterocycles pyrrole, furan and thiophene react almost exclusively at the position alpha to the heteroatom (Figure 1.6). The benzo-fused heterocycles react similarly and no products arising from activation of the benzo-fused ring are observed.^{13,36,46}

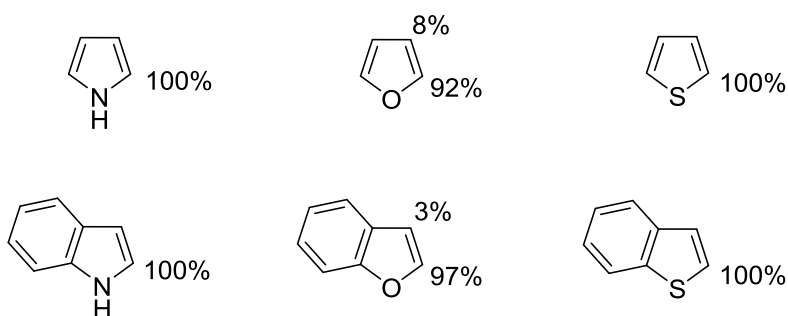


Figure 1.6: Regioselectivities for iridium-catalyzed borylation of unsubstituted 5-membered heteroarenes.

In 2002, Hartwig, Ishiyama, Miyaura and coworkers studied borylation of unsubstituted pyridine and quinoline and the observed regioselectivities are shown in Figure 1.7.¹³ In contrast to 5-membered heteroarenes, borylation of pyridine occurs at the 3- and 4-positions relative to the heteroatom and no 2-borylated products are observed.¹³ Quinoline also exhibits interesting selectivity with monoborylation occurring exclusively at the 3-position. The discrepancy between the regioselectivities of 5- and 6-membered heterocycles was suggested to be due to formation of a Lewis acid-base complex of the pyridines with either iridium or boron species in the reaction.¹³

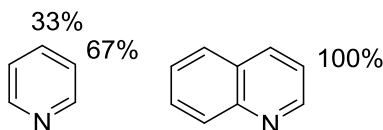


Figure 1.7: Regioselectivities for iridium-catalyzed borylation of pyridine and quinoline.

Substituted 5-membered heterocycles exhibit selectivity that results from a compromise between steric and electronic effects (Figure 1.8). In the case of 5-membered heterocycles, substitution at the 2-position results in borylation at the 5-position.^{52,53} Borylation at the 3-position will occur if both the 2-, and 5-positions are blocked.⁴⁷ Additionally, substituents on the nitrogen atom of pyrrole or indole can favor reactivity at the 3-position, with the 3-position reacting exclusively when the bulky triisopropylsilane (TIPS) group is utilized.¹³ Benzo-fused 5-membered heterocycles with substituents at the 2-position will borylate at the 7-position.^{54,55}

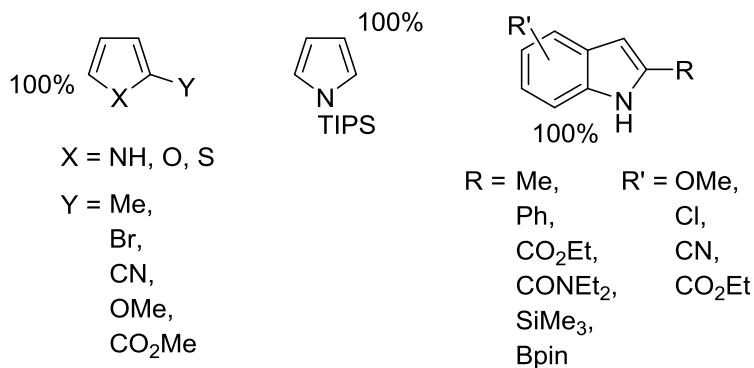


Figure 1.8: Regioselectivities for iridium-catalyzed borylation of substituted 5-membered heterocycles.

Experimental regioselectivity for pyridines is also heavily influenced by the presence of substituents (Figure 1.9). Pyridines substituted at the 2-position borylate at the 4- and 5-positions in a 50:50 ratio when the substituent is phenyl.⁵⁶ 2,6-Disubstituted pyridines borylate exclusively at the 4-position.⁴⁷ Pyridines with substituents at the 3-position favor borylation at the 5-position.⁵⁷

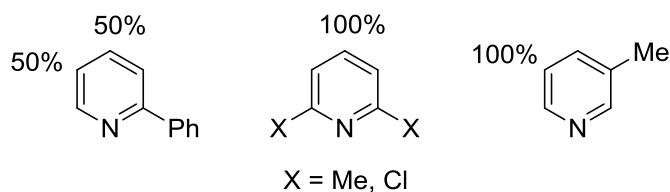


Figure 1.9: Regioselectivities for iridium-catalyzed borylation of substituted pyridines.

In a study published by Perutz, Marder and coworkers in 2006, 4,4'-disubstituted-2,2'-bipyridines were found to undergo borylation at either the 5-positions or the 6-positions (Figure 1.10).⁵⁶ For example, 4,4'-(MeO)₂-2,2'-bipyridine borylated exclusively at both of the 5-positions *ortho* to the methoxy substituents. The sterically hindered 4,4'-(*t*-Bu)₂-2,2'-bipyridine borylated exclusively at the 6-positions.

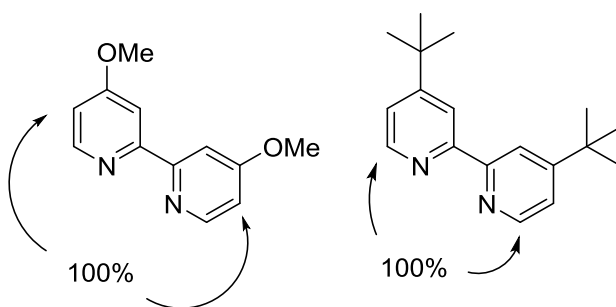


Figure 1.10: Observed Regioselectivities for bipyridines (Note mixture of mono and diborylated products was obtained).

Marder, Steel and coworkers recently conducted a thorough investigation on the borylation of substituted quinolines.¹² Substitution at the 2-position effectively inhibits borylation at the 3-position and favors borylation at both the 4-position and either the 6-, or 7-, positions depending on electronic factors (Figure 1.11). No monoborylated species were observed.

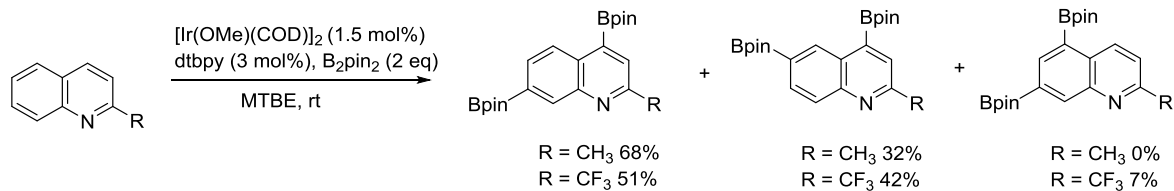


Figure 1.11: Regioselectivities for iridium-catalyzed diborylation of 2-substituted quinolines.

Quinolines disubstituted at the 4-, and 7-positions exhibit particularly interesting reactivity where borylation at the more sterically hindered 3-position is favored over the more accessible 2-position (Figure 1.12). Borylation of 2,7-disubstituted quinolines results in exclusive reactivity at the 4-position except when the substituent at the 2-position is a cyano group. These results show that reactivity at the sterically hindered *peri*-position is favored over reactivity *ortho* to a substituent unless the substituent is small.

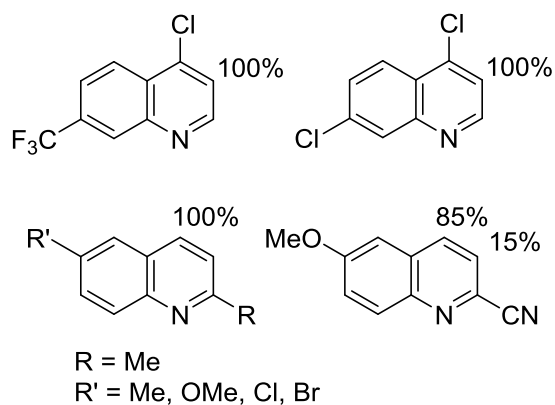
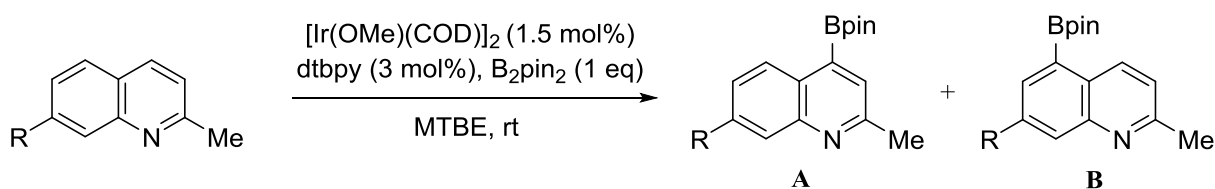


Figure 1.12: Regioselectivities for iridium-catalyzed diborylation of 4,7- and 2,6-disubstituted quinolines.

Borylations of 2,7-disubstituted quinolines occur at either the 4-, or 5-positions, though the 4-position is generally preferred.¹² Electron withdrawing substituents at the 7-position can help favor reactivity at the 5-position, but the product from borylation at the 4-position is always the major isomer (Table 1.4).

Table 1.4: Iridium-catalyzed borylation of 2,7-disubstituted quinolines.



R	Conversion	Ratio A:B ^a
Me	93	>95:<5
OMe	89	>95:<5
CN	92	>95:<5
Br	90	80:20
Cl	93	73:27
CF ₃	94	70:30

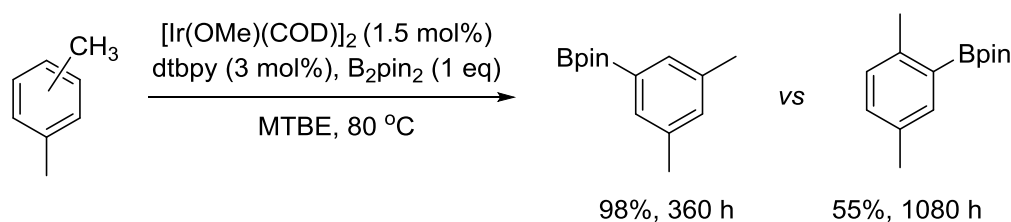
(a) Product ratios determined by GC-MS

REACTIVITY AND SUBSTITUENT EFFECTS:

While substituents clearly have a profound effect on the regioselectivity of borylation reactions, they also exert a strong influence on the reactivity of substrates via steric and electronic influences.

Steric effects on reactivity are pronounced in several cases of regioisomers which have similar electronic attributes but differ in steric attributes (Scheme 1.14). For example, borylation of 1,3-dimethyl benzene occurs in 98% yield after 360 h whereas borylation of 1,4-dimethylbenzene occurs in only 55% yield after 1080 h.⁴⁷ For comparison, Hartwig and coworkers reported borylation of benzene and toluene occurs in 96% yield after 16 h, and 82% yield after 16 h, respectively, under similar conditions.³⁵

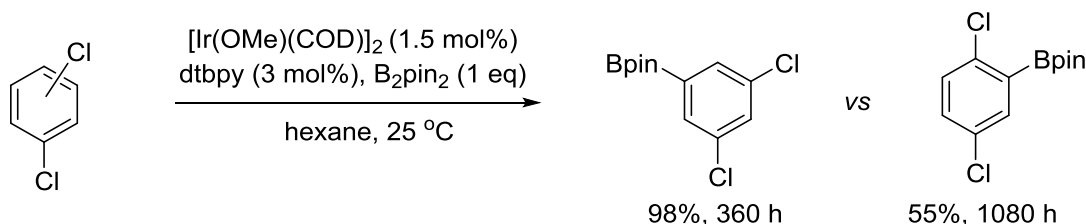
Scheme 1.14: Steric effect of methyl substituents on reactivity in 1,3-dimethylbenzene and 1,4-dimethylbenzene



Similarly, 1,3-dichlorobenzene borylates in 73% yield after 8 h whereas 1,4-dichlorobenzene borylates in only 22% yield after 24 h (Scheme 1.15).⁴⁶ Perhaps not

surprisingly, these results show that in cases where borylation must occur *ortho* to a substituent, reactivity is greatly reduced.

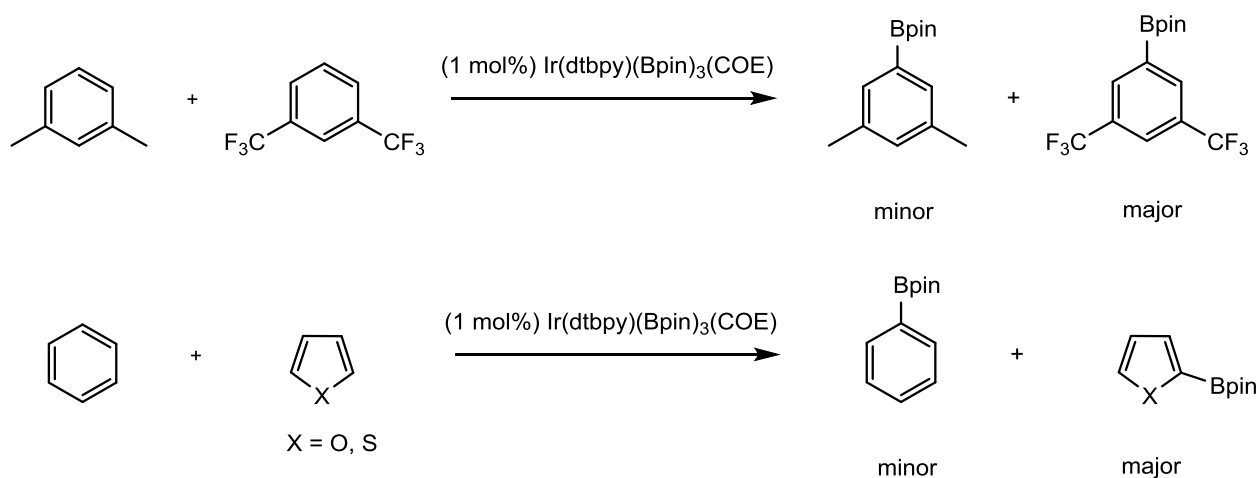
Scheme 1.15: Steric effect of chloro substituents on reactivity in 1,3-dichlorobenzene and 1,4-dichlorobenzene



A series of competition experiments with various arenes and heteroarenes performed by Hartwig, Ishiyama, Miyaura and coworkers highlight the importance of electronic effects on reactivity.⁵⁸ Starting from the catalyst precursor $\text{Ir}(\text{dtbpy})(\text{Bpin})_3(\text{COE})$, stoichiometric reaction of a 1:1 mixture of *m*-xylene and 1,3-bis(trifluoromethyl)benzene resulted in a >65% conversion of 1,3-bis(trifluoromethyl)benzene and <6% conversion of *m*-xylene (Scheme 1.16). A catalytic reaction utilizing 1 mol% of $\text{Ir}(\text{dtbpy})(\text{Bpin})_3(\text{COE})$ with a 1:1 mixture of *m*-xylene and 1,3-bis(trifluoromethyl)benzene yielded similar results. In contrast, analogous reactions between benzene vs. furan and benzene vs. thiophene resulted in borylation of the more electron-rich heterocycles as the major products. Based on these results, the authors suggest that reactivity is controlled by either the electronic properties of the sigma C–H bond or the stability of an 18-electron π complex that forms prior to C–H activation. The authors propose that the reactivity difference between thiophene and benzene is unlikely to be dominated by the electronic

properties of the σ C–H bond since sulfur and carbon have similar electronegativities. On this basis, the authors propose that the stability of the π complex is the factor controlling reactivity in competition experiments. To support their conclusion, the authors note that 1,3-bis(trifluoromethyl)benzene forms more stable π complexes than benzene⁵⁹ and that η^2 -complexes of heteroarenes are more stable than η^2 -complexes of arenes.⁶⁰

Scheme 1.16: Competition experiments between electron rich and electron poor arenes and between benzene and electron rich 5-membered heterocycles



Unsubstituted pyridines are substantially less reactive than benzene. While borylation of benzene occurs at room temperature, borylation of pyridine requires reaction temperatures in excess of 80 °C and yields are low. Low reactivity is not an inherent property of pyridines, however, since 2-substituted pyridines react faster than benzene.¹² Two proposals have been put forth to explain this reactivity: (1) pyridine acts as a ligand binding to iridium to form an 18 electron trisboryl complex leaving the *meta* and *para* positions of pyridine available for reaction

while the *ortho* position is disfavored due to steric congestion. (2) The pyridine forms a Lewis acid-base adduct with boron species in solution, disfavoring *ortho*-borylation due to steric effects.^{13,18} When pyridine is substituted at the 2-position the nitrogen atom is unable to form a Lewis adduct with either boron or iridium due to steric influences of the substituent.⁵⁶ Similar effects are observed for quinoline when quinoline is substituted at the 2-position.¹²

MECHANISM:

Over the past decade, much progress has been made towards understanding the mechanism of iridium-catalyzed borylation. For example, while it is now widely accepted that the active intermediate in these reactions is an iridium(III) trisboryl species, the nature of the C–H activation transition structure is still debated. Additionally, the regioselectivity for the borylation of pyridines cannot be fully explained by current models. A critical review of theoretical and experimental studies which have brought us to our current understanding about the mechanism of iridium-catalyzed borylation is presented in this section.

One of the original questions in the mechanism of iridium catalyzed borylation reactions was whether the active intermediate was an iridium(I) monoboryl or iridium(III) trisboryl species. As discussed previously, Smith and coworkers favored a catalytic borylation cycle involving Ir(III) and Ir(V) species over a pathway involving Ir(I) and Ir(III) (Scheme 1.8).³⁴

As mentioned previously, Ishiyama, Miyaura and Hartwig isolated a potential Ir(III) intermediate in the borylation of arenes with the $[\text{IrCl}(\text{COD})]_2/\text{dtbpy}$ catalyst system.³⁵ The Ir(III) species $\text{Ir}(\text{bpy})(\text{Bpin})_3(\text{COE})$ was isolated in 15% yield from $[\text{IrCl}(\text{COE})_2]_2$, 2 equiv of

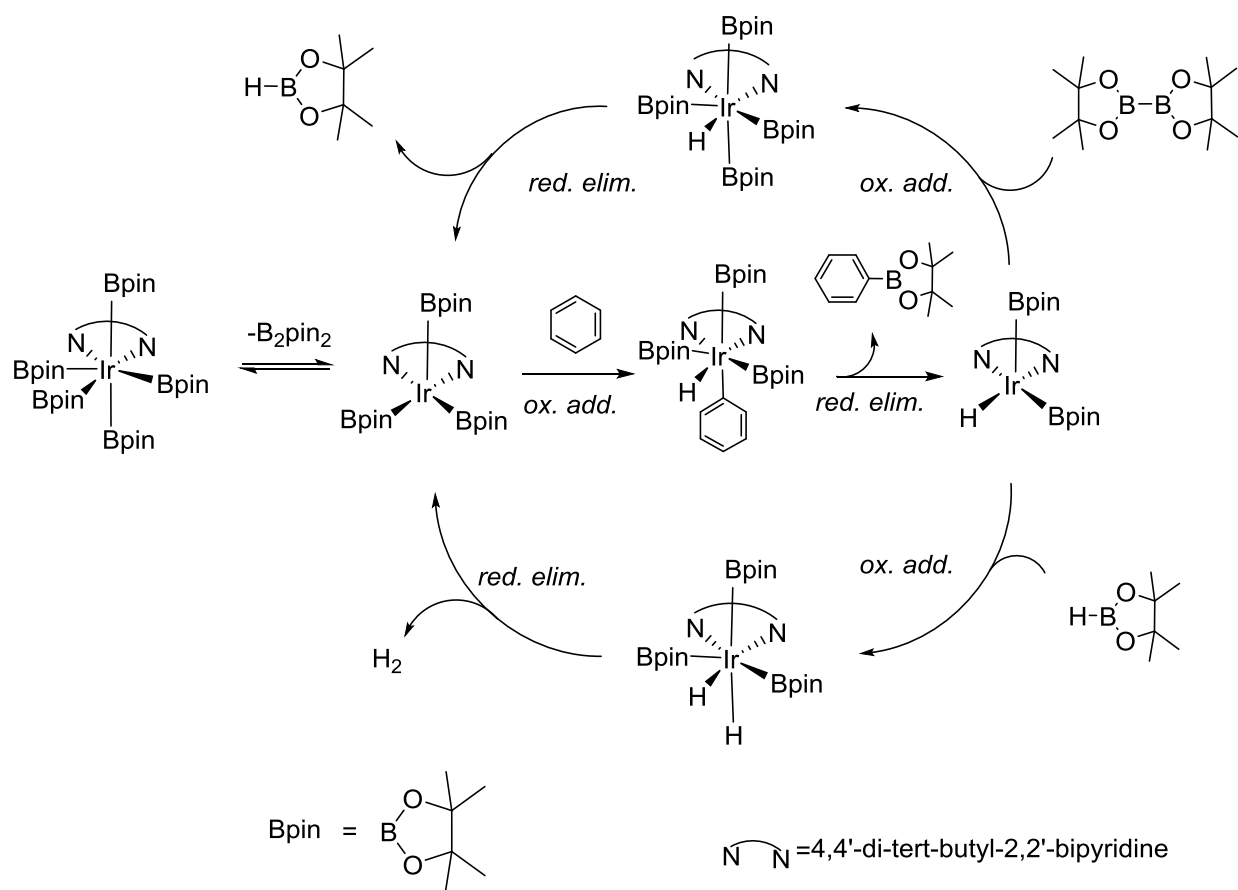
dtbpy and 10 equiv of B₂pin₂ in mesitylene solvent. When the isolated complex was dissolved in deuterated benzene, phenylboronic ester was formed in 80% yield. Kinetic isotope effect studies on this complex revealed a large KIE of 3.6 ± 0.2 which is essentially identical to the KIE of 3.8 ± 0.4 found for catalytic reactions in the same solvent mixture. From these results, the authors postulated that an iridium(III) trisboryl species was involved in the catalytic process.

Sakaki and coworkers published a theoretical study on the mechanism the iridium-catalyzed borylation of benzene.⁶¹ Using bpy and Beg (Beg = bis(ethyleneglycolato)diboron) as model ligands to simplify calculations, the authors found that the iridium(III) trisboryl complex was more likely to be the active intermediate than an iridium(I) monoboryl species for two reasons: (1) the Ir(I) complex is unstable in the presence of B₂(eg)₂, easily reacting to give the Ir(III) complex. In contrast, the iridium(III)trisboryl species, Ir(bpy)(Bpin)₃(COE) was experimentally isolated from a reaction with excess B₂pin₂;³⁵ and (2) reductive elimination of H₂ from Ir(III) is calculated to be highly endothermic (43.6 kcal/mol) whereas the Ir(V) species is sufficiently reactive to extrude H₂. In addition to these results, the authors also found C–H activation of the substrate to occur via an oxidative addition mechanism.

Based on their computational results, Sakaki and coworkers proposed a catalytic mechanism for the borylation of benzene (Scheme 1.17).⁶¹ Reductive elimination of HBpin from a hepta-coordinate Ir(V)tetraboryl hydride complex gives the active Ir(dtbpy)(Bpin)₃ complex. Reaction with benzene proceeds through a rate-limiting C–H activation step to give the hepta-coordinate aryl intermediate Ir(dtbpy)(Ph)(H)(Bpin)₃. Reductive elimination yields phenylpinacolboronate ester PhBpin and a five-coordinate Ir(III) hydride complex Ir(dtbpy)(H)(Bpin)₂. Oxidative addition of the iridium hydride complex with either (Bpin)₂ or

HBpin followed by reductive elimination regenerates the active catalyst and yields either HBpin or H₂, respectively.

Scheme 1.17: Proposed catalytic cycle for the catalytic borylation of benzene by Ir(dtpby)(Bpin)₃



Further data supporting an Ir(III) reactive intermediate over Ir(I) was published in a mechanistic study by Hartwig and coworkers in 2005.⁵⁸ The authors made several qualitative observations about the trisboryl intermediate. First, they noted that the trisboryl complex could

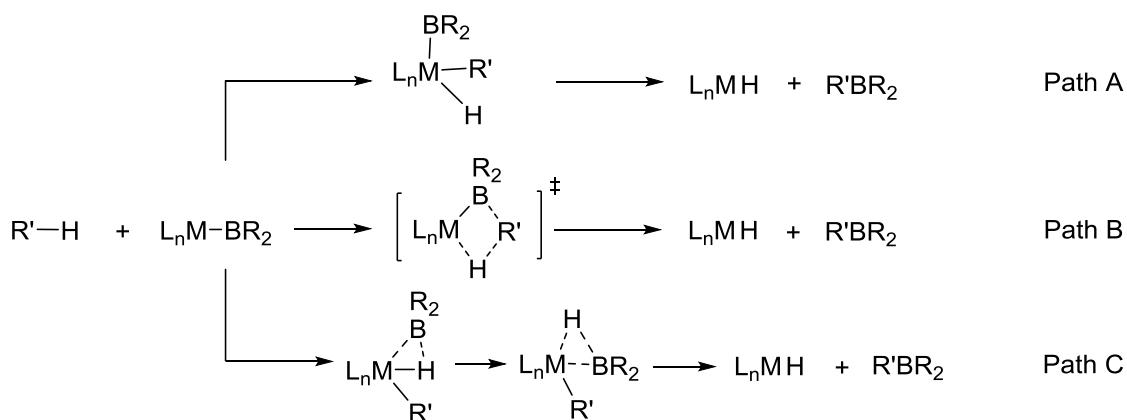
be isolated from the catalytic reaction mixture. Second, the authors noted that an induction period was required when they started from the precursor $[\text{Ir}(\text{OMe})(\text{COD})]_2/\text{dtbpy}$, whereas reactions starting from the trisboryl complex required no induction period. Third, they observed that the KIE for the catalytic reaction mixture was similar to the KIE for the isolated intermediate and that they both yielded the same products with similar regioselectivities. Additionally, kinetic studies showed that the complex $\text{Ir}(\text{bpy})(\text{Bpin})_3(\text{COE})$ rapidly and reversibly dissociates COE to form a 16-electron complex that lies on the proposed catalytic cycle. Again, these authors found that the C–H activation step was rate-limiting. These results firmly support the existence of an active iridium(III) intermediate in the catalytic cycle.

While the existence of an Ir(III) species in the catalytic pathway has been firmly established by experimental and computational studies, the mechanism of the rate-limiting C–H activation step is still debated. Two mechanisms for iridium-catalyzed borylation are favored, namely, oxidative addition involving an Ir(III)/Ir(V) cycle and sigma bond metathesis via an Ir(III) active intermediate. An electrophilic mechanism involving C–H activation on an empty p-orbital of a boryl ligand or on the iridium center is ruled out by the experimental observation that electron deficient arenes react more quickly than electron rich arenes.⁵⁸

Three pathways for C–H activation in iridium catalyzed borylation are shown in Scheme 1.18. Computational studies by Sakaki et al. support an oxidative addition type mechanism (Path A).⁶¹ In contrast, a computational study by Hartwig et al. on rhodium, tungsten and iron boryl complexes implies that C–H activation occurs via sigma bond metathesis.⁶² There are two pathways by which a sigma bond metathesis could occur: Path B formation of a C–B bond in a single step or Path C formation of a σ -borane complex prior to formation of the C–B bond.

Previous computational studies suggest that a sigma bond metathesis forming the C-B bond in the first step (Path B) is energetically disfavored.^{62,63}

Scheme 1.18: Possible C–H activation mechanisms for the iridium catalyzed borylation of arenes: Oxidative addition (Path A), sigma bond metathesis with the formation of the C-B bond in a single step (Path B), and sigma bond metathesis with formation of a borane σ complex prior to the formation of the C-B bond (Path C)



Studies by Smith, Singleton and Maleczka and coworkers demonstrated a strong correlation between the activation energy and the energy of the aryl intermediate formed as a result of C–H cleavage.¹¹ The authors reported that the transition structure is late and should be product-like according to the Hammond-Leffler postulate.^{64,65} Natural population analysis of arene charge in the intermediate demonstrated that there was a correlation between the energy of the intermediate and the buildup of negative charge on the arene ligand. By first order correlation

to the transition structures, the authors postulated that facilitating the transfer of charge to the arene is the key electronic factor that governs C–H activation.

Based on these results and the result that the more acidic, and hence less nucleophilic, bis(catecholato)boryl ligands resulted in slower reactivity, the authors proposed that proton transfer character contributes to the transition structure (Figure 1.13). Additionally, the authors noted a correlation between pK_a of the substrate and regioselectivity, where the more acidic C–H bonds tend to be the most reactive towards borylation. This study does not preclude or rule out an oxidative addition mechanism since the same factors that increase the negative charge on the arene will also increase the electron density on the metal center prior to activation, which is well known to facilitate oxidative addition.⁶⁶ Indeed, the authors point out that the intermediate product of C–H activation contains an Ir(V) center, thus ruling out a formal concerted metalation-deprotonation mechanism.

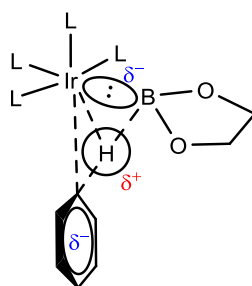


Figure 1.13: Proton-transfer description for transition state in iridium C–H borylation.

A related study by Smith, Singleton and coworkers showed that the correlation between arene charge and intermediate energy for pyrroles was primarily due to hydrogen bonding

interactions in the transition structure (Figure 1.14). In particular, the pyrrole N-hydrogen interacts with the oxygen atom of one of the equatorial boryl ligands in both the transition structure and the aryl intermediate. This hydrogen bonding interaction stabilizes the transition structure for borylation at the 2-position of pyrrole by as much as 2.3 kcal/mol. The authors successfully used this effect to prepare a number of *ortho*-borylated products of N-(*boc*)-protected anilines through an outer-sphere mechanism facilitated by hydrogen bonding of the substrate to a boryl ligand.⁵¹

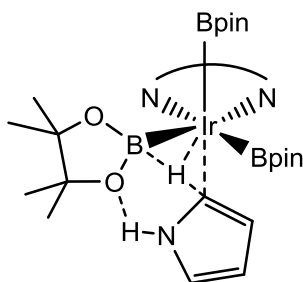


Figure 1.14: Proposed transition structure for borylation of pyrrole exhibiting hydrogen bonding between the substrate N–H hydrogen and the oxygen atom of an equatorial boryl ligand.

Further research by Marder, Steel and coworkers highlighted the correlation of pK_a to regioselectivity in the borylation of substituted quinolines, pyridine and substituted arenes.¹² While regioselectivity is dominated by steric effects, the authors noted that enhanced electronic selectivity could be observed when reactions were performed at room temperature. The authors found that the site of borylation could be estimated by analysis of the ^1H NMR spectrum of the substrate where preferential borylation occurred at the most deshielded hydrogen or carbon atom

as long as it was sterically accessible. The authors compared their experimental results to pK_a values determined by DFT and found good correlation with observed selectivity. Small differences in selectivity, however, led them to suggest that M–C bond strength may be a better quantitative predictor of selectivity.

Several computational studies support the use of M–C bond strength as a predictor of selectivity. Eisenstein and Perutz et al. reported good correlation between regioselectivity and Pd–C bond strengths of the aryl palladium intermediates or C–H activation transition structures in palladium-catalyzed C–H activations.^{67,68} The authors found that correlation between Pd–C bond dissociation energy (BDE) of the reaction intermediates and the activation energy in the direct arylation of fluorinated benzenes was better than the correlation between pK_a and activation energy.⁶⁸ Recently, in a related study on palladium-catalyzed C(sp^2)–H activation, Ess *et al.* found a linear correlation between the C–H bond activation energy and the transition state Pd–C bond energy.⁶⁹ Taken together, these results illustrate that the stability of the forming Pd–aryl bonds determines regioselectivity for a variety of arene and heteroarene substrates. Thus, extending this model to the C–H bond activation step in iridium-catalyzed borylation reactions may provide useful insights into the origins of observed regioselectivities.

CONCLUSION:

Iridium-catalyzed borylation of arenes and heterocycles has been the subject of much attention. Numerous studies have highlighted the importance of steric effects on the regioselectivity of borylation such that there is a simple rule for borylation: reaction does not occur *ortho* to a substituent when a C–H bond lacking an *ortho* substituent is available. This rule

is valid in most cases though there are important exceptions such as benzodioxole which borylates preferentially at the *ortho* position, highlighting the effect of electronic factors when steric factors are small.

Steric factors also have a large effect on the reactivity of the substrate especially when borylation is required to occur *ortho* to a substituent. Electronic factors also have an effect on reactivity, wherein more electron poor arenes react faster than electron rich arenes. In a somewhat contradictory result, electron rich heterocycles borylate considerably faster than benzene in competition experiments. These results have been proposed to the consequence of formation of more stable η^2 π -complexes in the case of electron deficient arenes and 5-membered heterocycles, though, strikingly, pyridines react with exclusive selectivity disfavoring borylation at the C–H bond alpha to the heteroatom. In addition, pyridines that do not bear substituents at positions alpha to the heteroatom are considerably less reactive than other substrates suggesting the possibility that pyridine forms a Lewis adduct with either an iridium complex or boron species in solution.

More than ten years after the initial discovery of iridium-catalyzed borylation of arenes and heterocycles, questions still remain regarding the origins of observed regioselectivities. It has been firmly established that the active species is an iridium(III) trisboryl complex. Based upon the regioselectivity and reactivity observed with a variety of substrates, two mechanisms are currently favored for catalytic borylation. Computational studies by Sakaki et al. as well as experimental results that showing the greater reactivity of electron poor arenes support a traditional Ir(III)/Ir(V) oxidative addition mechanism while theoretical and experimental work performed by the groups of Smith, Maleczka, Singleton, Marder and Steel support an oxidative

addition mechanism with significant proton-transfer character. Neither mechanism has been definitively established. Future work will need to focus on elucidating the nature of the rate-limiting—and regioselectivity-determining—step in order to provide an encompassing model for all substrates.

REFERENCES:

- (1) Pelter, A.; Smith, K.; Brown, H. C. *Borane Reagents*; Academic Press: Ann Arbor, 1988.
- (2) Brown, H. C. *Organic Syntheses via Boranes*; Wiley: New York, 1975.
- (3) Miyaura, N.; Suzuki, A. *Chem. Rev.* **1995**, *95*, 2457.
- (4) Chan, D. G.; Winternheimer, D. J.; Merlic, C. A. *Org. Lett.* **2011**, *13*, 2778.
- (5) Winternheimer, D. J.; Merlic, C. A. *Org. Lett.* **2010**, *12*, 2508.
- (6) Shade, R. E.; Hyde, A. M.; Olsen, J.-C.; Merlic, C. A. *J. Am. Chem. Soc.* **2010**, *132*, 1202.
- (7) Sanjeeva Rao, K.; Wu, T.-S. *Tetrahedron* **2012**, *68*, 7735.
- (8) Qiao, J. F.; Patrick, Y. S. *Synthesis* **2011**, *2011*, 829.
- (9) Bunescu, A.; Qian, W.; Zhu, J. *Synthesis* **2012**, *44*, 3811.
- (10) Gillis, E. P.; Burke, M. D. *Adrichim. Acta* **2009**, *42*, 17.
- (11) Vanchura, I. I. B. A.; Preshlock, S. M.; Roosen, P. C.; Kallepalli, V. A.; Staples, R. J.; Maleczka, J. R. E.; Singleton, D. A.; Smith, I. I. I. M. R. *Chem. Commun.* **2010**, *46*, 7724.
- (12) Tajuddin, H.; Harrisson, P.; Bitterlich, B.; Collings, J. C.; Sim, N.; Batsanov, A. S.; Cheung, M. S.; Kawamorita, S.; Maxwell, A. C.; Shukla, L.; Morris, J.; Lin, Z.; Marder, T. B.; Steel, P. G. *Chem. Sci.* **2012**.

- (13) Takagi, J.; Sato, K.; Hartwig, J. F.; Ishiyama, T.; Miyaura, N. *Tetrahedron Lett.* **2002**, *43*, 5649.
- (14) Ishiyama, T.; Miyaura, N. *Pure Appl. Chem.* **2006**, *78*, 1369.
- (15) Mkhaliid, I. A. I.; Barnard, J. H.; Marder, T. B.; Murphy, J. M.; Hartwig, J. F. *Chem. Rev.* **2010**, *110*, 890.
- (16) Hartwig, J. F. *Chem. Soc. Rev.* **2011**, *40*, 1992.
- (17) Hartwig, J. F. *Acc. Chem. Res.* **2012**, *45*, 864.
- (18) Ishiyama, T.; Miyaura, N. *J. Organomet. Chem.* **2003**, *680*, 3.
- (19) Chemler, S. R.; Trauner, D.; Danishefsky, S. J. *Angew. Chem. Int. Ed.* **2001**, *40*, 4544.
- (20) Imao, D.; Glasspoole, B. W.; Laberge, V. r. S.; Crudden, C. M. *J. Am. Chem. Soc.* **2009**, *131*, 5024.
- (21) Ohmura, T.; Awano, T.; Suginome, M. *J. Am. Chem. Soc.* **2010**, *132*, 13191.
- (22) Sandrock, D. L.; Jean-Gérard, L.; Chen, C.-y.; Dreher, S. D.; Molander, G. A. *J. Am. Chem. Soc.* **2010**, *132*, 17108.
- (23) Lee, J. C. H.; McDonald, R.; Hall, D. G. *Nature Chem.* **2011**, *3*, 894.
- (24) Suzuki, A. *Angew. Chem. Int. Ed.* **2011**, *50*, 6722.
- (25) Nguyen, P.; Blom, H. P.; Westcott, S. A.; Taylor, N. J.; Marder, T. B. *J. Am. Chem. Soc.* **1993**, *115*, 9329.
- (26) Waltz, K. M.; He, X.; Muhoro, C.; Hartwig, J. F. *J. Am. Chem. Soc.* **1995**, *117*, 11357.
- (27) Waltz, K. M.; Hartwig, J. F. *Science* **1997**, *277*, 211.
- (28) Iverson, C. N.; Smith, M. R. *J. Am. Chem. Soc.* **1999**, *121*, 7696.
- (29) Chen, H.; Hartwig, J. F. *Angew. Chem. Int. Ed.* **1999**, *38*, 3391.

- (30) Ball, R. G.; Campen, A. K.; Graham, W. A. G.; Hamley, P. A.; Kazarian, S. G.; Ollino, M. A.; Poliakoff, M.; Rest, A. J.; Sturgeoff, L.; Whitwell, I. *Inorg. Chim. Acta* **1997**, *259*, 137.
- (31) Chen, H.; Schlecht, S.; Semple, T. C.; Hartwig, J. F. *Science* **2000**, *287*, 1995.
- (32) Cho, J.-Y.; Iverson, C. N.; Smith, M. R. *J. Am. Chem. Soc.* **2000**, *122*, 12868.
- (33) Shimada, S.; Batsanov, A. S.; Howard, J. A. K.; Marder, T. B. *Angew. Chem. Int. Ed.* **2001**, *40*, 2168.
- (34) Cho, J.-Y.; Tse, M. K.; Holmes, D.; Maleczka, R. E.; Smith, M. R. *Science* **2002**, *295*, 305.
- (35) Ishiyama, T.; Takagi, J.; Ishida, K.; Miyaura, N.; Anastasi, N. R.; Hartwig, J. F. *J. Am. Chem. Soc.* **2002**, *124*, 390.
- (36) Ishiyama, T.; Takagi, J.; Hartwig, J. F.; Miyaura, N. *Angew. Chem. Int. Ed.* **2002**, *41*, 3056.
- (37) Olsson, V. J.; Szabó, K. J. *Angew. Chem. Int. Ed.* **2007**, *46*, 6891.
- (38) Brown, J. M.; Lloyd-Jones, G. C. *J. Am. Chem. Soc.* **1994**, *116*, 866.
- (39) Coapes, R. B.; Souza, F. E. S.; Thomas, R. L.; Hall, J. J.; Marder, T. B. *Chem. Commun.* **2003**, 614.
- (40) Mkhaliid, I. A. I.; Coapes, R. B.; Edes, S. N.; Coventry, D. N.; Souza, F. E. S.; Thomas, R. L.; Hall, J. J.; Bi, S.-W.; Lin, Z.; Marder, T. B. *Dalton Trans.* **2008**, 1055.
- (41) Olsson, V. J.; Szabó, K. I. n. *J. Org. Lett.* **2008**, *10*, 3129.
- (42) Kikuchi, T.; Takagi, J.; Isou, H.; Ishiyama, T.; Miyaura, N. *Chem. Asian J.* **2008**, *3*, 2082.
- (43) Kikuchi, T.; Takagi, J.; Ishiyama, T.; Miyaura, N. *Chem. Lett.* **2008**, *37*, 664.
- (44) Sasaki, I.; Doi, H.; Hashimoto, T.; Kikuchi, T.; Ito, H.; Ishiyama, T. *Chem. Commun.* **2013**, *49*, 7546.
- (45) Itoh, H.; Kikuchi, T.; Ishiyama, T.; Miyaura, N. *Chem. Lett.* **2011**, *40*, 1007.
- (46) Ishiyama, T.; Nobuta, Y.; Hartwig, J. F.; Miyaura, N. *Chem. Commun.* **2003**, 2924.

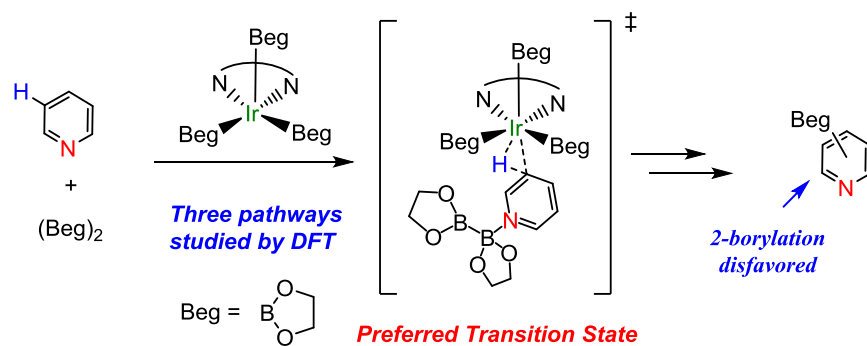
- (47) Harrisson, P.; Morris, J.; Marder, T. B.; Steel, P. G. *Org. Lett.* **2009**, *11*, 3586.
- (48) Chotana, G. A.; Rak, M. A.; Smith, M. R. *J. Am. Chem. Soc.* **2005**, *127*, 10539.
- (49) Boebel, T. A.; Hartwig, J. F. *J. Am. Chem. Soc.* **2008**, *130*, 7534.
- (50) Robbins, D. W.; Boebel, T. A.; Hartwig, J. F. *J. Am. Chem. Soc.* **2010**, *132*, 4068.
- (51) Roosen, P. C.; Kallepalli, V. A.; Chattopadhyay, B.; Singleton, D. A.; Maleczka, R. E.; Smith, M. R. *J. Am. Chem. Soc.* **2012**, *134*, 11350.
- (52) Ishiyama, T.; Takagi, J.; Yonekawa, Y.; Hartwig, J. F.; Miyaura, N. *Adv. Synth. & Catal.* **2003**, *345*, 1103.
- (53) Chotana, G. A.; Kallepalli, V. A.; Maleczka Jr, R. E.; Smith Iii, M. R. *Tetrahedron* **2008**, *64*, 6103.
- (54) Paul, S.; Chotana, G. A.; Holmes, D.; Reichle, R. C.; Maleczka, R. E.; Smith, M. R. *J. Am. Chem. Soc.* **2006**, *128*, 15552.
- (55) Lo, W. F.; Kaiser, H. M.; Spannenberg, A.; Beller, M.; Tse, M. K. *Tetrahedron Lett.* **2007**, *48*, 371.
- (56) Mkhaliid, I. A. I.; Coventry, D. N.; Albesa-Jove, D.; Batsanov, A. S.; Howard, J. A. K.; Perutz, R. N.; Marder, T. B. *Angew. Chem. Int. Ed.* **2006**, *45*, 489.
- (57) Murphy, J. M.; Liao, X.; Hartwig, J. F. *J. Am. Chem. Soc.* **2007**, *129*, 15434.
- (58) Boller, T. M.; Murphy, J. M.; Hapke, M.; Ishiyama, T.; Miyaura, N.; Hartwig, J. F. *J. Am. Chem. Soc.* **2005**, *127*, 14263.
- (59) Chin, R. M.; Dong, L.; Duckett, S. B.; Partridge, M. G.; Jones, W. D.; Perutz, R. N. *J. Am. Chem. Soc.* **1993**, *115*, 7685.
- (60) Rauchfuss, T. B. In *Progress in Inorganic Chemistry*; John Wiley & Sons, Inc.: 2007, p 259.

- (61) Tamura, H.; Yamazaki, H.; Sato, H.; Sakaki, S. *J. Am. Chem. Soc.* **2003**, *125*, 16114.
- (62) Webster, C. E.; Fan, Y.; Hall, M. B.; Kunz, D.; Hartwig, J. F. *J. Am. Chem. Soc.* **2003**, *125*, 858.
- (63) Lam, W. H.; Lin, Z. *Organometallics* **2003**, *22*, 473.
- (64) Hammond, G. S. *J. Am. Chem. Soc.* **1955**, *77*, 334.
- (65) Leffler, J. E. *Science* **1953**, *117*, 340.
- (66) Hartwig, J. F. *Organotransition Metal Chemistry: From Bonding to Catalysis*; Univ. Science Books: Sausalito, 2010.
- (67) Clot, E.; Mégret, C.; Eisenstein, O.; Perutz, R. N. *J. Am. Chem. Soc.* **2006**, *128*, 8350.
- (68) Guihaume, J.; Clot, E.; Eisenstein, O.; Perutz, R. N. *Dalton Trans.* **2010**, *39*, 10510.
- (69) Petit, A.; Flygare, J.; Miller, A. T.; Winkel, G.; Ess, D. H. *Org. Lett.* **2012**, *14*, 3680.

Chapter 2: Mechanism and Regioselectivity of the Iridium-Catalyzed Borylation of Pyridine Elucidated with Density Functional Theory

ABSTRACT:

The origins of the regioselectivity observed in the iridium-catalyzed borylation of pyridine have been studied using density functional theory with the B3LYP and M06 functionals. Three pathways for the functionalization of pyridine were examined: direct borylation of pyridine (Pathway A), borylation of a Lewis acid-base adduct with pyridine bound to a diboron species (Pathway B), and borylation of a Lewis acid-base adduct with pyridine bound to a second equivalent of the iridium catalyst (Pathway C). Pathway B is found to be energetically preferred and gives good agreement with the reported experimental selectivities for pyridine borylation. Computations predict that the Lewis acid-base substrate pyridine trifluoroborane will be activated towards C–H borylation at the 3- and 4-positions and highly deactivated at the 2-position.

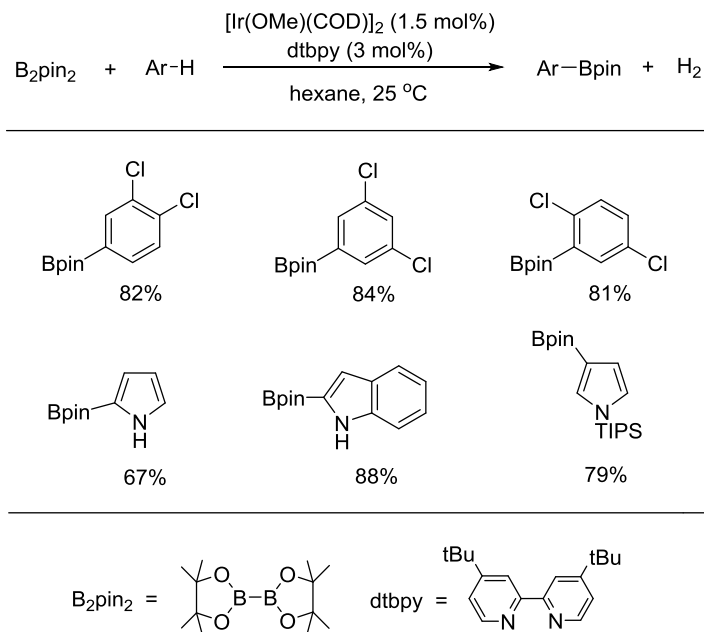


INTRODUCTION:

Arylboron reagents have numerous applications as essential building blocks in modern synthetic organic chemistry.¹⁻⁵ The iridium-catalyzed direct borylation of sp^2 C–H bonds is a particularly powerful method for accessing a wide range of arylboron compounds from simple arenes.^{3,6-8} The regioselectivity of these C–H borylation reactions is often exquisite, and is predominantly controlled by steric effects. With rare exceptions,⁹⁻¹¹ Ir-catalyzed C–H borylation occurs preferentially at sites that do not bear an *ortho* substituent, and functionalization of *ortho*-substituted C–H bonds occurs only in the absence of less-hindered sites. For example, in the Ir-catalyzed C–H borylation of 1,2- and 1,3-dichlorobenzene with bis(pinacolato)diboron (B_2pin_2), no functionalization of the sites *ortho* to the chlorine substituents is observed (Chart 2.1).¹² This sterically-controlled regioselectivity provides access to products which are often complementary to those of well-developed nucleophilic and electrophilic substitution reactions.¹³

For less hindered substrates with diminished steric considerations, electronic effects become increasingly important to regioselectivity. For example, unsubstituted 5-membered heteroarenes undergo borylation exclusively at the position alpha to the heteroatom,^{12,14-16} as seen in the 2-borylation of pyrrole.¹⁶ However, a bulky substituent on the nitrogen can alter this regioselectivity; for instance, borylation occurs preferentially at the 3-position of 1-(triisopropylsilyl)pyrrole (Chart 2.1).¹⁶

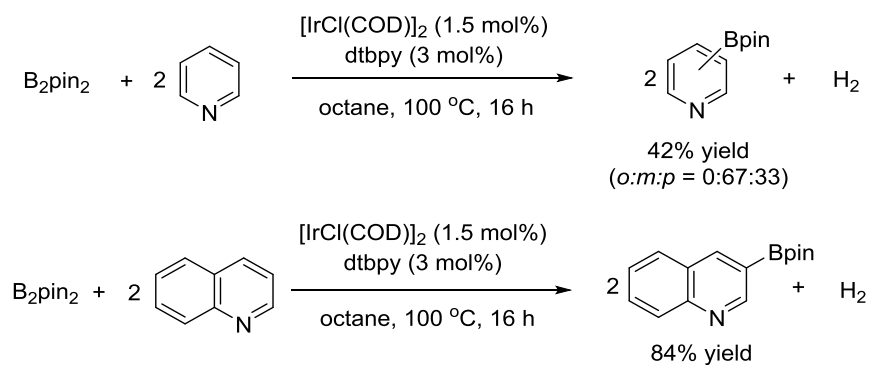
Chart 2.1: Products from the Ir-catalyzed borylation of arene and heteroarene C–H bonds (Bpin = 4,4,5,5-tetramethyl-1,3,2-dioxaborolanyl).^{12,16}



In contrast to reactions with unhindered 5-membered heterocycles, no borylation is observed at the position alpha to the nitrogen of pyridine or quinoline substrates.^{16,17} Borylation of pyridine yields a statistical mixture of 3- and 4-functionalized products (67:33), and no 2-borylation is observed (Scheme 2.1). Quinoline undergoes borylation exclusively at the 3-position. To date, the origin of the observed regioselectivity for Ir-catalyzed borylation of pyridine and derivatives has remained unclear.^{7,8,16,18,19} Hartwig, Ishiyama, and Miyaura suggested that 2-borylation may be inhibited due to the formation of a Lewis acid-base adduct between the pyridine nitrogen and either a boron species or the iridium catalyst in solution.^{16,20}

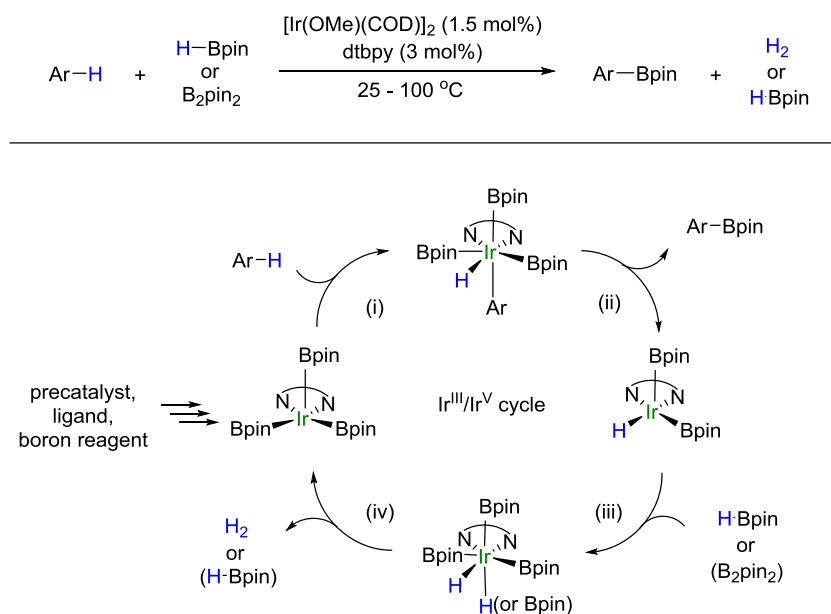
However, such a hypothesis has not been investigated experimentally or computationally until now.

Scheme 2.1: Ir-catalyzed borylation of pyridine and quinoline



Experimental studies by Hartwig and coworkers utilizing $Ir(dtbpy)(Bpin)_3(COE)$ ($COE =$ cyclooctene) as a precatalyst support a mechanism (Scheme 2.2) where $Ir^{III}(dtbpy)(Bpin)_3$ is the active catalyst that mediates C–H cleavage via oxidative addition (step i). Reductive elimination (step ii) yields the arylboronate ester.²¹ In this mechanism, regeneration of the active catalyst can occur with either $HBpin$ or B_2pin_2 (steps iii and iv). While no computational studies on the mechanism of Ir-catalyzed borylation of substituted aromatic compounds or pyridine have been reported, Sakaki et al. reported calculations on the borylation of benzene which support the mechanism shown in Scheme 2.2.²² The calculations were conducted on a simplified system, in which the $dtbpy$ ligand was substituted with bpy ($bpy = 2,2'$ -bipyridine) and $Bpin$ was substituted with (ethyleneglycolato)boron (Beg), and revealed that oxidative addition of $Ir(bpy)(Beg)_3$ (**2.1**) into the Ph–H bond is the rate-limiting step for benzene borylation.

Scheme 2.2: Proposed catalytic cycle for the Ir-catalyzed borylation of benzene²¹

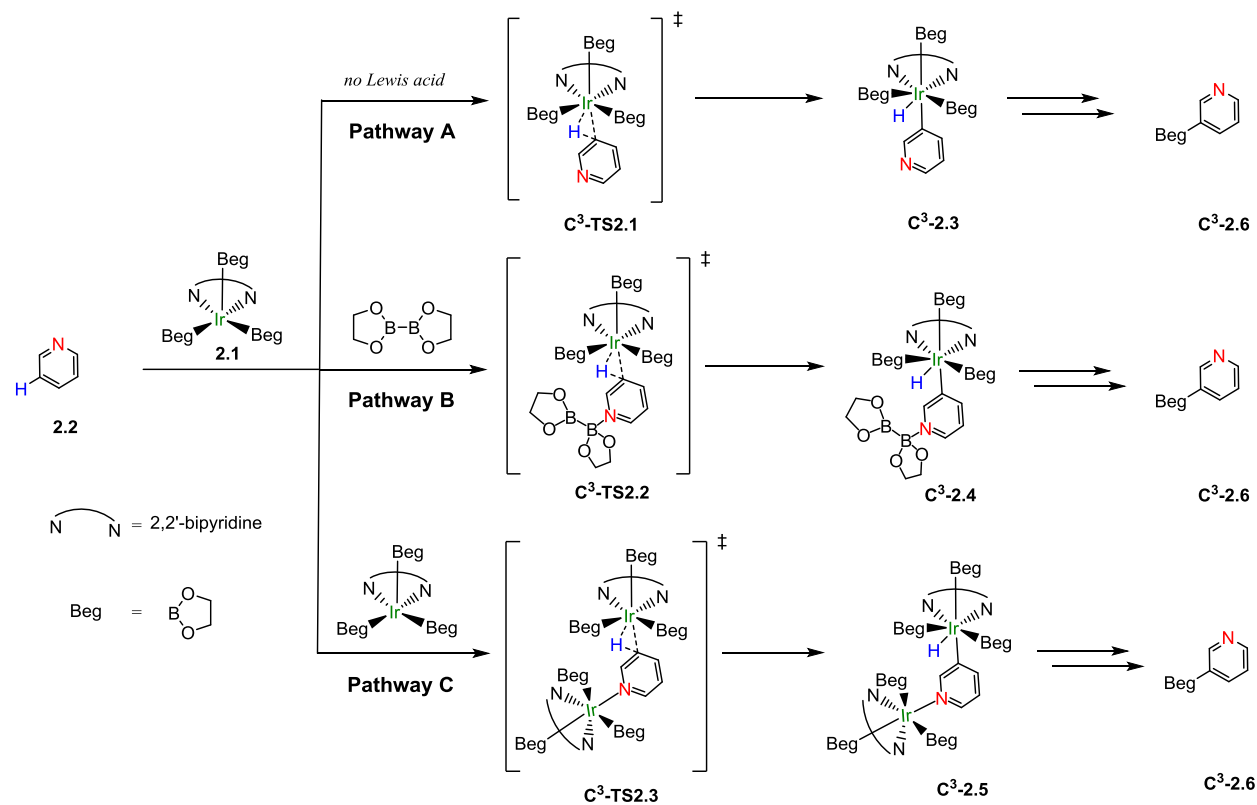


As discussed above, the mechanism of pyridine borylation might deviate from that of benzene borylation due to potential Lewis acid-base interactions involving the pyridine nitrogen. We explored computationally the three most likely pathways for the activation of pyridine: borylation of free pyridine (Scheme 2.3, Pathway A), borylation of pyridine complexed to a diboron species (Pathway B), and borylation of pyridine coordinated to a second equivalent of Ir catalyst (Pathway C).

Each of these three possible pathways is apparently consistent with experimental results. Pathway A involves the direct Ir-catalyzed borylation of pyridine via **TS2.1**. In cases where steric factors are minimal (as expected for Pathway A) and do not control regioselectivity of borylation, it has been observed that the pK_a 's of C-H bonds are inversely correlated to their

reactivity toward functionalization (i.e., more acidic bonds react preferentially).^{9,19} By this analysis, Pathway A would lead to the observed site-selectivity for borylation, as the C–H bonds at the 2-position of pyridine should be the least reactive (least acidic). Notably, however, experimental correlation between C–H bond pK_a and reactivity toward functionalization fails in many cases.¹⁹ In Pathway B, pyridine binds to one equivalent of the diboron reagent to give a Lewis acid-base adduct which is then borylated via **TS2.2**. Precedent for formation of pyridine adducts of diboron moieties is provided by Marder, who showed that 4-picoline forms mono- and bis-adducts with bis(catecholato)diboron.^{23,24} In Pathway C, pyridine binds to one equivalent of Ir(bpy)(Beg)₃ to form the complex Ir(bpy)(Beg)₃(pyr) (pyr = pyridine). The pyridine ligand of this complex is then borylated by a second equivalent of Ir(bpy)(Beg)₃ via **TS2.3**. This mechanistic proposal is consistent with Hartwig's choice of dtbpy (instead of bpy) as a ligand to prevent ligand borylation,⁸ a known side reaction that could presumably occur via an analogous mechanistic pathway involving borylation of the Ir-coordinated bpy ligand with another equivalent of Ir catalyst.

Scheme 2.3: The three reaction pathways studied for pyridine borylation by the model system Ir(bpy)(Beg)₃, illustrated for 3-functionalization



COMPUTATIONAL METHODS:

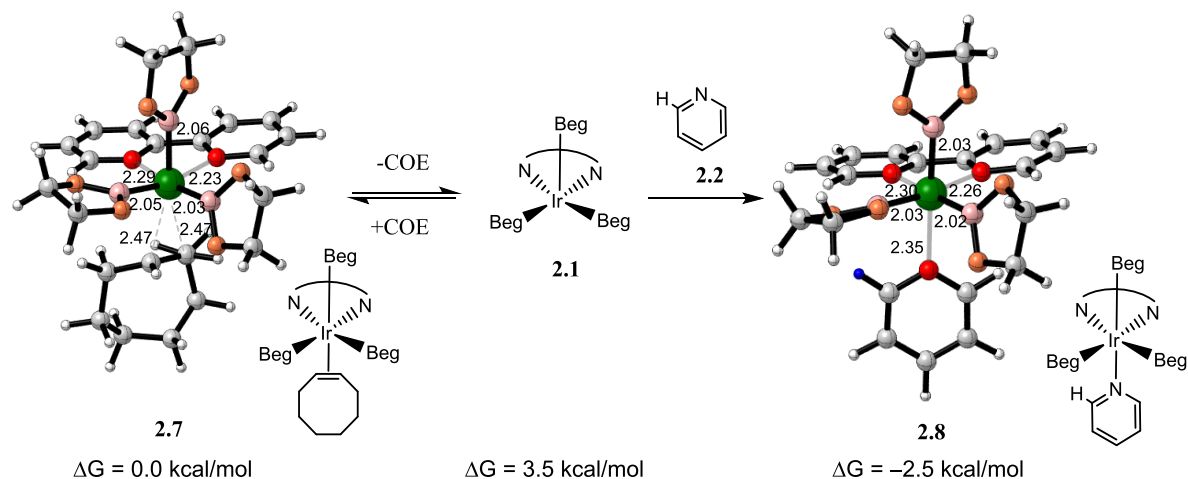
Geometry optimizations for transition states and minima were carried out using the B3LYP functional and a mixed basis set of LANL2DZ for Ir and the double- ζ split-valence 6-31G(d) basis set for all other atoms. Vibrational frequencies confirmed that structures were either minima or transition states. Electronic energies were calculated on the B3LYP geometries using Truhlar's M06 functional with a mixed basis set consisting of SDD for Ir and the triple- ζ split-

valence 6-311G(d,p) basis set for other atoms. Solvation by n-octane was taken into account in the single point calculations using the SMD model. The use of B3LYP for geometry optimization and M06 energy refinement has been demonstrated by numerous studies to produce successfully energy profiles of reactions involving transition-metal systems.²⁵⁻³² All of the calculations were performed with Gaussian 09.³³

RESULTS AND DISCUSSION:

The compounds Ir(bpy)(Beg)₃ **2.1** (Beg = (ethyleneglycolato)boron) and B₂eg₂ were used as models for Ir(dtbp)(Bpin)₃ and B₂pin₂ analogous to previous calculations by Sakaki et al.²² In the absence of pyridine, the π -olefin complex Ir(bpy)(Beg)₃(COE) **2.7** was found to be the stable resting state for catalyst **2.1** (Scheme 2.4). The geometry and Ir–N and Ir–B bond lengths of **2.7** correspond favorably to the similar complex [Ir(dtbp)(Bpin)₃(COE)], for which an X-ray crystal structure was previously obtained.³⁴ We next examined formation of the Lewis acid-base adduct Ir(bpy)(Beg)₃(pyr) **2.8**. Species **2.8** is readily formed by coordination of one equivalent of pyridine **2.2** to iridium complex **2.1** (Scheme 2.4). The calculated stability of this adduct was unsurprising ($\Delta G = -2.5$ kcal/mol relative to **2.7**), as iridium readily forms isolable complexes with pyridine ligands.^{35,36} This result also supports the conclusion of Marder and coworkers, who suggested that the observed lower reactivity of pyridine relative to 2-substituted pyridines toward Ir-catalyzed borylation is due to the formation of a stable Ir–pyridine complex in the absence of pyridine 2-substitution.³⁷

Scheme 2.4: Structures and free energies of 2.7 and 2.8



The free energy profile for 2-, 3-, and 4-borylation of pyridine via Pathway A was calculated starting from iridium-pyridine adduct **2.8** (Figure 2.1). The profile is analogous to that described for the borylation of benzene,²² with a rate-limiting oxidative addition step. The reaction involves formation of a higher energy π -complex **2.9** which undergoes oxidative addition into the C–H bond via transition structure **TS2.1** to yield an Ir–heteroaryl intermediate **2.3**. Complex **2.3** then undergoes facile C–B bond-forming reductive elimination via transition structure **TS2.4** to provide the oxygen-bound adduct **2.10**. Dissociation yields the heteroarylboron product **2.6** and iridium hydride complex **2.11**. Plausible mechanistic details for subsequent steps to regenerate the catalyst have been previously described by Sakaki et al. and are not rate-limiting.²² Figure 2.1 depicts regeneration of **2.8** via the reaction of **2.11** with B_2eg_2 , followed by pyridine coordination. We observe that formation of products (regardless of the site of functionalization) is exergonic, indicating that regioselectivity is not controlled

thermodynamically, but rather kinetically by the rate-limiting oxidative addition step. Regeneration of the catalyst employing HBeg, instead of B₂eg₂ (Figure 2.1), is also exergonic (Figure 2.2).

Most importantly, no regioselectivity is predicted by these calculations, as the transition states for 2-, 3-, and 4-borylation are calculated to have nearly the same energies ($\Delta G^\ddagger = 29.2$, 28.7 and 29.0 kcal/mol, respectively). This result is at odds with the reported experimental selectivities for Ir-catalyzed pyridine borylation with B₂pin₂ (2-:3-:4-borylation = 0:2:1),¹⁶ and consequently indicates that Pathway A is unlikely to be the primary operative pathway for this transformation.

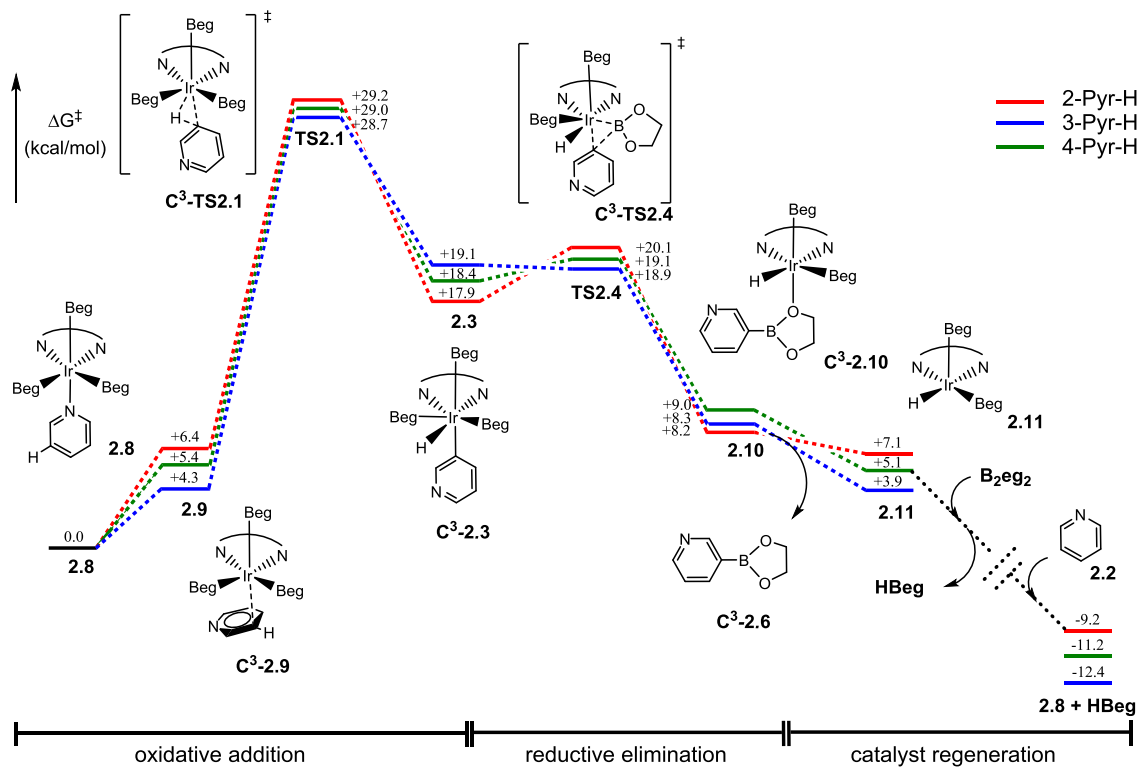


Figure 2.1: Free energy profile for Pathway A with catalyst regeneration by B_2eg_2 . Structures for borylation at the 3-position of pyridine are shown. Results for 2-, 3-, and 4-C–H activation are denoted by red, blue and green lines, respectively.

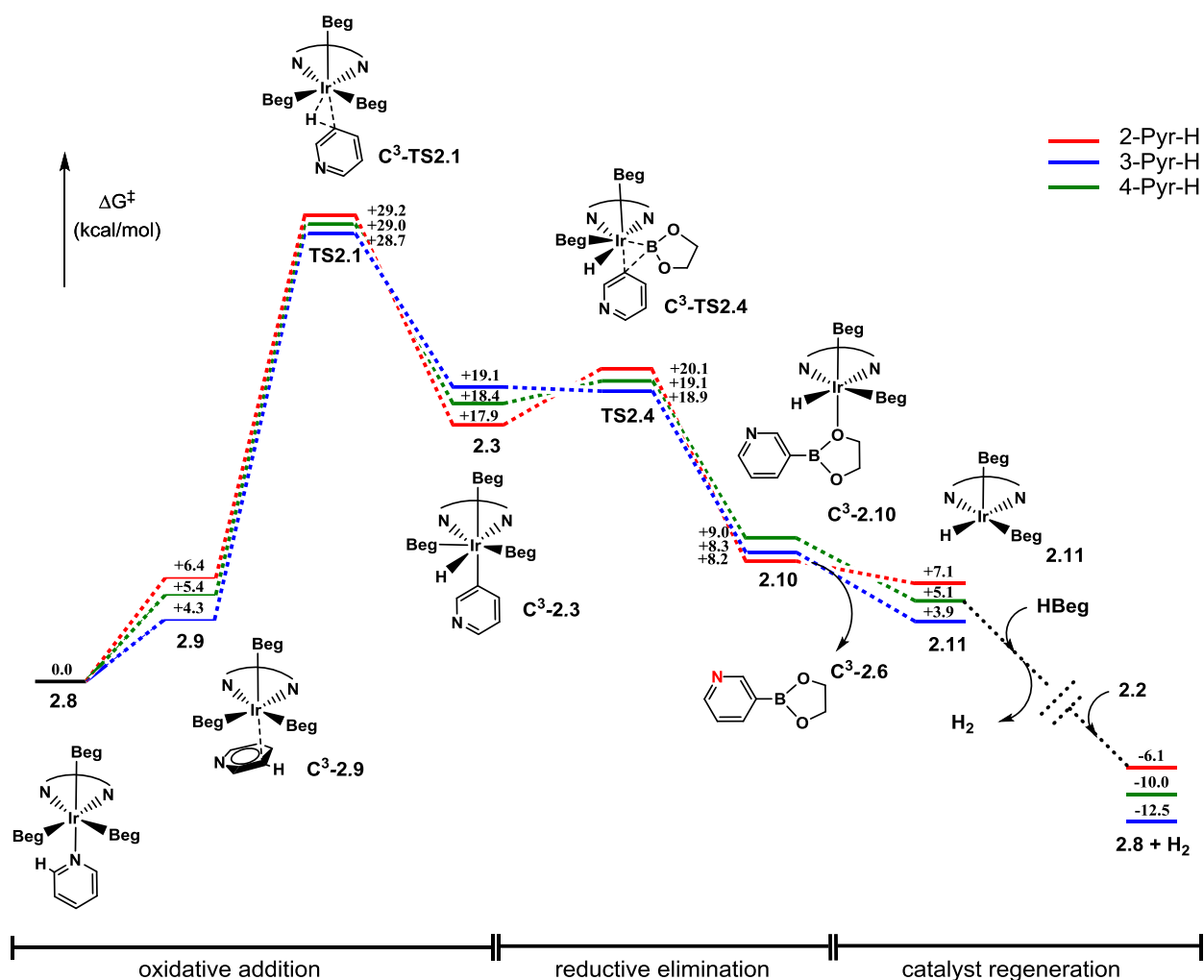


Figure 2.2: Free energy profile for Pathway A with catalyst regeneration by HBeg. Structures for borylation at the 3-position of pyridine are shown. Results for 2-, 3-, and 4-C-H activation are denoted by red, blue and green lines, respectively.

The computational results for Pathway B are shown in Figure 2.3. One equivalent of pyridine coordinates to B₂eg₂ to form a Lewis acid-base adduct **2.12** ($\Delta G = -1.6$ kcal/mol). Adduct **2.12** can react with coordinatively unsaturated Ir complex **2.1**, formed by dissociation of

pyridine from **2.8**. The overall energy of formation of this unstable mixture of **2.12**, **2.1**, and pyridine is energetically uphill ($\Delta G = 6.0$ kcal/mol). Attempts to find a stable π -complex intermediate similar to **2.9** (Figure 2.1) were unsuccessful due to the steric influence of the bulky B_2eg_2 moiety coordinated to pyridine. The 16-electron complex **2.1** then undergoes oxidative addition to a C–H bond of **2.12** to form the aryl intermediate **2.4** via transition structure **TS2.2**. Subsequent C–B bond-forming reductive elimination proceeds readily through transition structure **TS2.5**, providing the oxygen-bound intermediate **2.13**. Dissociation of Ir and B_2eg_2 from **2.13** yields the pyridyl–Beg product **2.6** and iridium hydride complex **2.11**, from which the starting catalyst **2.8** can be regenerated.

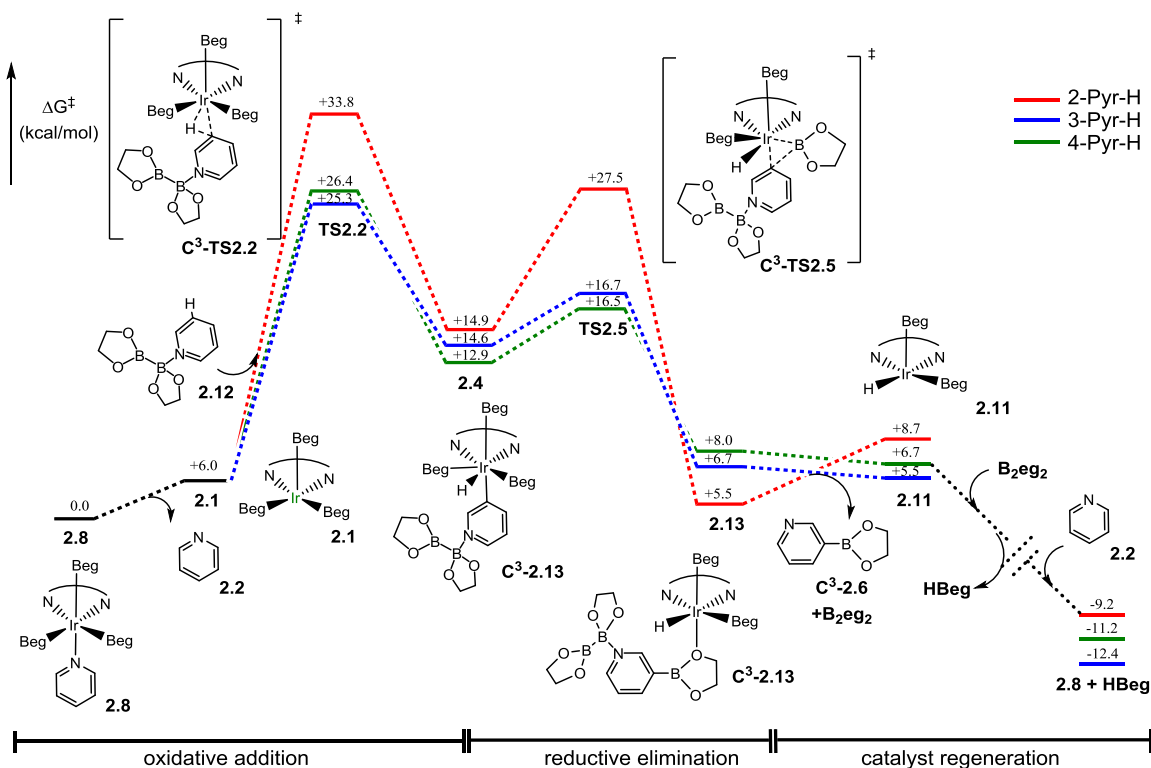


Figure 2.3: Free energy profile for Pathway B. Structures for borylation at the 3-position of pyridine are shown. Results for 2-, 3-, and 4-C–H activation are denoted by red, blue and green lines, respectively.

Notably, Pathway B is characterized by a large calculated difference between the activation free energy for 2-borylation ($\Delta G^\ddagger = 33.8$ kcal/mol) and the activation free energies for 3- and 4-borylation ($\Delta G^\ddagger = 25.3$ and 26.4 kcal/mol, respectively). The large activation free energy for 2-borylation arises from steric effects, and is in accord with the experimentally observed absence of 2-borylated products.¹⁶ Significantly, the activation free energies for 3- and 4-borylation are lower in Pathway B than in Pathway A. This result is expected because pyridine

is more electron deficient when coordinated to the Lewis acid (B_2eg_2), which should promote its reactivity toward oxidative addition of Ir.³⁸ We do note that the activation free energies for C^3 -**TS2.2** and C^4 -**TS2.2** are lower than that of benzene ($\Delta G^\ddagger = 25.5$ kcal/mol for benzene), yet benzene is known to undergo borylation at room temperature whereas pyridine requires forcing conditions (80-100 °C). Thus, we may be underestimating the stability of the complex **2.8**. Indeed, a recent report by Goddard and Periana on a dihydroxo iridium(III) pyridine complex suggests that the free energy associated with the iridium-pyridine Ir–N bond formation is on the order of -13.5 kcal/mol,³⁹ more than 7 kcal/mol more stable than our calculations, though it should be pointed out this large difference is due in part to greater steric repulsions in our case. Therefore, the activation energies for Pathways A and B may be systemically underestimated in our calculations, but our predicted regioselectivities would not change.

Transition structures for the oxidative addition step in Pathway B are depicted in Figure 2.4. The length of the forming Ir–C bond is indicative of the steric strain between the metal center and the substrate. Interestingly, this bond length is nearly identical in the transition structures C^3 -**TS2.2** and C^4 -**TS2.2** for 3- and 4-C–H activation (2.25 Å and 2.23 Å, respectively). Conversely, the forming Ir–C and the B_2eg_2 -Pyr B–N bond lengths in C^2 -**TS2.2** (2.30 Å and 1.78 Å, respectively) are both longer than the corresponding bond lengths in C^3 - and C^4 -**TS2.2**. This result highlights the greater steric effects involved during activation at the 2-position. The length of the activated C–H bond in **TS2.2** does not appear to be correlated with steric effects; the C–H bond length in C^2 -**TS2.2** (which is the most sterically hindered) is slightly shorter than the C–H bond in C^4 -**TS2.2** (which has the least steric hindrance).

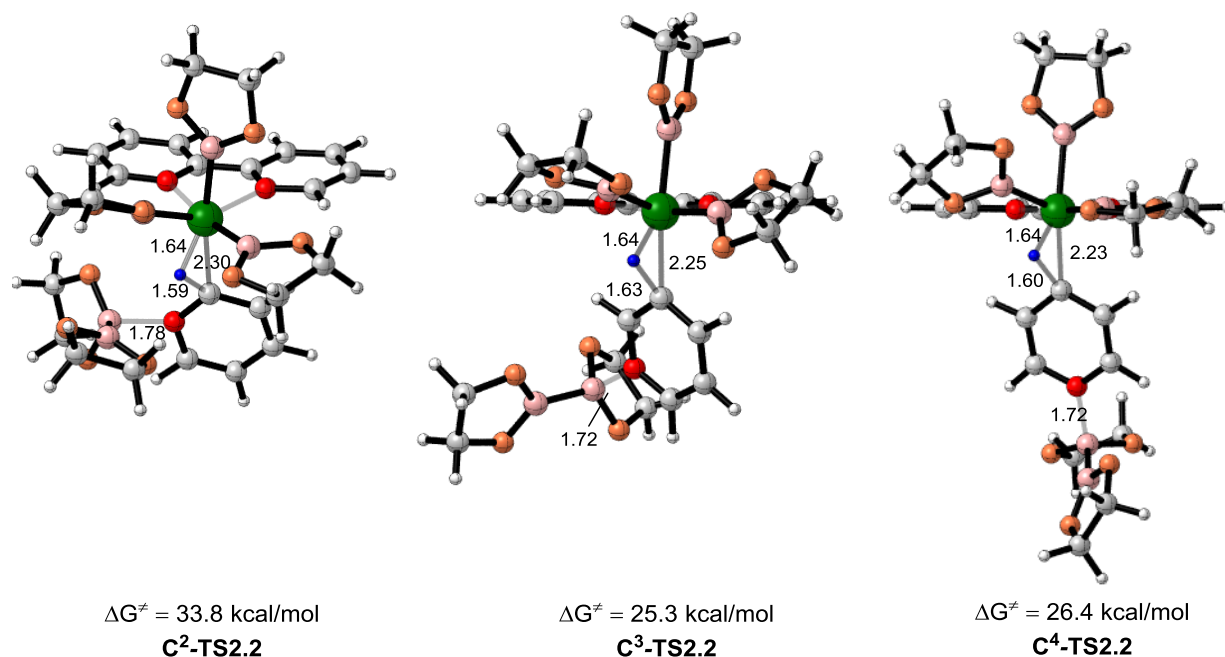


Figure 2.4: Transition structures for the oxidative addition step of Pathway B.

Finally, the free energy profile calculated for Pathway C is shown in Figure 2.5. Starting from Ir–pyridine complex **2.8**, dissociation of pyridine **2.2** yields the active trisboryl iridium(III) intermediate **2.1**. Subsequently, **2.1** undergoes oxidative addition into a C–H bond of the pyridine ligand of another equivalent of **2.8** via transition structure **TS2.3**, providing the homobimetallic complex **2.5**. Due to the high steric congestion involved in the activation of the 2-position through this pathway, we were unable to locate a transition structure for the 2-activated substrate, which is presumably high in energy. Facile C–B bond-forming reductive elimination at complex **2.5** occurs through transition structure **TS2.6** to afford bimetallic complex **2.14**. Subsequent dissociation of product **2.6** from **2.14** provides Ir–H complex **2.11**, which is then converted to the starting catalyst **2.8** as described above for Pathways A and B.

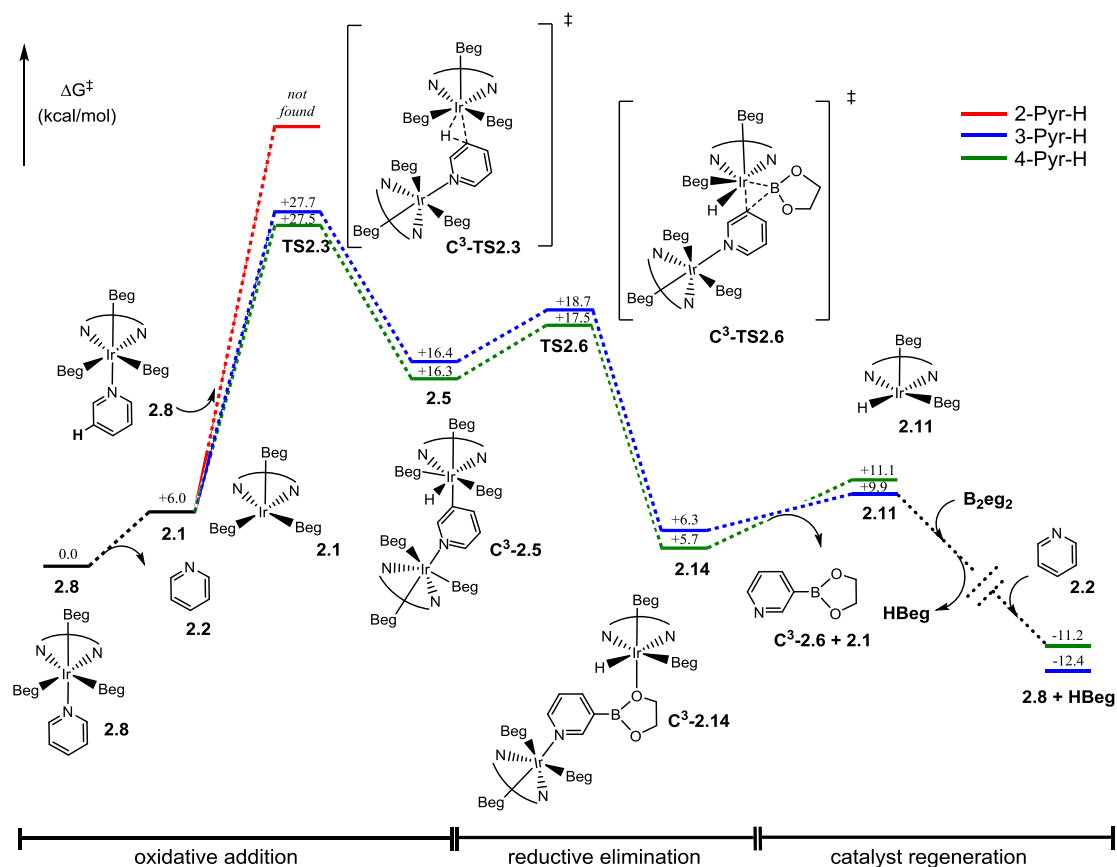


Figure 2.5: Free energy profile for Pathway C. Structures for borylation at the 3-position of pyridine are shown. Results for 2-, 3-, and 4-C–H activation are denoted by red, blue and green lines, respectively.

In agreement with the experimentally observed equal reactivity of the 3- and 4-positions of pyridine, 3- and 4-borylation in Pathway C have similar activation free energies ($\Delta G^\ddagger = 27.7$ and 27.5 kcal/mol, respectively). The 3-borylation transition structure exhibits an Ir–N distance of 2.35 Å (Figure 2.6), which is the same as the Ir–N distance in **2.8**. In contrast, the Ir–N

distance in the transition structure for 4-borylation decreases slightly to 2.33 Å. The forming Ir–C bond length of 2.22 Å for 3-borylation is slightly shorter than that of the forming Ir–C bond for 4-borylation (2.29 Å). Since there are no appreciable differences in the steric interactions between the 3- and 4-borylation transition structures, this difference in Ir–C bond length can be attributed to more favorable bonding interaction between the metal center and the carbon at the 3-position.

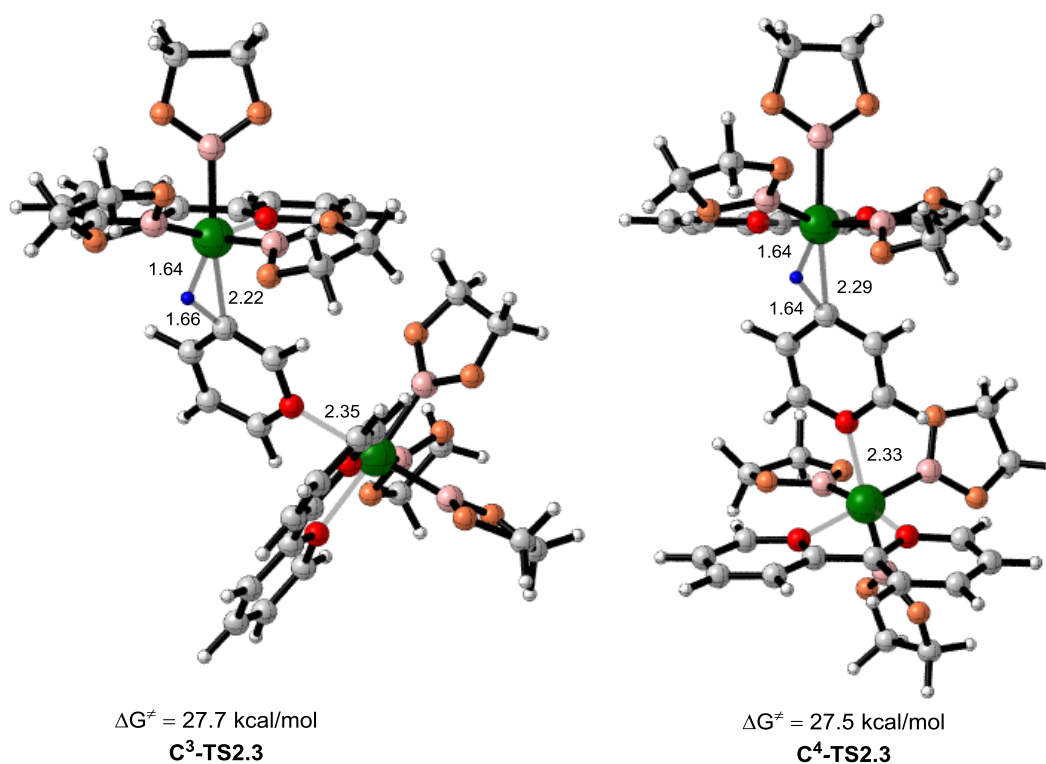


Figure 2.6: Transition structures for the C–H oxidative addition step of Pathway C.

Activation free energies for the 2-, 3- and 4-borylation of pyridine via Pathways A–C are summarized in Table 2.1. The theoretical results for Pathway A suggest that C–H

functionalization via this pathway should yield a mixture of products that includes 2-borylated pyridine, a prediction that does not agree with the experimentally observed selectivities. On the other hand, the theoretical results for Pathways B and C both predict high selectivity for activation of the 3- and 4-positions of pyridine. These latter two pathways involve borylation of pyridine that is complexed as a Lewis acid-base adduct of a diboron (**2.12**) or an iridium species (**2.8**) for Pathways B and C, respectively. The activation free energy for 2-borylation in Pathway C could not be determined, and is presumably even larger than that calculated for Pathway B, since the Ir–pyridine Lewis acid-base adduct found in Pathway C is more bulky than the the pyridine–B₂eg₂ adduct of Pathway B. Overall, Pathway B is predicted to be more favorable than Pathway C by 2.4 and 1.1 kcal/mol for 3- and 4-borylation, respectively. Additionally, Pathway B is expected to be more likely than Pathway C because the concentration of iridium catalyst is low relative to B₂pin₂. The computations correctly predict that both 3- and 4-borylation should be more favored than 2-borylation; however, a small preference for 3- over 4-selectivity is predicted that has not been observed experimentally.

Table 2.1: Activation free energies for 2-, 3-, and 4-borylation of pyridine by Pathways A–C.

Pathway	Activation Free Energy (kcal/mol)		
	C ² –H	C ³ –H	C ⁴ –H
A	29.2	28.7	29.0
B	33.8	25.3	26.4
C	--	27.7	27.5

Finally, noting that the formation of a Lewis acid-base adduct increases reactivity and selectivity for the 3- and 4-positions in pyridine **2.2**, we turned our attention to the pyridine trifluoroborane complex **2.15** as a reference substrate for iridium-catalyzed borylation. The computational results for borylation of **2.15** are shown in Figure 2.7. Complex **2.15** undergoes rate-limiting C–H oxidative addition to catalyst **2.1** via transition structure **TS2.7**. Subsequent C–B bond-forming reductive elimination proceeds readily through transition structure **TS2.8**, providing the oxygen-bound intermediate **2.17**. Dissociation of Ir from **2.17** yields the pyridyl–Borane product **2.18** and iridium hydride complex **2.11**, from which the starting catalyst **2.8** can be regenerated.

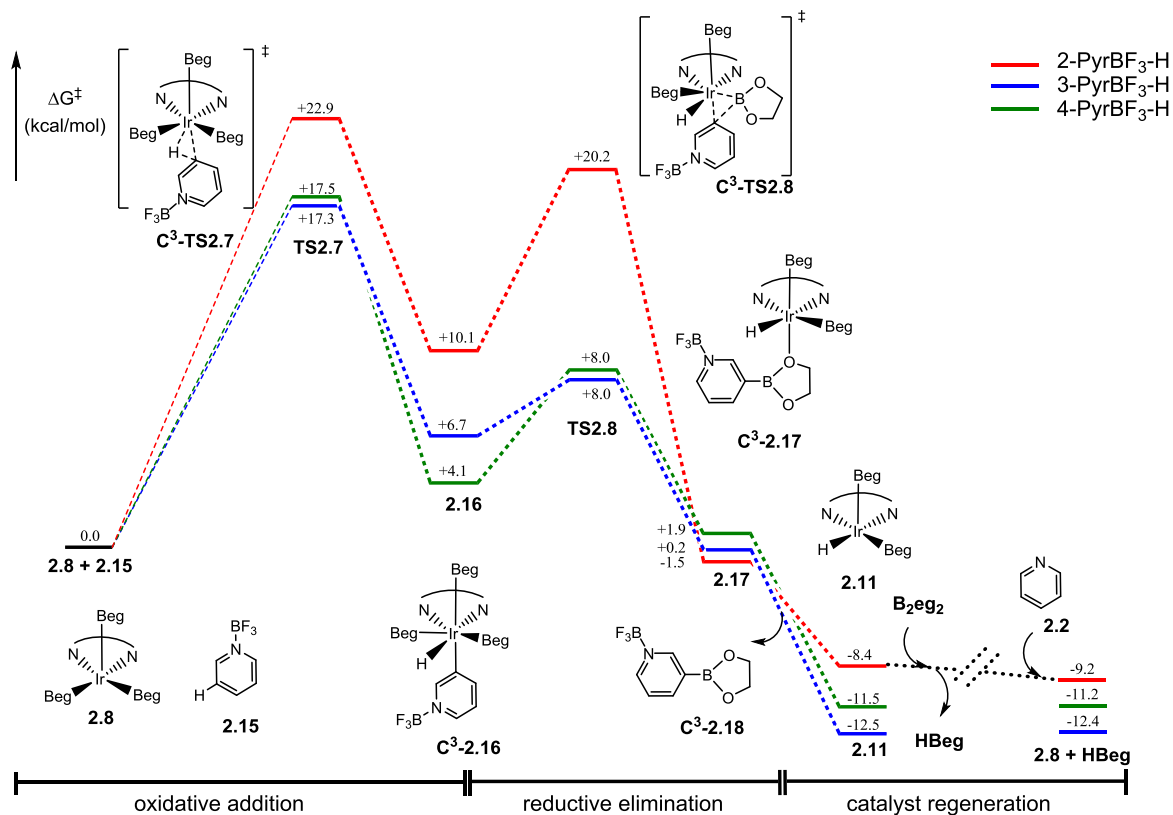


Figure 2.7: Free energy profile for activation of trifluoroborane pyridine complex **2.15**. Structures for borylation at the 3-position of **2.15** are shown. Results for 2-, 3-, and 4-C-H activation are denoted by red, blue and green lines, respectively.

Figure 2.8 shows the transition structures for the rate-limiting oxidative addition of **2.15** via **TS2.7**. The forming Ir-C bond length of 2.27 Å for 2-borylation is slightly longer than that of the forming Ir-C bond for 3- and 4-borylation (2.25 and 2.24 Å, respectively). The activation energy for borylation at the 2-position (22.9 kcal/mol) is significantly higher than the activation energies for the borylation at the 3- and 4-positions (17.3 and 17.5 kcal/mol, respectively) due to steric strain imposed by the trifluoroborane substituent in **C2-TS2.7**. In addition, activation

energies for both the 3- and 4-position are very low relative to free pyridine due to the strong Lewis acidity of BF_3 . Activation energies suggest experimental statistical selectivities $\text{C}^2:\text{C}^3:\text{C}^4$ of approximately 0:67:33.

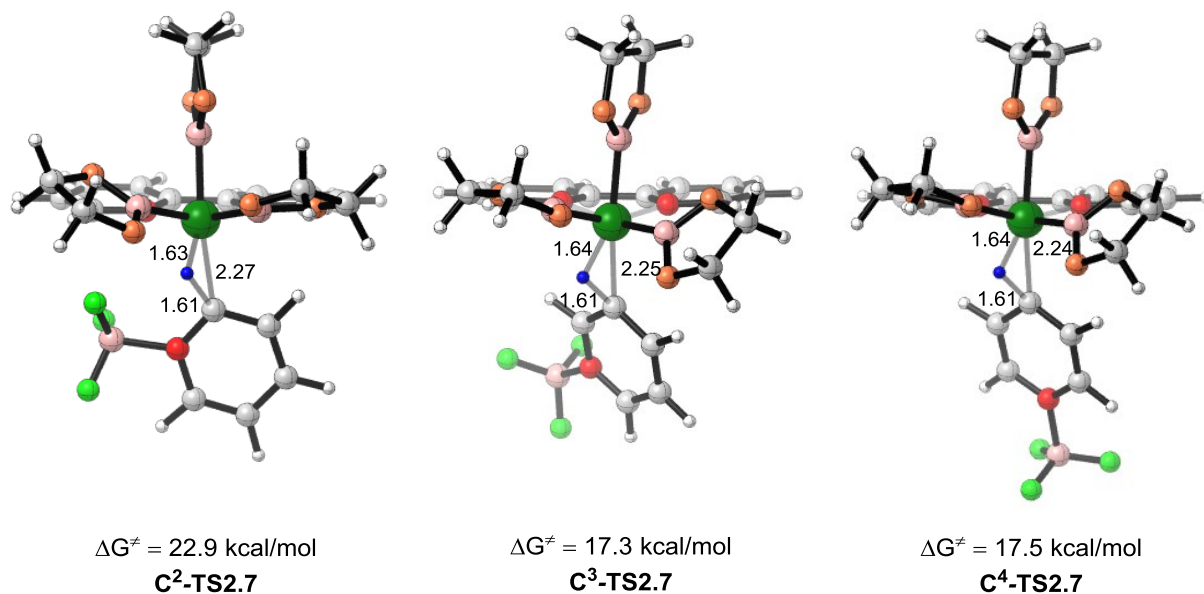


Figure 2.8: Transition structures for the C–H oxidative addition step for the borylation of **2.15**.

CONCLUSION:

In summary, free energy profiles of four different C–H-activation pathways for borylation of pyridine were determined using DFT computational methods. A pathway involving C–H activation of a Lewis acid-base adduct between boron and pyridine (Pathway B), is found to be preferred relative to C–H activation of free pyridine (Pathway A). Coordination of pyridine to

the diboryl species activates the pyridine substrate (relative to free pyridine) towards 3- and 4-borylation, and provides steric hindrance that renders 2-borylation unfavorable. Computations predict Lewis acid-base complex **2.15** is highly activated and C–H borylation will yield 3- and 4-borylation products.

REFERENCES:

- (1) Brown, H. C. *Organic Syntheses via Boranes*; Wiley: New York, 1975.
- (2) Pelter, A.; Smith, K.; Brown, H. C. *Borane Reagents*; Academic Press: Ann Arbor, 1988.
- (3) Miyaura, N. *Bull. Chem. Soc. Jpn.* **2008**, *81*, 1535.
- (4) Magano, J.; Dunetz, J. R. *Chem. Rev.* **2011**, *111*, 2177.
- (5) Suzuki, A. *Angew. Chem. Int. Ed.* **2011**, *50*, 6722.
- (6) Mkhaliid, I. A. I.; Barnard, J. H.; Marder, T. B.; Murphy, J. M.; Hartwig, J. F. *Chem. Rev.* **2010**, *110*, 890.
- (7) Hartwig, J. F. *Chem. Soc. Rev.* **2011**, *40*, 1992.
- (8) Hartwig, J. F. *Acc. Chem. Res.* **2012**, *45*, 864.
- (9) Vanchura, I. I. B. A.; Preshlock, S. M.; Roosen, P. C.; Kallepalli, V. A.; Staples, R. J.; Maleczka, J. R. E.; Singleton, D. A.; Smith, I. I. I. M. R. *Chem. Commun.* **2010**, *46*, 7724.
- (10) Roosen, P. C.; Kallepalli, V. A.; Chattopadhyay, B.; Singleton, D. A.; Maleczka, R. E.; Smith, M. R. *J. Am. Chem. Soc.* **2012**, *134*, 11350.
- (11) Robbins, D. W.; Boebel, T. A.; Hartwig, J. F. *J. Am. Chem. Soc.* **2010**, *132*, 4068.
- (12) Ishiyama, T.; Takagi, J.; Hartwig, J. F.; Miyaura, N. *Angew. Chem. Int. Ed.* **2002**, *41*, 3056.

- (13) Davies, H. M. L.; Manning, J. R. *Nature* **2008**, *451*, 417.
- (14) Ishiyama, T.; Takagi, J.; Yonekawa, Y.; Hartwig, J. F.; Miyaura, N. *Adv. Synth. & Catal.* **2003**, *345*, 1103.
- (15) Ishiyama, T.; Nobuta, Y.; Hartwig, J. F.; Miyaura, N. *Chem. Commun.* **2003**, 2924.
- (16) Takagi, J.; Sato, K.; Hartwig, J. F.; Ishiyama, T.; Miyaura, N. *Tetrahedron Lett.* **2002**, *43*, 5649.
- (17) Harrisson, P.; Morris, J.; Marder, T. B.; Steel, P. G. *Org. Lett.* **2009**, *11*, 3586.
- (18) Ishiyama, T.; Miyaura, N. *Pure Appl. Chem.* **2006**, *78*, 1369.
- (19) Tajuddin, H.; Harrisson, P.; Bitterlich, B.; Collings, J. C.; Sim, N.; Batsanov, A. S.; Cheung, M. S.; Kawamorita, S.; Maxwell, A. C.; Shukla, L.; Morris, J.; Lin, Z.; Marder, T. B.; Steel, P. G. *Chem. Sci.* **2012**.
- (20) Ishiyama, T.; Miyaura, N. *J. Organomet. Chem.* **2003**, *680*, 3.
- (21) Boller, T. M.; Murphy, J. M.; Hapke, M.; Ishiyama, T.; Miyaura, N.; Hartwig, J. F. *J. Am. Chem. Soc.* **2005**, *127*, 14263.
- (22) Tamura, H.; Yamazaki, H.; Sato, H.; Sakaki, S. *J. Am. Chem. Soc.* **2003**, *125*, 16114.
- (23) Nguyen, P.; Dai, C.; Taylor, N. J.; Power, W. P.; Marder, T. B.; Pickett, N. L.; Norman, N. *C. Inorg. Chem.* **1995**, *34*, 4290.
- (24) Clegg, W.; Dai, C.; J. Lawlor, F.; B. Marder, T.; Nguyen, P.; C. Norman, N.; L. Pickett, N.; P. Power, W.; J. Scott, A. *J. Chem. Soc., Dalton Trans.* **1997**, *0*, 839.
- (25) Benitez, D.; Tkatchouk, E.; Goddard Iii, W. A. *Chem. Commun.* **2008**, 6194.
- (26) Balcells, D.; Clot, E.; Eisenstein, O. *Chem. Rev.* **2010**, *110*, 749.
- (27) Lin, M.; Kang, G.-Y.; Guo, Y.-A.; Yu, Z.-X. *J. Am. Chem. Soc.* **2011**, *134*, 398.

- (28) Yeom, H.-S.; Koo, J.; Park, H.-S.; Wang, Y.; Liang, Y.; Yu, Z.-X.; Shin, S. *J. Am. Chem. Soc.* **2011**, *134*, 208.
- (29) Tang, S.-Y.; Guo, Q.-X.; Fu, Y. *Chem. Eur. J.* **2011**, *17*, 13866.
- (30) Giri, R.; Lan, Y.; Liu, P.; Houk, K. N.; Yu, J.-Q. *J. Am. Chem. Soc.* **2012**, *134*, 14118.
- (31) Herbert, M. B.; Lan, Y.; Keitz, B. K.; Liu, P.; Endo, K.; Day, M. W.; Houk, K. N.; Grubbs, R. H. *J. Am. Chem. Soc.* **2012**, *134*, 7861.
- (32) Liu, P.; Xu, X.; Dong, X.; Keitz, B. K.; Herbert, M. B.; Grubbs, R. H.; Houk, K. N. *J. Am. Chem. Soc.* **2012**, *134*, 1464.
- (33) Gaussian 09, Revision C.01, Frisch, M. J.; Trucks, G. W.; Schlegel, H. B.; Scuseria, G. E.; Robb, M. A.; Cheeseman, J. R.; Scalmani, G.; Barone, V.; Mennucci, B.; Petersson, G. A.; Nakatsuji, H.; Caricato, M.; Li, X.; Hratchian, H. P.; Izmaylov, A. F.; Bloino, J.; Zheng, G.; Sonnenberg, J. L.; Hada, M.; Ehara, M.; Toyota, K.; Fukuda, R.; Hasegawa, J.; Ishida, M.; Nakajima, T.; Honda, Y.; Kitao, O.; Nakai, H.; Vreven, T.; Montgomery, J. A.; Peralta, J. E.; Ogliaro, F.; Bearpark, M.; Heyd, J. J.; Brothers, E.; Kudin, K. N.; Staroverov, V. N.; Kobayashi, R.; Normand, J.; Raghavachari, K.; Rendell, A.; Burant, J. C.; Iyengar, S. S.; Tomasi, J.; Cossi, M.; Rega, N.; Millam, J. M.; Klene, M.; Knox, J. E.; Cross, J. B.; Bakken, V.; Adamo, C.; Jaramillo, J.; Gomperts, R.; Stratmann, R. E.; Yazyev, O.; Austin, A. J.; Cammi, R.; Pomelli, C.; Ochterski, J. W.; Martin, R. L.; Morokuma, K.; Zakrzewski, V. G.; Voth, G. A.; Salvador, P.; Dannenberg, J. J.; Dapprich, S.; Daniels, A. D.; Farkas; Foresman, J. B.; Ortiz, J. V.; Cioslowski, J.; Fox, D. J. Wallingford CT, 2009.
- (34) Ishiyama, T.; Takagi, J.; Ishida, K.; Miyaura, N.; Anastasi, N. R.; Hartwig, J. F. *J. Am. Chem. Soc.* **2002**, *124*, 390.

- (35) Śliwa, W. *Transition Met. Chem.* **1995**, *20*, 1.
- (36) In *Chemistry of Heterocyclic Compounds*; Tomasik, P. R., Zbigniew; Newkome, George R.; Sktrekowski, Lucjan, Ed.; John Wiley & Sons, Inc.: 2008, p 186.
- (37) Mkhaliid, I. A. I.; Coventry, D. N.; Albesa-Jove, D.; Batsanov, A. S.; Howard, J. A. K.; Perutz, R. N.; Marder, T. B. *Angew. Chem. Int. Ed.* **2006**, *45*, 489.
- (38) Hartwig, J. F. *Organotransition Metal Chemistry: From Bonding to Catalysis*; Univ. Science Books: Sausalito, 2010.
- (39) Meier, S. K.; Young, K. J. H.; Ess, D. H.; Tenn, W. J.; Oxgaard, J.; Goddard, W. A.; Periana, R. A. *Organometallics* **2009**, *28*, 5293.

CHAPTER 3: Distortion/Interaction Analysis Reveals the Origins of the Selectivities in Iridium-Catalyzed C–H Borylation of Substituted Arenes and 5-Membered Heterocycles

Reproduced with permission from Journal of the American Chemical Society, submitted for publication. Unpublished work copyright 2013 American Chemical Society.

ABSTRACT:

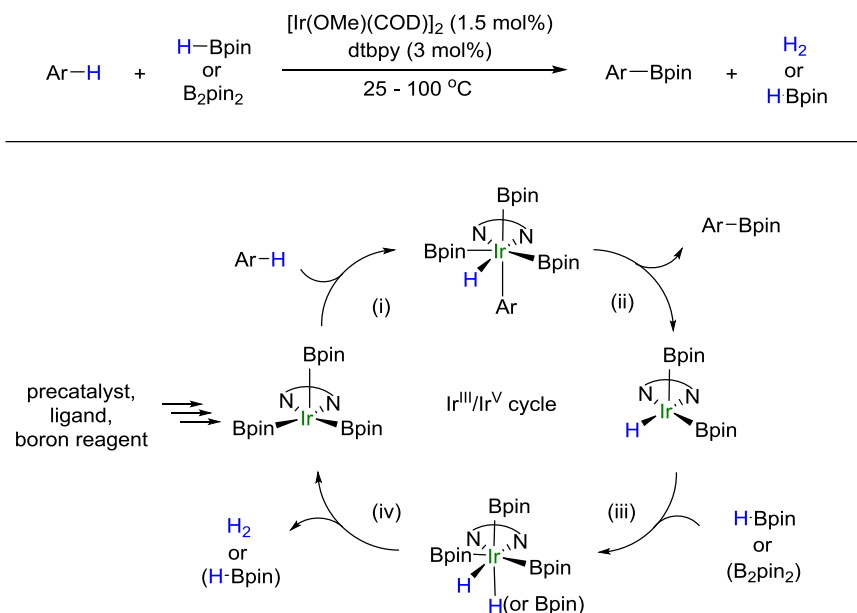
The iridium-catalyzed borylation of mono- and di-substituted arenes and heteroarenes has been studied with density functional theory. The distortion/interaction model was employed to understand the origins of the selectivities in these reactions. Computations revealed that the transition states for C–H oxidative addition are very late, resembling the aryl iridium hydride intermediate with a fully formed Ir–C bond. Consequently, regioselectivity is mainly controlled by differences in the interaction energies between the iridium catalyst and arene carbon. The regioselectivity does not correlate with the substrate distortion energy, which is mostly controlled by the length of the breaking C–H bond in the transition state.

INTRODUCTION:

Selective functionalization of aromatic C–H bonds is an important area of research that can lead to new approaches for the synthesis of complex organic molecules.^{1,2} The regioselective borylation of C(*sp*²)–H bonds is a particularly attractive target because of the well-

known utility of arylboron starting materials in a variety of synthetic applications.^{3,4} Recently, iridium-catalyzed borylation of aromatic compounds has emerged as a viable alternative to well-known palladium-catalyzed borylations.⁵⁻⁷ A common borylation protocol involves the use of $[\text{Ir}(\text{OMe})(\text{COD})]_2$ as a catalyst precursor with dtbpy (dtbpy = 4,4'-di-*tert*-butyl-2,2'-bipyridine) as the ligand and either bis(pinacolato)diboron (B_2pin_2) or pinacolborane (HBpin) as the boron source (Scheme 3.1). Experimental studies by Hartwig and coworkers utilizing $\text{Ir}(\text{dtbpy})(\text{Bpin})_3(\text{COE})$ (COE = cyclooctene) as a precatalyst support a mechanism where $\text{Ir}^{\text{III}}(\text{dtbpy})(\text{Bpin})_3$ is the active catalyst that mediates C–H cleavage via rate-limiting oxidative addition (step i).⁸ Subsequent, reductive elimination (step ii) yields the arylboronate ester. In this mechanism, regeneration of the active catalyst can occur with either HBpin or B_2pin_2 (steps iii and iv). This mechanism has been supported computationally.⁹

Scheme 3.1: Catalytic cycle for the iridium-catalyzed borylation of aromatic rings



Despite remarkable progress in the use of iridium catalysts, the origins of the regioselectivity in this reaction are not well understood. For example, in the case of substituted arenes, the regioselectivity appears to be largely controlled by steric factors. Monosubstituted benzene rings react nearly exclusively at the *meta*- and *para*-positions and regioselectivity is only slightly perturbed by changing the electronic properties of the substituent (Figure 1).¹⁰⁻¹² Additionally, in the case of 1,2-disubstituted benzene rings, no 3- or 6-borylated products are observed. The selectivity for the 4- or 5-position is influenced by electronic properties the preferred site of C–H activation is *para* to the weaker electron donating substituent (Figure 3.1).¹³

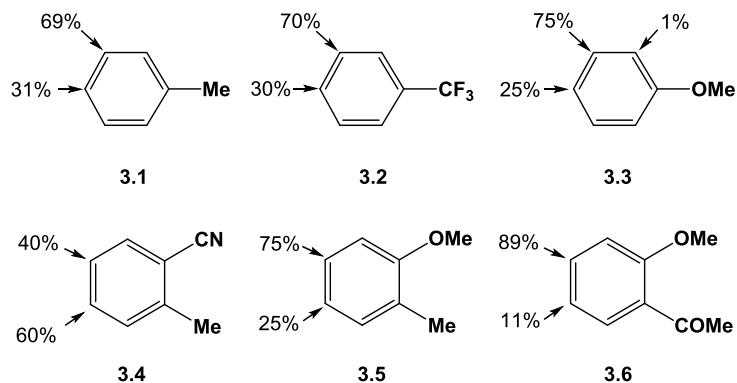


Figure 3.1: Regioselectivities of various substituted benzene rings.

Experimental selectivities for a select group of 5-membered- and benzo-fused 5-membered heterocycles **3.7-3.14** are shown in Figure 3.2. Unsubstituted 5-membered heterocycles react exclusively at the 2-position, suggesting a strong electronic effect with these substrates.^{11,12,14} Only after placing a sterically hindering group on the heteroatom does the regioselectivity begin to favor the 3-position.¹⁵ In the case of pyrrole derivatives, reaction with

N-methylpyrrole yields a mixture of 2- and 3-borylated products. In the presence of a bulky TIPS group at the nitrogen, the reaction of **14** occurs at the 3-position exclusively.¹⁵

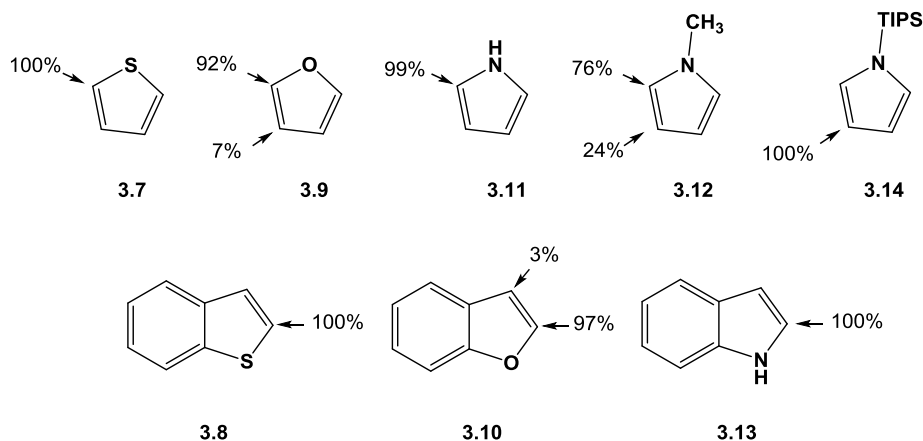


Figure 3.2: Regioselectivities of C–H activation of select 5-membered heterocycles.

A number of factors may contribute to the reactivity of C–H bonds in the oxidative addition transition states, such as steric effects, the homolytic or heterolytic dissociation energy of the C–H bond, and the stability of the forming Ir–C bond. Recent studies by Maleczka, Singleton, Smith suggest that the regioselectivity of iridium-catalyzed borylation is governed by the pK_a 's of the C–H bond; in the absence of external factors, the most acidic bonds are borylated preferentially.¹⁶ A recent study on iridium-catalyzed borylation by Marder, Steel and coworkers demonstrated that pK_a 's of the C–H bonds may provide an indicator of selectivity.¹³ However, while some success predicting the preferred borylation position was achieved using NMR spectroscopy, the correlation between substrate pK_a values and selectivity is not perfect.¹³ Interestingly, recent computational studies on palladium-catalyzed C–H activations have demonstrated a correlation between regioselectivity and Pd–C bond strengths of the aryl

palladium intermediates or C–H activation transition structures. Eisenstein and Perutz *et al.* found a better correlation between Pd–C bond dissociation energy (BDE) of the reaction intermediates and the activation energy in the direct arylation of fluorinated benzenes than the correlation between pK_a and activation energy.¹⁷ In a related study on palladium-catalyzed C(sp^2)–H activation, Ess *et al.* found a linear correlation between the C–H bond activation energy and the transition state Pd–C bond energy, demonstrating that the stability of the forming Pd–aryl bonds determines regioselectivity for a variety of arene and heteroarene substrates.¹⁸

We recently employed the distortion/interaction model to investigate the origins of reactivity and selectivities in a variety of organic and organometallic reactions.^{19–23} The distortion/interaction analysis has also been called the activation-strain model by Bickelhaupt.^{24–26} In the distortion/interaction model, the activation energy (ΔE^\ddagger) of a bimolecular process is divided into the energy to distort the reactants to the transition state geometry ($\Delta E_{\text{dist}}^\ddagger$) and the energy of interaction between the distorted fragments ($\Delta E_{\text{int}}^\ddagger$). In a study on the Pd-catalyzed cross-coupling of polyhalogenated heterocycles, we reported that regioselectivities are controlled by both the energy to distort the C–X bond (related to BDE) and the interaction energy of the metal with the substrate.²⁰ In related studies, Gorelsky and Fagnou applied the distortion/interaction model to the palladium-catalyzed C–H activation of aromatic substrates involving the concerted metalation-deprotonation (CMD) mechanism.^{27,28} They found that regioselectivity was determined by distortion energy or interaction energy or both depending on the substrate. Borovik and Shaik applied the distortion/interaction model to investigate the reactivity of C–H, N–H, and O–H bonds with non-heme iron oxo complexes and concluded the activation energy is mainly controlled by distortion energy, which they referred to as deformation energy.²⁹ Recently, Bickelhaupt *et al.* studied the palladium-induced activation of

C–H, C–C, C–F, and C–Cl bonds in alkanes using the distortion/interaction (activation-strain) model.³⁰ They pointed out that the location of the transition state along the reaction coordinate has a large effect on the distortion and interaction energies and is an important consideration for understanding activation barriers. We have now for the first time applied the distortion/interaction model to study the factors that control regioselectivity of C–H oxidative additions in iridium-catalyzed borylations, and provide a model to understand the origins of selectivities in these reactions.

COMPUTATIONAL METHODS:

Geometry optimizations were carried out using B3LYP and a mixed basis set of LANL2DZ for Ir and the double- ζ split-valence 6-31G(d) basis set for all other atoms. Vibrational frequency analysis confirmed that the structure was either a minimum or a transition state. Electronic energies were obtained from single point calculations on the B3LYP geometries using Truhlar's M06 functional with a mixed basis set consisting of SDD for Ir and the triple- ζ split-valence 6-311G(d,p) basis set for other atoms. Solvation by n-octane was computed by single point calculations using the SMD model. The effectiveness of B3LYP for geometry optimization and M06 energy refinement has been demonstrated by numerous studies to successfully produce energy profiles of reactions involving transition-metal complexes.³¹⁻³⁸ All of the calculations in this study were performed with Gaussian 09.³⁹

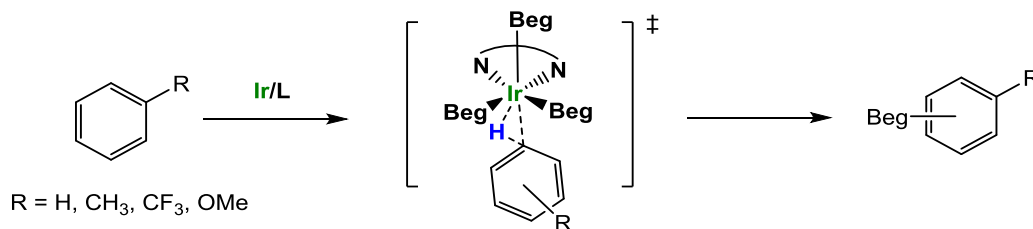
RESULTS AND DISCUSSION:

The complex lacking the four methyl groups on each Bpin, (bpy)Ir(Beg)₃ (bpy = 2,2'-bipyridine; Beg = (ethyleneglycolato)boron)^{9,16,40} was used as a model for (dtbpy)Ir(Bpin)₃.

Although Beg is a poorer electron donor and thus expected to be less reactive in C–H oxidative addition than the Bpin-ligated catalyst,⁴¹ the effects on regioselectivity employing Beg in place of Bpin are expected to be small. The transition states for the C–H oxidative addition of these substrates have been calculated: benzene, three monosubstituted benzenes (**3.1-3.3**), three 1,2-disubstituted benzene rings (**3.4-3.6**), and seven 5-membered heterocycles (**3.7-3.13**).

Monosubstituted Benzene Rings. Substrates **3.1-3.3** have different electronic properties but similar steric properties. The activation energies for the rate- and regioselectivity-determining C–H activation step are given in Table 3.1. The structures of the *ortho*-, *meta*-, and *para*-C–H oxidative addition transition states for toluene **3.1** are shown in Figure 3.3 (**TS3.1-o**, **TS3.1-m**, and **TS3.1-p**, respectively). The differences between the ΔG^\ddagger values (weighted Boltzmann average at 298 K: 1% *ortho*; 70% *meta*; 29% *para*) correspond well to the experimentally observed selectivity (0% *ortho*; 69% *meta*; 31% *para*). **TS3.1-o** is 2.5 kcal/mol less stable than the *meta*- and *para*-transition states, due to steric repulsions between the *ortho*-methyl group of the substrate and the oxygen atom of one of the equatorial Beg groups (2.48 Å). Notably, the breaking C–H bond length for the *ortho* transition state (1.74 Å) is longer than the C–H bond length for the *meta* and *para* transition states (both are 1.67 Å), indicating that the *ortho* transition state is later than the *meta* and *para* transition states. Although being a later TS as indicated by the C–H bond length, the forming Ir–C bond is longer in the *ortho* transition state (2.28 Å) than those in *meta*- or *para*-transition states (both are 2.24 Å) due to the Beg–substrate steric repulsions. The relatively short Ir–C distances in all three regioisomeric transition states indicate that the transition state is late and the Ir–C bond is almost fully formed.

Table 3.1: Activation energies and C–H/Ir–C distances in the oxidative addition transition states in the C–H borylation reaction with monosubstituted benzenes and the BDE of C–H bonds in the substrates.



Substrate	Borylation position	Exptl. product ratio	ΔG^\ddagger (kcal/mol)	ΔE^\ddagger (kcal/mol)	TS C–H length (Å)	TS Ir–C length (Å)	Reactant C–H BDE (kcal/mol)
Benzene	-	100	25.5	13.7	1.672	2.237	110.7
	<i>o</i>	0	28.2	14.6	1.742	2.276	110.5
3.1 R = CH ₃	<i>m</i>	69	25.6	13.6	1.670	2.236	110.6
	<i>p</i>	31	25.7	13.6	1.672	2.234	111.1
3.2 R = CF ₃	<i>o</i>	0	25.7	12.1	1.676	2.228	116.9
	<i>m</i>	70	23.1	11.0	1.640	2.234	116.2
	<i>p</i>	30	23.3	11.5	1.641	2.235	116.1
3.3 R = OMe	<i>o</i>	1	26.4	14.5	1.662	2.242	110.4
	<i>m</i>	74	24.7	12.8	1.676	2.238	110.4
3.3 R = OMe	<i>p</i>	25	25.6	13.8	1.680	2.235	111.8

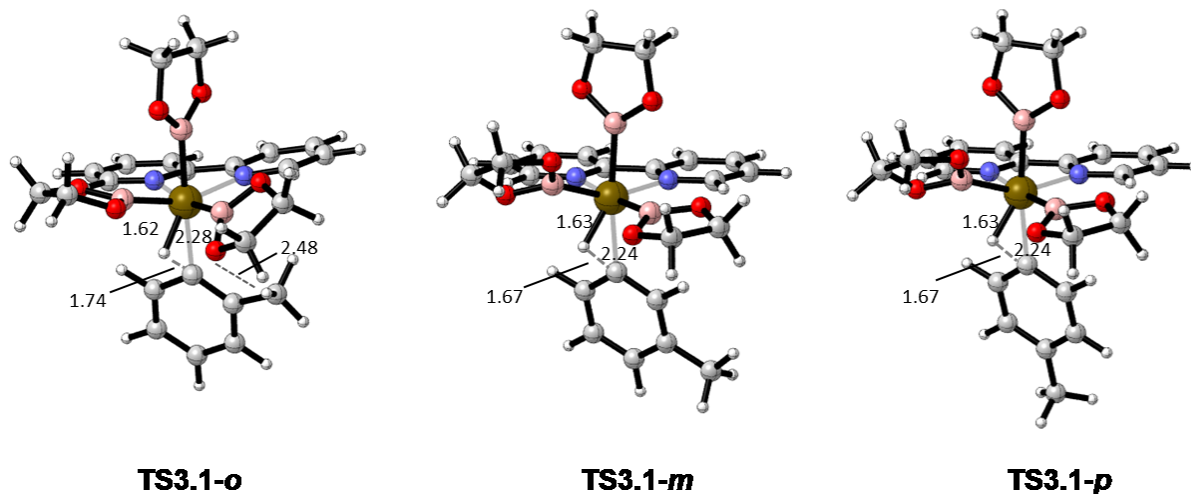


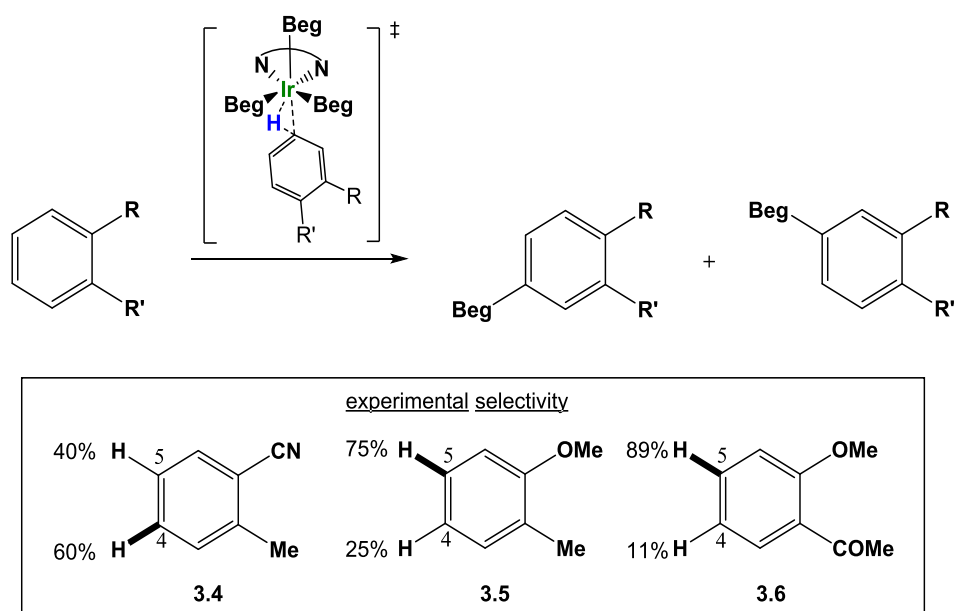
Figure 3.3: Oxidative addition transition states for the reaction of toluene, **3.1**.

As expected,⁴² the activation energy for the more electron-poor trifluoromethylbenzene **3.2** is lower than that of toluene **3.1**, consistent with the experiment with a similar substrate 1,3-bis(trifluoromethyl)-benzene.⁸ The trifluoromethyl group has an inverse electronic effect to that of the methyl group, but the relative *meta/para*-selectivities of **3.1** and **3.2** remain the same. Borylation at the *ortho*-positions of the monosubstituted benzene rings (**3.1**, **3.2** and **3.3**) are all disfavored due to steric effects.

1,2-Disubstituted Benzenes. The disubstituted benzenes, 2-methylbenzonitrile, 1-methoxy-2-methylbenzene and 1-(2-methoxyphenyl)ethanone (**3.4-3.6**) all have sterically unhindered 4- and 5-positions, which differ only in electronic properties. Indeed, the C–H and Ir–C bond lengths in the transition state structures for the activation of either the 4- or the 5-positions for **3.4-3.6** are all similar suggesting that the steric effects are comparable (Table 3.2). The computed selectivities agree well with the experimental product ratios. In the case of **3.4**, there is little selectivity between the 4- and 5-positions. For both **3.5** and **3.6**, activation at the 4-

position leads to a slightly later transition state which coincides with a higher activation energy. Reactions occurring at the 3- and 6- positions were not computed, because steric effects prevent the reaction from occurring at these positions, as indicated in the calculations with mono-substituted benzenes.

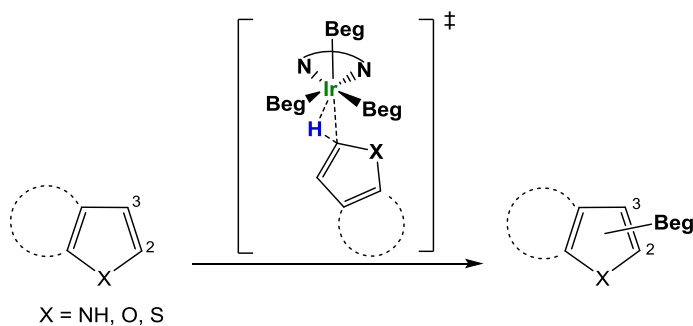
Table 3.2: Activation energies and C–H/Ir–C distances for the oxidative addition transition states in the C–H borylation reaction with 1,2-disubstituted benzenes and the BDE of C–H bonds in the substrates.



Substrate	Borylation position	Exptl. product ratio	ΔG^\ddagger (kcal/mol)	ΔE^\ddagger (kcal/mol)	TS C–H length (Å)	TS Ir–C length (Å)	Reactant C–H BDE (kcal/mol)
3.4	4	60	22.3	10.8	1.641	2.232	111.0
	5	40	22.8	11.2	1.631	2.236	111.7
3.5	4	25	26.2	14.0	1.688	2.234	111.6
	5	75	24.8	12.9	1.674	2.236	110.7
3.6	4	11	24.2	12.6	1.644	2.236	111.8
	5	89	23.2	11.1	1.658	2.231	110.5

5-Membered and Benzo-fused Heterocycles. The 5-membered heterocycles predominantly borylate at the 2-position. Calculations correlate excellently with experimental results (Table 3.3). In reaction with substrates **3.7-3.10**, the breaking C–H bond length is longer in transition state for attack at the 3-position relative to the 2-position. The reverse trend is seen in substrates **3.11** and **3.12** where the activation at the 2-position occurs later (1.75 Å) than the 3-position (1.67 Å), but the 2-position is still favored energetically. Detailed analysis of the transition structure of **3.11** revealed hydrogen bonding between the N-H hydrogen of the pyrrole substrate and an oxygen atom of one of the Beg ligands—a result that was previously demonstrated by Smith and Singleton and is confirmed in this study (Figure 3.4).⁴⁰

Table 3.3: Activation energies and C–H/Ir–C distances for the oxidative addition transition states in the C–H borylation reaction with 5-membered heterocycles and the BDE of C–H bonds in the substrates.



Compound	Borylation position	Exptl. product ratio	ΔG^\ddagger (kcal/mol)	ΔE^\ddagger (kcal/mol)	TS C–H length (Å)	TS Ir–C length (Å)	Reactant C–H BDE (kcal/mol)
3.7	2	100	19.3	6.8	1.615	2.206	116.6
	3	0	24.0	11.8	1.717	2.234	113.7
3.8	2	100	16.9	5.6	1.597	2.206	115.7
	3	0	22.0	9.2	1.648	2.248	113.7
3.9	2	92	19.8	8.1	1.597	2.179	118.3
	3	7	24.2	12.8	1.703	2.214	118.3
3.10	2	97	18.2	6.9	1.569	2.177	117.7
	3	3	21.3	8.6	1.612	2.217	118.3
3.11	2	99	20.9	8.2	1.749	2.201	118.1
	3	0	25.5	13.7	1.686	2.209	117.6
3.12	2	76	26.2	13.1	1.725	2.223	117.9
	3	24	26.0	13.7	1.683	2.207	117.4
3.13	2	100	19.7	4.3	1.639	2.209	117.4
	3	0	26.1	11.6	1.664	2.216	118.0

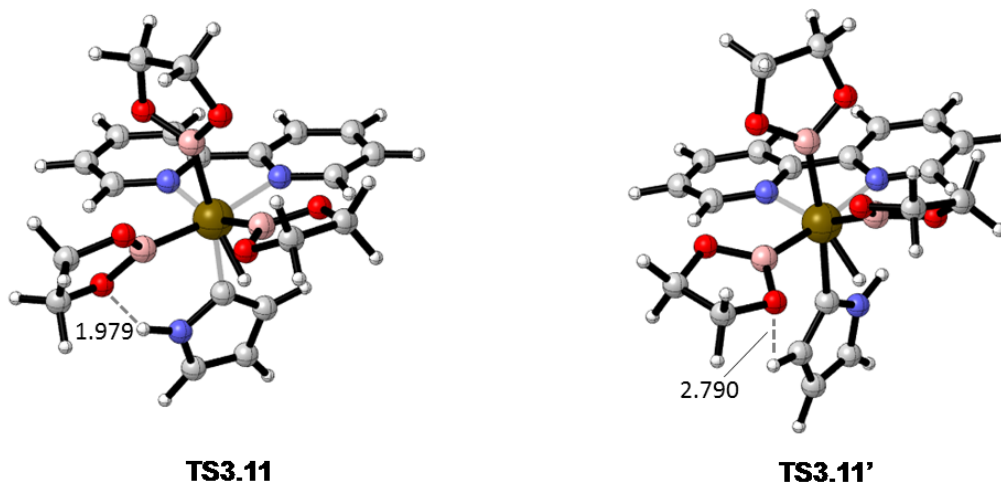


Figure 3.4: Transition state conformer for activation at the 2-position of **3.11**. **TS3.11'** does not exhibit hydrogen bonding.

Interestingly, the transition state of **3.12** is also late, even though hydrogen bonding cannot occur. This is likely due to steric repulsion with the methyl group on the nitrogen; the late transition state is stabilized by the favorable interaction of the metal and substrate at the electron-rich 2-position. The transition structure for the borylation of the 2-position of **3.13** does not exhibit hydrogen bonding and the transition state for the 2-borylation occurs earlier (1.64 Å) than in **3.11** or **3.12**.

Correlation between Activation Energy and Stability of the Aryl Palladium Hydride Intermediate. Recently, Smith, Maleczka, Singleton, and coworkers reported good correlation between the activation barrier (ΔE^\ddagger) and the energies of the intermediates after oxidative addition (ΔE_{rxn}) for iridium-catalyzed borylation reactions using the B3LYP/6-31G(d,p)-SDD method and (bpy)Ir(Beg)₃ as a model catalyst.¹⁶ The correlation is indicative of a late transition state according to the Hammond-Leffler postulate.^{43,44} The correlation is best when ΔE^\ddagger vs. ΔE_{rxn} is

plotted separately for arenes and heterocycles. We obtain similar results for **3.1-3.13** (Figure 3.5; $R^2 = 0.85$). The linear correlation increases dramatically when we do not include *N*-heterocycles in the analysis (Figure 3.6; $R^2 = 0.94$), similar to previous results.

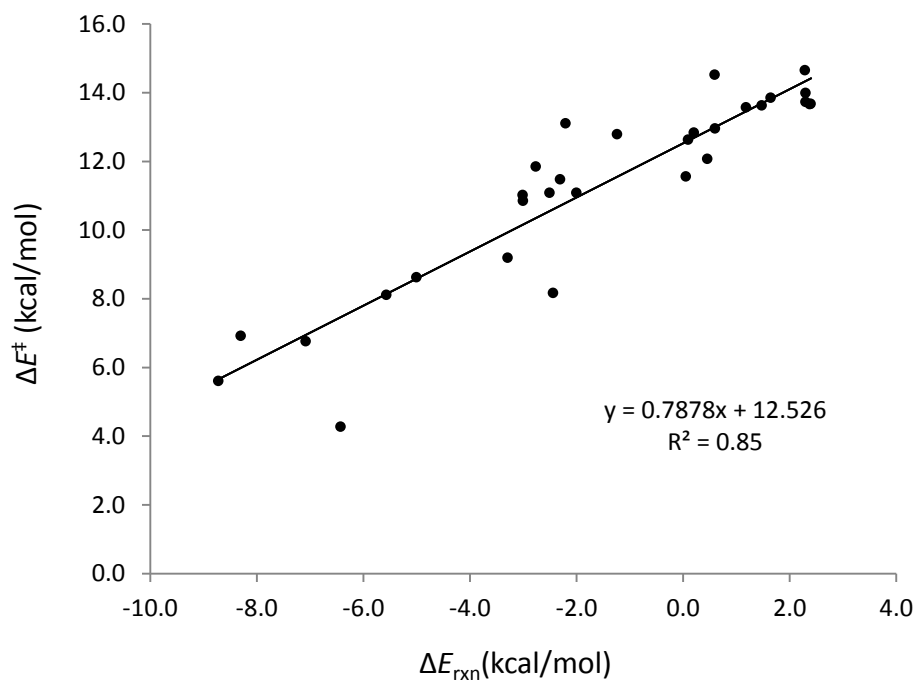


Figure 3.5: ΔE^\ddagger vs. ΔE_{rxn} for **3.1-3.13**.

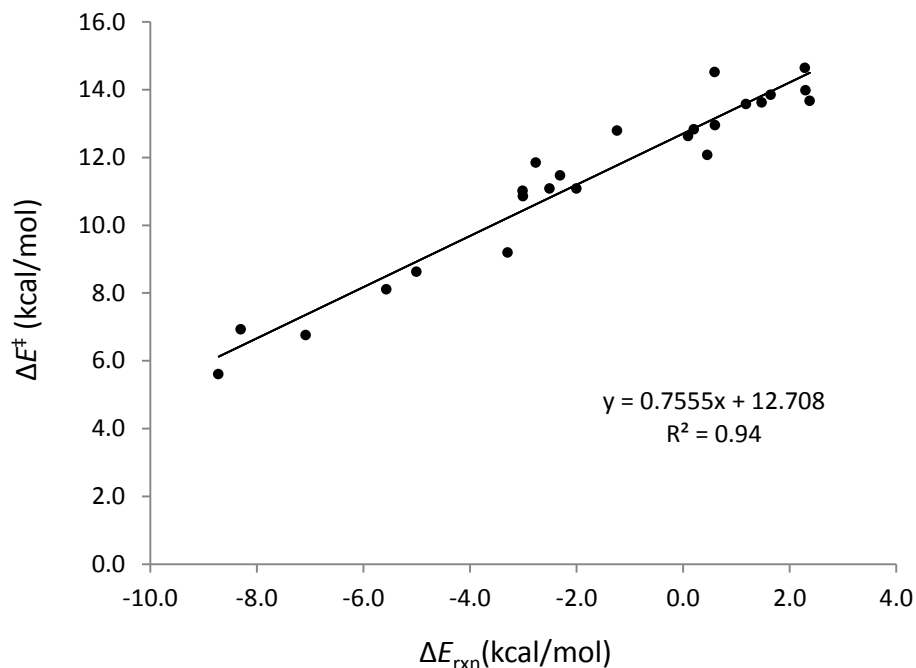


Figure 3.6: ΔE^\ddagger vs. ΔE_{rxn} for **3.1-3.10**.

Eisenstein *et al.* demonstrated that increasing Pd–aryl bond strengths in the product led to lower activation energies for Pd-catalyzed direct arylation of polyfluorinated benzenes which occurs through a concerted deprotonation-metalation (CMD) mechanism.¹⁷ While they noted a good correlation of the activation energy with pK_a , an even better correlation to Pd–aryl bond strengths was observed.¹⁷ We calculated the Ir–C BDEs for the intermediate products resulting from the C–H activation of **3.1-3.13**. A plot of ΔE^\ddagger vs. Ir–C BDE for substrates **3.1-3.13** shows a definitive trend between the activation energy and the strength of the forming Ir–C bond; the stronger the bond, the lower the activation energy (Figure 3.7). The linear relationship in Figure 3.7 is not great ($R^2 = 0.74$). This might be expected, since ΔE^\ddagger and Ir–C BDE represent properties of the transition state and the intermediate, respectively, and the correlation is affected by the position of the transition state on the reaction coordinate. However, the relative Ir–C BDE

of different regioisomeric products is a useful tool to predict regioselectivities of the C–H activations. The relative strengths of the Ir–C bonds correctly predicted the regioselectivities for C–H activations of all substrates studied (Table 3.4).

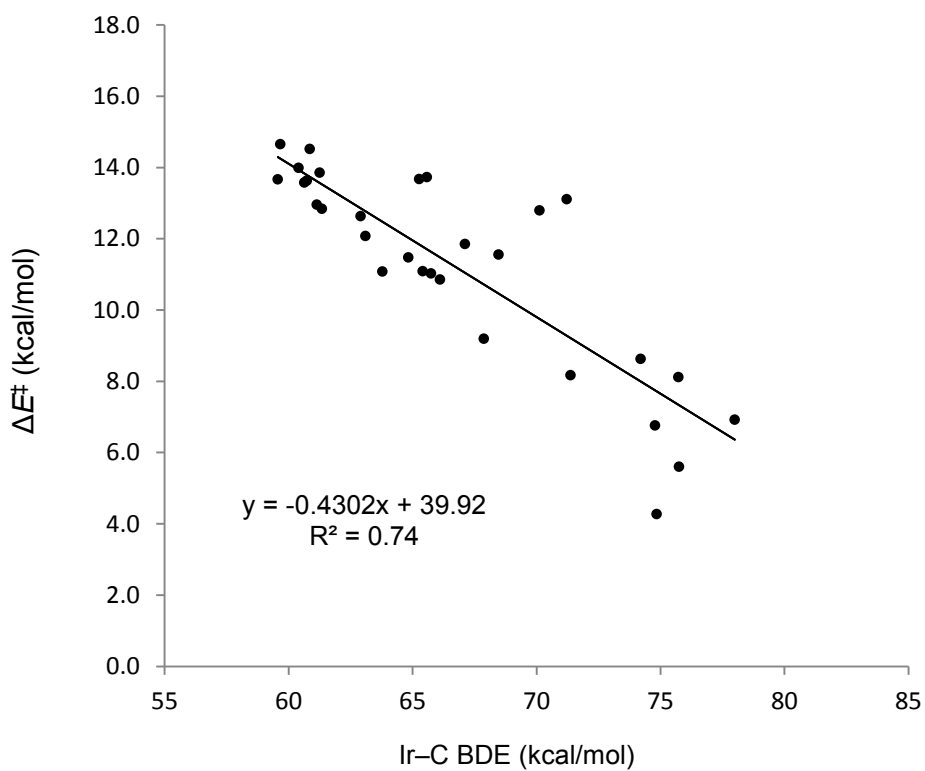


Figure 3.7: Plot for ΔE^\ddagger vs. Ir–C BDE for substrates **3.1-3.13**.

Table 3.4: Ir-Aryl BDEs and transition state energies for **3.1-3.13**.

Compound	ΔE^\ddagger (kcal/mol)	Ir-C BDE (kcal/mol)
Benzene	13.7	59.6
3.1	14.6	59.7
	13.6	60.6
	13.6	60.7
3.2	12.1	63.1
	11.0	65.8
	11.5	64.8
3.3	14.5	60.9
	12.8	61.4
	13.8	61.3
3.4	10.8	66.1
	11.1	65.4
3.5	14.0	60.4
	12.9	61.1
3.6	12.6	62.9
	11.1	63.8
3.7	6.8	74.8
	11.8	67.1
3.8	5.6	75.8
	9.2	67.9
3.9	8.1	75.7
	12.8	70.1
3.10	6.9	78.0
	8.6	74.2
3.11	8.2	71.4
	13.7	65.6
3.12	13.1	71.2
	13.7	65.3
3.13	4.3	74.9
	11.6	68.5

Distortion/Interaction Analysis of the Transition States of 3.1-3.13. We explored the origins of reactivities and regioselectivities in the C–H activations of different substrates **3.1-3.13** using the distortion/interaction model (Table 3.5). The $\Delta E^\ddagger_{\text{dist}}(\text{Ir cat.})$ is the energy to distort the

Ir and its ligands into the transition state geometry, while $\Delta E_{\text{dist}}^{\ddagger}(\text{arene})$ is the energy to distort the arene substrate into the transition state geometry. $\Delta E_{\text{int}}^{\ddagger}$ is the energy of interaction between these distorted fragments. The distortion energies of the iridium catalyst in all reactions are very similar, typically within ± 1 kcal/mol of that in the reaction with benzene (11.2 kcal/mol). Thus, the distortion of the catalyst does not noticeably affect the regioselectivities of C–H activation. The energy required to distort the aromatic substrates into the transition state geometry ($\Delta E_{\text{dist}}^{\ddagger}(\text{arene})$) correlates well with the C–H bond distance in the transition state (Figure 3.8, $R^2 = 0.92$), indicating that distortion energy is mainly controlled by the early or late location of the transition state on the reaction coordinate. The distortion energy does not correlate with either the activation energy or the regioselectivity. The distortion energy does not correlate well with the activation energy or the strength of the C–H bond in the substrate (See Figures 3.9 and 3.10). This indicates that substrate distortion is not the major factor that controls regioselectivities.

Table 3.5: Distortion/Interaction analysis for the oxidative addition transition states of **3.1-3.13**.

The activation energies, ΔE^\ddagger , the distortion energies of the iridium catalyst, $\Delta E^\ddagger_{\text{dist}}(\text{Ir cat.})$, the distortion energies of the substrate, $\Delta E^\ddagger_{\text{dist}}(\text{arene})$, and the interaction energies, $\Delta E^\ddagger_{\text{int}}$, are given in kcal/mol.

Substrate	Borylation position	ΔE^\ddagger	$\Delta E^\ddagger_{\text{dist}}(\text{Ir cat.})$	$\Delta E^\ddagger_{\text{dist}}(\text{arene})$	$\Delta E^\ddagger_{\text{int}}$	TS C-H length (Å)
Benzene	-	13.7	11.2	65.9	-63.4	1.672
	<i>o</i>	14.6	11.8	68.7	-65.9	1.742
3.1	<i>m</i>	13.6	10.1	66.0	-62.5	1.670
	<i>p</i>	13.6	11.2	66.0	-63.6	1.672
3.2	<i>o</i>	12.1	10.2	67.3	-65.4	1.676
	<i>m</i>	11.0	10.9	62.8	-62.8	1.640
3.3	<i>p</i>	11.5	11.0	63.1	-62.7	1.641
	<i>o</i>	14.5	11.0	67.4	-63.9	1.662
3.4	<i>m</i>	12.8	11.0	66.0	-64.2	1.676
	<i>p</i>	13.8	11.2	66.6	-64.0	1.680
3.5	4	10.8	10.8	63.0	-62.9	1.641
	5	11.1	10.7	61.8	-61.5	1.631
3.6	4	14.0	11.2	67.4	-64.6	1.688
	5	12.9	11.1	66.2	-64.3	1.674
3.7	4	12.6	10.9	64.5	-62.8	1.644
	5	11.1	10.9	63.7	-63.5	1.658
3.8	2	6.8	10.9	59.3	-63.5	1.615
	3	11.8	10.2	70.8	-69.2	1.717
3.9	2	5.6	10.8	57.5	-62.6	1.597
	3	9.2	10.6	64.3	-65.7	1.648
3.10	2	8.1	10.9	58.7	-61.5	1.597
	3	12.8	9.9	71.2	-68.3	1.703
3.11	2	6.9	10.8	56.0	-59.9	1.569
	3	8.6	10.6	61.0	-63.0	1.612
3.12	2	8.2	10.7	74.0	-76.5	1.749
	3	13.7	11.5	68.4	-66.2	1.686
3.13	2	13.1	10.3	72.8	-70.0	1.725
	3	13.7	11.7	68.1	-66.1	1.683
3.13	2	4.3	9.8	63.9	-69.4	1.639
	3	11.6	11.3	66.6	-66.3	1.664

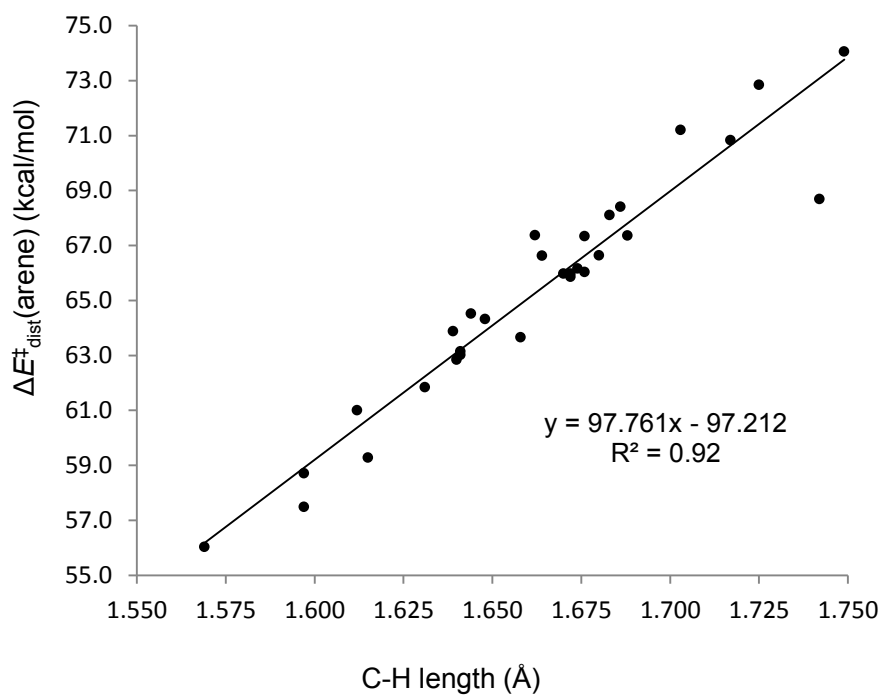


Figure 3.8: Plot of substrate distortion energy ($\Delta E_{\text{dist}}^{\ddagger}(\text{arene})$) versus the C–H bond length in the transition state for **3.1-3.13**.

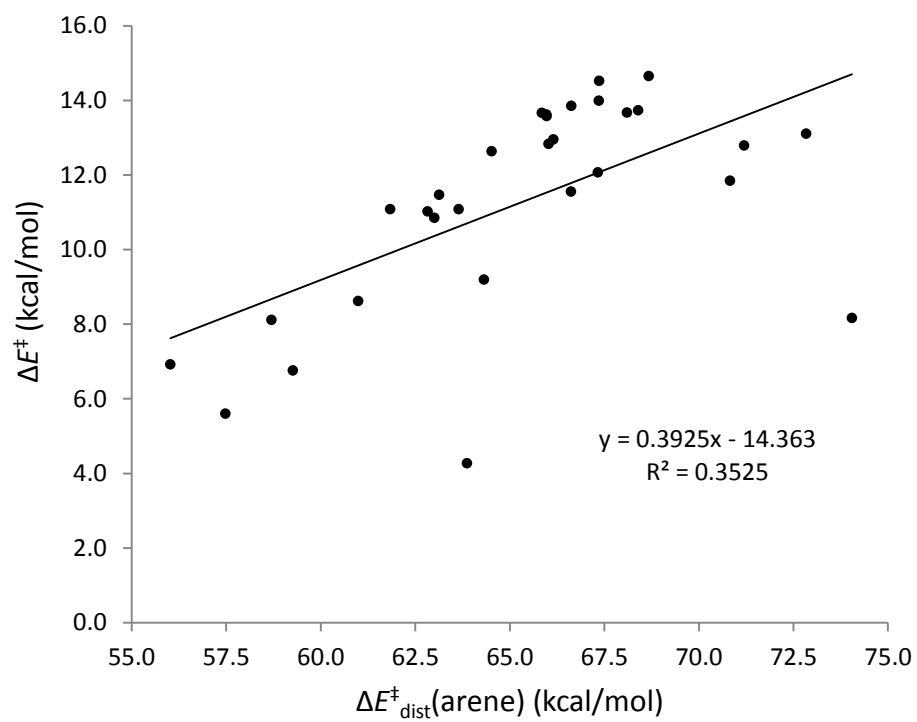


Figure 3.9: ΔE^\ddagger vs. $\Delta E^\ddagger_{\text{dist(arene)}}$ for 3.1-3.13.

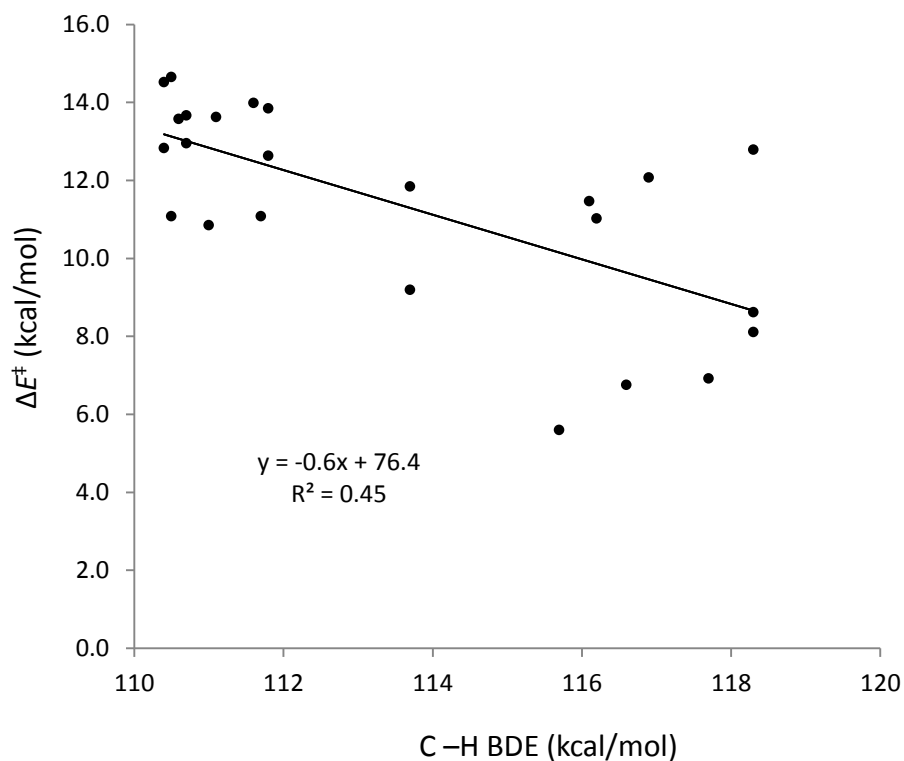


Figure 3.10: ΔE^\ddagger vs. C-H BDE for **3.1-3.13**.

There is no obvious correlation between the interaction energy and the activation energy, as the interaction energy between the substrate and the catalyst in the transition state is also affected by the early or late location of the transition state. For example, in the reaction with thiophene (**3.7**), the interaction energy for the C3-activation (-69.2 kcal/mol) is much greater than that for the C2-activation (-63.5 kcal/mol), although the C-H activation occurs exclusively at the 2-position. This is due to the much earlier transition state for C2-activation. Similarly, in reactions with heterocycles **3.8**, **3.9**, and **3.10**, interaction energies for C3-activations, which all involve earlier transition states, are greater than those for C2-activations. The trend is reversed in the reaction with pyrrole (**3.11**), in which the large interaction energy for the activation at the 2-

position (-76.6 kcal/mol) is partly due to hydrogen bonding of the N–H hydrogen with one of the oxygen atoms on an equatorial Beg ligand (O–H bond length of 1.98 Å) as mentioned previously. A higher energy conformer of the transition state was found that did not exhibit hydrogen bonding and the interaction energy (-66.8 kcal/mol) was similar to the interaction energy for activation at the 3-position (-66.2 kcal/mol).

In order to understand the effect of an early vs. late transition state on the distortion and interaction energies, we performed a distortion/interaction analysis along the reaction coordinate for C2 and C3-activations of thiophene (**3.7**) (Figure 3.11; for **3.1** and **3.6**, see Figure 3.12 and Figure 3.13, respectively). The data points for each geometry along the reaction coordinate were obtained by performing a relaxed scan of the breaking C–H bond from 1.350 Å to 1.900 Å in intervals of 0.025 Å. The total energy, distortion energy, and interaction energy for each point along the reaction paths were computed. As discussed earlier, the distortion energies of the iridium catalyst are very similar along the two different reaction paths, and thus are not plotted in Figure 3.11. The total energy curve along each reaction path is relatively flat in the transition state region. This explains why the locations of the transition states are easily affected by the C2 or C3-activations. In all three reactions investigated, the distortion energy becomes more positive and the interaction energy becomes more negative when increasing the breaking C–H bond length. At all points along the reaction coordinate with thiophene (**3.7**), the difference between distortion energies for the C2- and C3-activations is relatively small (<4 kcal/mol). However, at all points along the reaction coordinate, the interaction energy for the 2-activation is significantly greater than the 3-activation (>10 kcal/mol). Since the transition state for 2-borylation is much earlier than 3-borylation, the interaction energy of the 2-borylation TS is smaller than the 3-borylation TS (-63.5 and -69.2 kcal/mol for 2- and 3-positions, respectively). Nonetheless, the

dramatic difference of interaction energies between 2- and 3-activations along the reaction coordinate indicates the origin of the high selectivity of 2-borylation is the greater interaction energy between the catalyst and the substrate. This is a case that, as Bickelhaupt pointed out, simply using the interaction energies at the transition states is not adequate to describe the effects of distortions and interactions, due to the effects of different locations of the isomeric transition states on the reaction coordinate.³⁰ Similar results were obtained for substrates **3.1** and **3.6** (Figure 3.12 and Figure 3.13, respectively). These results indicate that Ir–substrate interaction energy is the driving factor in the respective selectivities for the C–H activation of **3.1-3.13**. This agrees with the correlation between activation energy and the Ir–Aryl bond strength discussed earlier.

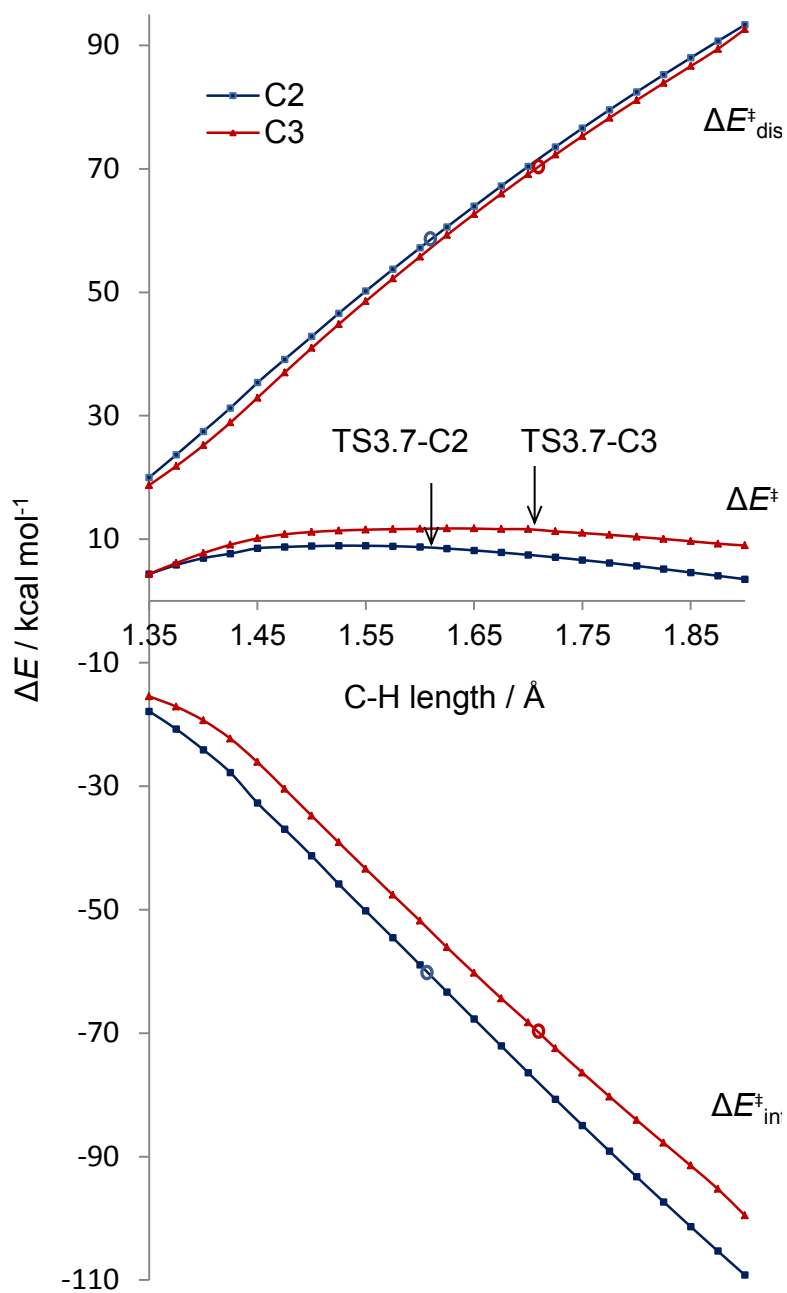


Figure 3.11: Energy (ΔE^\ddagger), distortion energy ($\Delta E^\ddagger_{\text{dist}}(\text{thiophene})$) and interaction energy of toluene ($\Delta E^\ddagger_{\text{int}}$) with the iridium complex as a function of the breaking C–H bond length in the reaction of **3.7**.

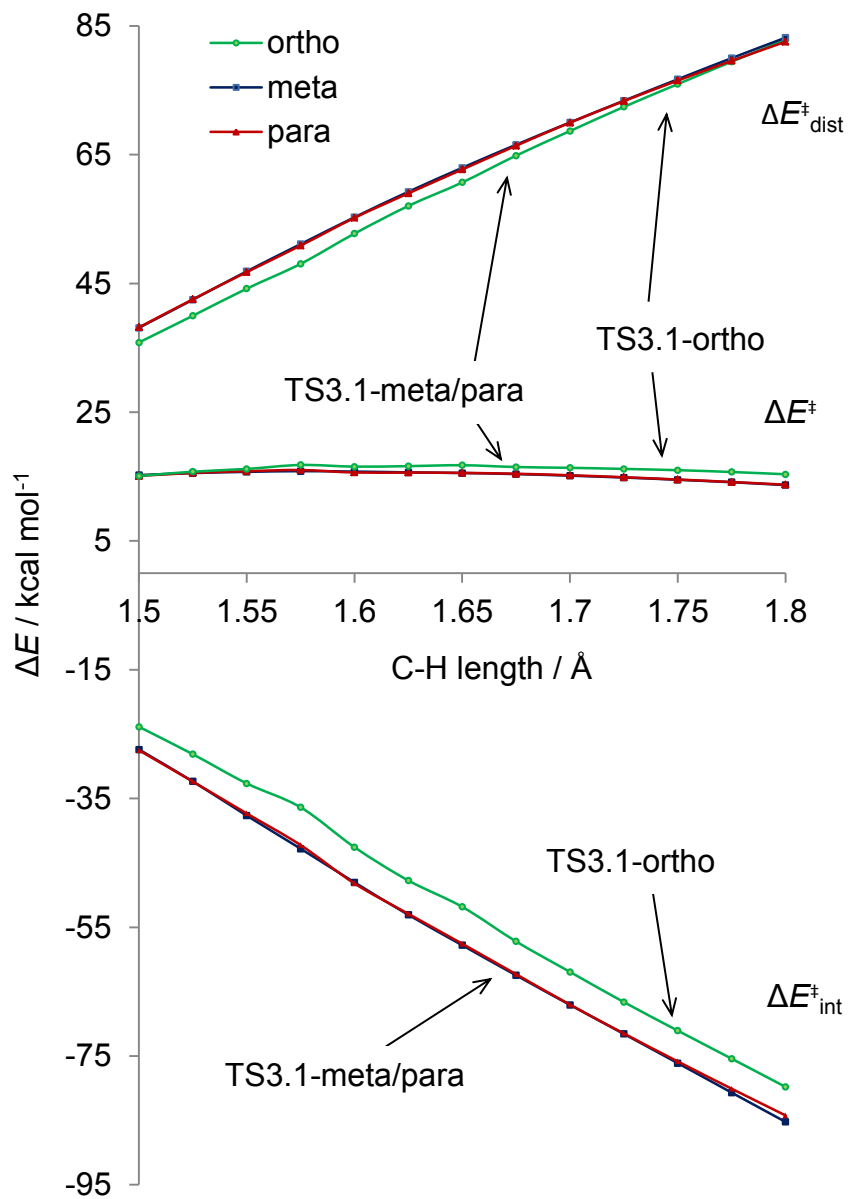


Figure 3.12: Energy (ΔE^{\ddagger}), distortion energy ($\Delta E_{\text{dist}}^{\ddagger}$ (toluene)) and interaction energy of toluene ($\Delta E_{\text{int}}^{\ddagger}$) with the iridium complex as a function of the breaking C–H bond length in the reaction of 3.1.

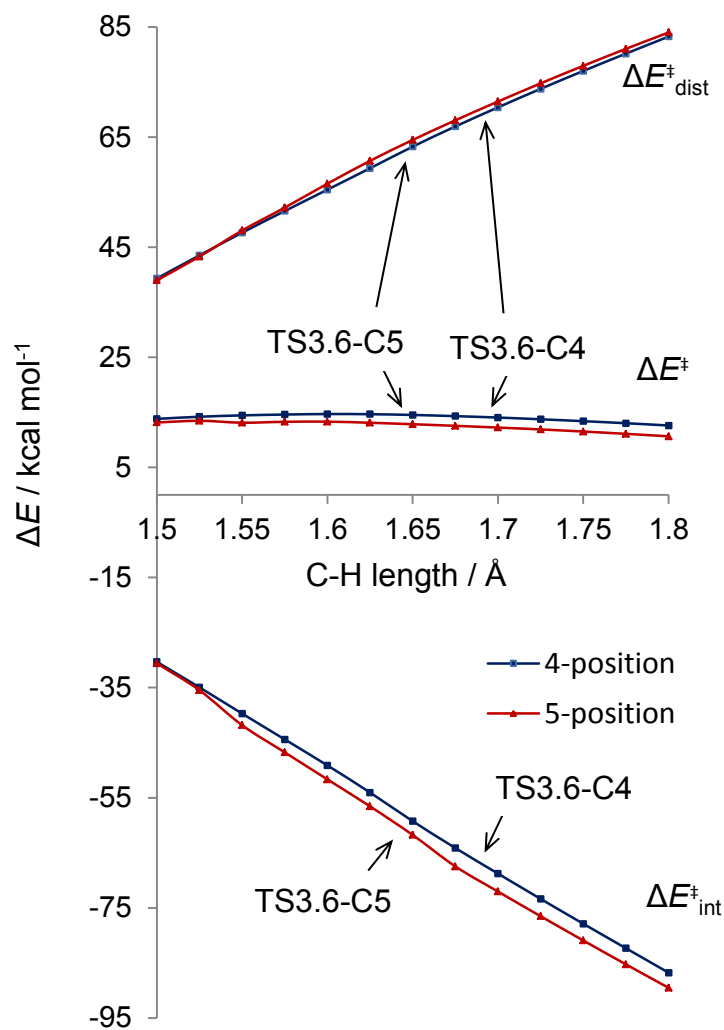


Figure 3.13: Energy (ΔE^\ddagger), distortion energy ($\Delta E^\ddagger_{\text{dist}}$ (acetoanisole)) and interaction energy of toluene ($\Delta E^\ddagger_{\text{int}}$) with the iridium complex as a function of the breaking C–H bond length in the reaction of **3.6**.

In order to understand the driving factors behind the interaction energy, we probed a number of different factors. Interaction energies have previously been explained on the basis HOMO-LUMO interactions between the substrate and the catalyst.²⁰ However, analysis of the

fragment orbital contributions between thiophene and Ir(bpy)(Beg)₃ shows that these interactions are complex (Figure 3.14) and simple arguments based on secondary orbital overlap are not feasible.

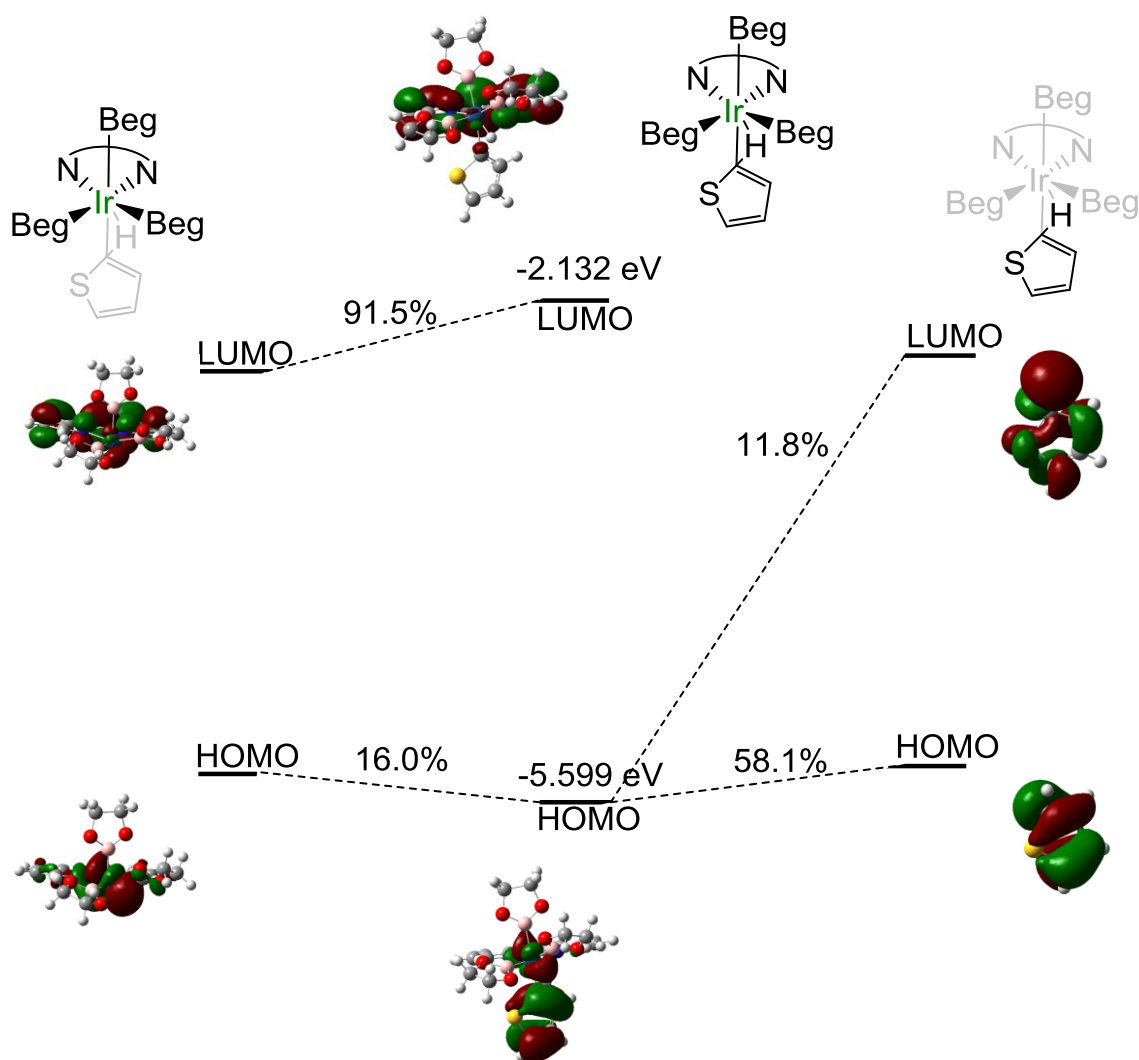


Figure 3.14: Fragment orbital analysis of the transition structure of 3.7 activated at the 2-position.

To quantify more directly how the iridium–aryl bonding interaction influences the activation energy, we calculated the TS Ir–C bond energies,¹⁸ ΔE_{tbe} , for **3.1-3.13**. Figure 3.15 illustrates how we define the TS Ir–C bond energies, following the approach of Ess.¹⁸ This involves calculation of the Ir–C bond energy at the transition state structure without geometry relaxation ($[\text{Ir}(\text{bpy})(\text{Beg})_3(\text{Ar})]^\ddagger \rightarrow [\text{Ir}(\text{bpy})(\text{Beg})_3\cdot]^\ddagger + [\text{Ar}\cdot]^\ddagger$). Figure 3.15 also shows a plot of ΔE^\ddagger vs. ΔE_{tbe} for the activation of all C–H bonds in arenes and heteroarenes **3.1-3.13**. There is a good linear correlation ($R^2 = 0.81$) between these values, which reveals that the Ir–C bonding interaction that develops along the reaction coordinate for C–H bond activation contributes significantly to stabilizing the TS and determines regioselectivity. Indeed, deviation from a perfect linear correlation is expected, due to the differences in early vs. late C–H activation on the reaction coordinate for the respective positions activated in **3.1-3.13**. There is no correlation between computed C–H BDEs and ΔE^\ddagger values (Figure 3.16), since it is the developing Ir–aryl bond and not the breaking of the C–H bond that determines relative barrier heights.

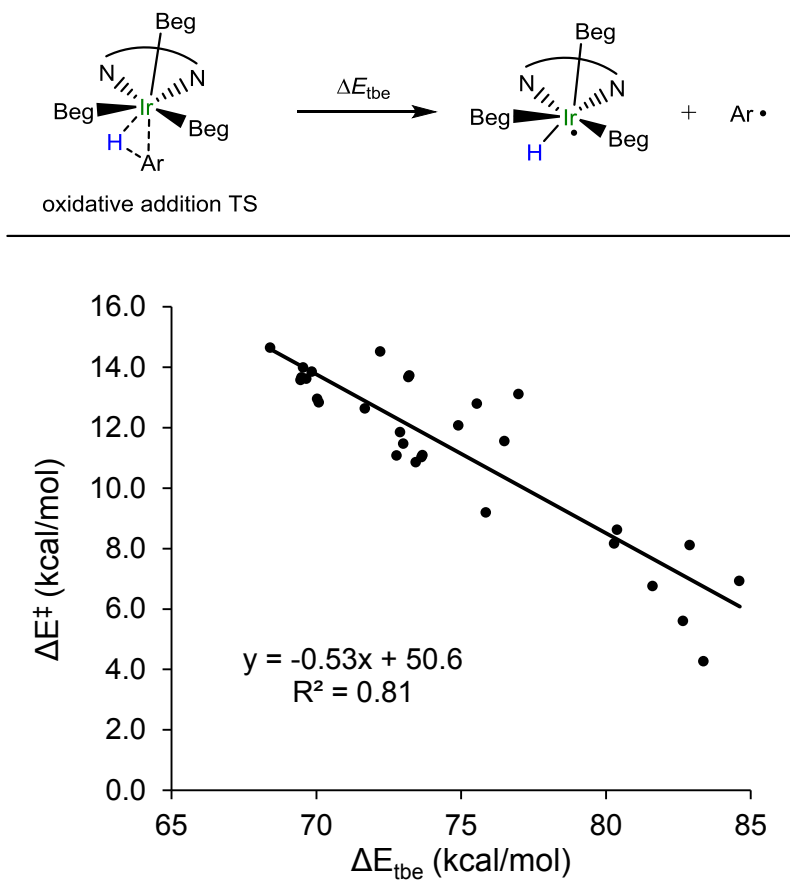


Figure 3.15. Plot of activation energy ΔE^\ddagger versus transition state Ir–C bond energy ΔE_{tbe} for reactions with 3.1-3.13.

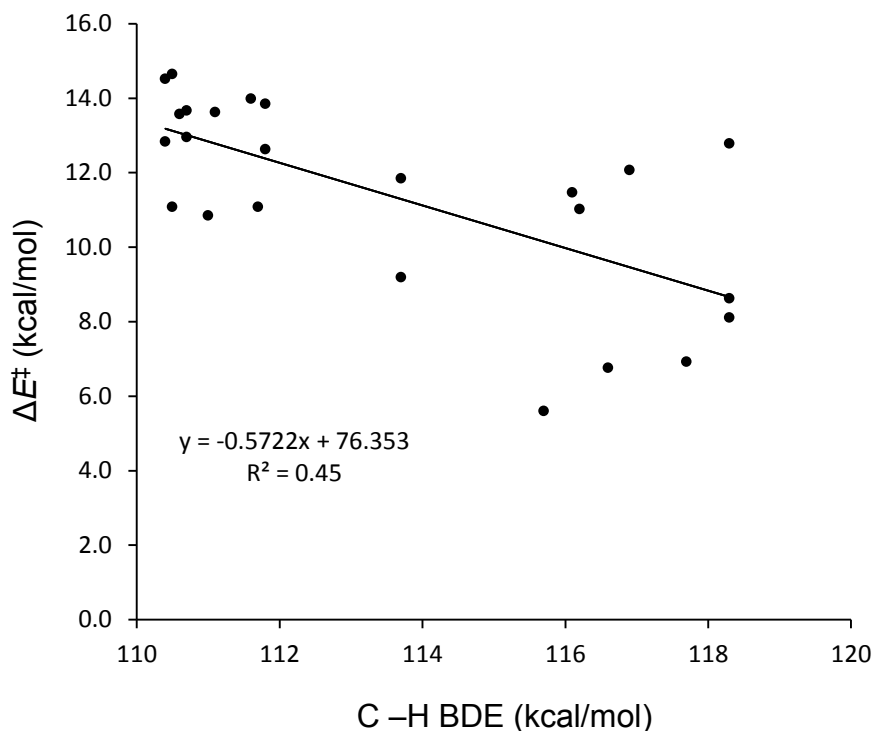


Figure 3.16: C–H BDE (B3LYP) vs. ΔE^\ddagger for **3.1-3.13**.

CONCLUSION:

We have studied the origins of regioselectivity in iridium-catalyzed C–H borylation reaction of substituted benzene rings and heterocycles. Distortion/interaction analyses show that regioselectivity is determined primarily by the interaction energy between the iridium catalyst and the substrate in the oxidative addition transition state. As a result, Ir–C bond energies in the aryl iridium hydride intermediates or in the C–H oxidative addition transition states both correlate well with the activation energy and can be used to determine the regioselectivity of the C–H activation reaction.

REFERENCES:

- (1) Godula, K.; Sames, D. *Science* **2006**, *312*, 67.
- (2) Davies, H. M. L.; Manning, J. R. *Nature* **2008**, *451*, 417.
- (3) Brown, H. C. *Organic Syntheses via Boranes*; Wiley: New York, 1975.
- (4) Pelter, A.; Smith, K.; Brown, H. C. *Borane Reagents*; Academic Press: Ann Arbor, 1988.
- (5) Ishiyama, T.; Miyaura, N. *Pure Appl. Chem.* **2006**, *78*, 1369.
- (6) Mkhaldid, I. A. I.; Barnard, J. H.; Marder, T. B.; Murphy, J. M.; Hartwig, J. F. *Chem. Rev.* **2010**, *110*, 890.
- (7) Hartwig, J. F. *Acc. Chem. Res.* **2012**, *45*, 864.
- (8) Boller, T. M.; Murphy, J. M.; Hapke, M.; Ishiyama, T.; Miyaura, N.; Hartwig, J. F. *J. Am. Chem. Soc.* **2005**, *127*, 14263.
- (9) Tamura, H.; Yamazaki, H.; Sato, H.; Sakaki, S. *J. Am. Chem. Soc.* **2003**, *125*, 16114.
- (10) Ishiyama, T.; Takagi, J.; Ishida, K.; Miyaura, N.; Anastasi, N. R.; Hartwig, J. F. *J. Am. Chem. Soc.* **2002**, *124*, 390.
- (11) Ishiyama, T.; Takagi, J.; Hartwig, J. F.; Miyaura, N. *Angew. Chem. Int. Ed.* **2002**, *41*, 3056.
- (12) Ishiyama, T.; Nobuta, Y.; Hartwig, J. F.; Miyaura, N. *Chem. Commun.* **2003**, 2924.
- (13) Tajuddin, H.; Harrisson, P.; Bitterlich, B.; Collings, J. C.; Sim, N.; Batsanov, A. S.; Cheung, M. S.; Kawamorita, S.; Maxwell, A. C.; Shukla, L.; Morris, J.; Lin, Z.; Marder, T. B.; Steel, P. G. *Chem. Sci.* **2012**.
- (14) Ishiyama, T.; Takagi, J.; Yonekawa, Y.; Hartwig, J. F.; Miyaura, N. *Adv. Synth. & Catal.* **2003**, *345*, 1103.
- (15) Takagi, J.; Sato, K.; Hartwig, J. F.; Ishiyama, T.; Miyaura, N. *Tetrahedron Lett.* **2002**, *43*, 5649.

- (16) Vanchura, I. I. B. A.; Preshlock, S. M.; Roosen, P. C.; Kallepalli, V. A.; Staples, R. J.; Maleczka, J. R. E.; Singleton, D. A.; Smith, I. I. I. M. R. *Chem. Commun.* **2010**, *46*, 7724.
- (17) Guihaume, J.; Clot, E.; Eisenstein, O.; Perutz, R. N. *Dalton Trans.* **2010**, *39*, 10510.
- (18) Petit, A.; Flygare, J.; Miller, A. T.; Winkel, G.; Ess, D. H. *Org. Lett.* **2012**, *14*, 3680.
- (19) Ess, D. H.; Houk, K. N. *J. Am. Chem. Soc.* **2007**, *129*, 10646.
- (20) Legault, C. Y.; Garcia, Y.; Merlic, C. A.; Houk, K. N. *J. Am. Chem. Soc.* **2007**, *129*, 12664.
- (21) Ess, D. H.; Houk, K. N. *J. Am. Chem. Soc.* **2008**, *130*, 10187.
- (22) Hayden, A. E.; Houk, K. N. *J. Am. Chem. Soc.* **2009**, *131*, 4084.
- (23) Schoenebeck, F.; Ess, D. H.; Jones, G. O.; Houk, K. N. *J. Am. Chem. Soc.* **2009**, *131*, 8121.
- (24) van Zeist, W.-J.; Bickelhaupt, F. M. *Org. Biomol. Chem.* **2010**, *8*, 3118.
- (25) Fernández, I.; Cossío, F. P.; Bickelhaupt, F. M. *J. Org. Chem.* **2011**, *76*, 2310.
- (26) Fernández, I.; Bickelhaupt, F. M. *J. Comp. Chem.* **2012**, *33*, 509.
- (27) Gorelsky, S. I.; Lapointe, D.; Fagnou, K. *J. Org. Chem.* **2011**, *77*, 658.
- (28) Gorelsky, S. I.; Lapointe, D.; Fagnou, K. *J. Am. Chem. Soc.* **2008**, *130*, 10848.
- (29) Usharani, D.; Lacy, D. C.; Borovik, A. S.; Shaik, S. *J. Am. Chem. Soc.* **2013**, *ASAP*.
- (30) de Jong, G. T.; Bickelhaupt, F. M. *ChemPhysChem* **2007**, *8*, 1170.
- (31) Benitez, D.; Tkatchouk, E.; Goddard III, W. A. *Chem. Commun.* **2008**, 6194.
- (32) Lin, M.; Kang, G.-Y.; Guo, Y.-A.; Yu, Z.-X. *J. Am. Chem. Soc.* **2011**, *134*, 398.
- (33) Zhou, M.; Balcells, D.; Parent, A. R.; Crabtree, R. H.; Eisenstein, O. *ACS Catal.* **2011**, *2*, 208.
- (34) Tang, S.-Y.; Guo, Q.-X.; Fu, Y. *Chem. Eur. J.* **2011**, *17*, 13866.
- (35) Yeom, H.-S.; Koo, J.; Park, H.-S.; Wang, Y.; Liang, Y.; Yu, Z.-X.; Shin, S. *J. Am. Chem. Soc.* **2011**, *134*, 208.

- (36) Liu, P.; Xu, X.; Dong, X.; Keitz, B. K.; Herbert, M. B.; Grubbs, R. H.; Houk, K. N. *J. Am. Chem. Soc.* **2012**, *134*, 1464.
- (37) Giri, R.; Lan, Y.; Liu, P.; Houk, K. N.; Yu, J.-Q. *J. Am. Chem. Soc.* **2012**, *134*, 14118.
- (38) Herbert, M. B.; Lan, Y.; Keitz, B. K.; Liu, P.; Endo, K.; Day, M. W.; Houk, K. N.; Grubbs, R. H. *J. Am. Chem. Soc.* **2012**, *134*, 7861.
- (39) Gaussian 09, Revision B.01, Frisch, M. J., et al. Gaussian, Inc., Wallingford CT, 2009.
- (40) Roosen, P. C.; Kallepalli, V. A.; Chattopadhyay, B.; Singleton, D. A.; Maleczka, R. E.; Smith, M. R. *J. Am. Chem. Soc.* **2012**, *134*, 11350.
- (41) Liskey, C. W.; Wei, C. S.; Pahls, D. R.; Hartwig, J. F. *Chem. Commun.* **2009**, 5603.
- (42) Hartwig, J. F. *Organotransition Metal Chemistry: From Bonding to Catalysis*; Univ. Science Books: Sausalito, 2010.
- (43) Leffler, J. E. *Science* **1953**, *117*, 340.
- (44) Hammond, G. S. *J. Am. Chem. Soc.* **1955**, *77*, 334.

CHAPTER 4: Defying Torquoselectivity in Cyclobutene Ring-Opening via Strain-Induced Thermal Selectivity

ABSTRACT:

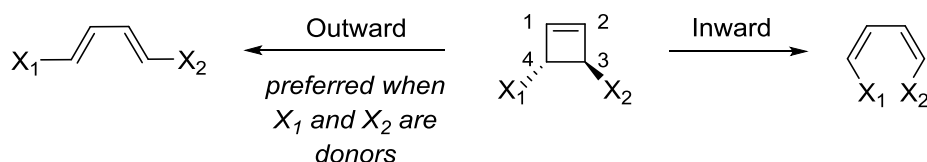
Outward ring-opening of donor substituted cyclobutene rings is preferred according the rules of torquoselectivity. However, results obtained by Byron Boon demonstrate that thermolysis of a bicyclic trans-cyclobutene resulted in the unexpected formation of (*Z,Z*)-1,3-diene product. Furthermore, computations revealed the (*Z,Z*)-1,3-diene product of inward ring-opening to be highly favorable under thermal conditions. Additional computations identified the feasibility of bicyclic trans-cyclobutenes containing either a sulfide or a sulfone linkage to undergo similar inward ring-opening electrocyclization reactions. The results show that the reversal of typically observed selectivity is due to the large ring-strain inherent in the (*E,E*)-1,3-diene macrocycles, which are the products of outward ring-opening. These results suggest a general strategy for the synthesis of cyclic (*Z,Z*)-1,3-dienes based on thermodynamic selectivity. We term this phenomenon strain-induced thermal selectivity.

INTRODUCTION:

Under thermal conditions, cyclobutenes are well known to form 1,3-dienes via conrotatory electrocyclic ring-opening.¹ For trans-substituted cyclobutenes with substituents at the 3- and 4- positions, two modes of ring-opening can occur: inward ring-opening to give the (*Z,Z*)-1,3-diene or outward ring-opening to give the (*E,E*)-1,3-diene (Scheme 4.1). Of the two

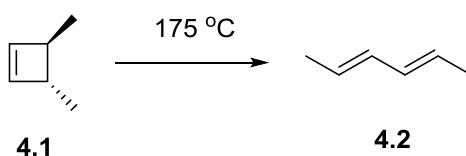
possible modes of ring-opening, however, only one is favored based on torquoselectivity.^{2,3} According to the rules of torquoselectivity developed by Houk,³⁻⁵ ring-opening of trans-3,4-cyclobutene rings containing donor substituents ($X = \text{CH}_3, \text{OR}, \text{halides}$) at the 3- and 4-positions favor outward rotation over inward rotation, while trans-3,4-cyclobutene rings containing accepting substituents [$X = \text{CHO}, \text{COOR}, \text{NO}, \text{SiR}_3, \text{B(OR)}_2$] favor inward rotation over outward rotation.^{2,6}

Scheme 4.1: Outward (favored) and inward (disfavored) ring-opening



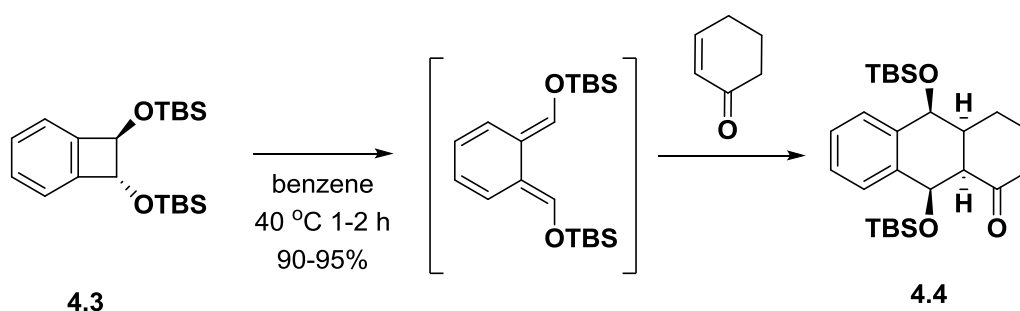
This preference for outward rotation provides an approach for stereoselective synthesis of substituted 1,3-dienes. In a seminal study, Winter showed that trans-3,4-dimethylcyclobutene **4.1** underwent clean isomerization to the outward ring-opening product (*E,E*)-2,4-hexadiene **4.2** (Scheme 4.2).⁷ In 1985, Houk computed the activation energy for outward rotation of **4.1** at the RHF/3-21G level of theory to be lower than inward rotation by 13 kcal/mol.²

Scheme 4.2: Thermal isomerization of trans-3,4-dimethylcyclobutene



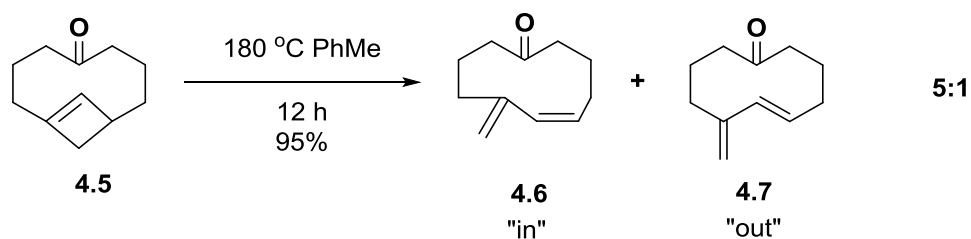
More recently, Danishefsky reported that upon the conrotatory thermal ring-opening of trans-1,2-disilyloxybenzocyclobutene **4.3** to form *ortho*-quinone dimethides, Diels-Alder cycloaddition with a range of dienophiles provided tetrahydronaphthalene products, such as **4.4**, in excellent yields (Scheme 4.3).

Scheme 4.3: Formation of tetrahydronaphthalene products via outward ring-opening of trans-cyclobutene 4.3



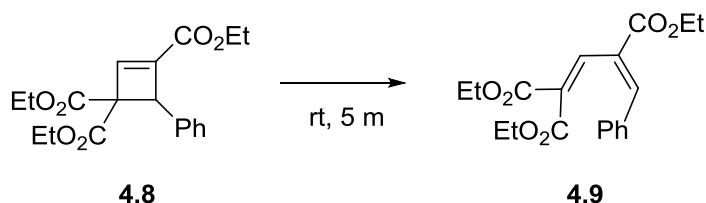
To date, no violations of the principle of torquoselectivity are known and the outward rotation product is always kinetically favored when the 3- and 4-positions of the cyclobutene ring contain donor substituents. There exist, however, several examples in the literature in which cyclobutenes ring-open to give the torquoselectively disfavored—but thermodynamically preferred—inward rotation products, particularly in the case of strained trans-3,4-cyclobutene rings containing alkyl substituents. In the 1980's, Schreiber and coworkers reported the electrocyclic ring-opening of bridgehead olefins as an access point to the germacranes.^{8,9} In a series of reactions starting from the bicyclic enone **4.5**, formation of the torquoselectively preferred “in” isomer **4.6** was obtained over the “out” isomer **4.7** in a 5:1 ratio (Scheme 4.4). The more energetic “out” isomers were able to be accessed by UV-irradiation of the “in” isomers.

Scheme 4.4: Stereoselective ring-opening of bicyclic cyclobutene 4.5 to give torquoselectively disfavored “in” product 4.6



In 2009, Tang et al. reported an unexpected inward rotation of donors in ring-opening reactions of triester cyclobutenes.¹⁰ For example, triester cyclobutene **4.8** ring-opens to give the product of inward “in” product **4.9** exclusively (Scheme 4.5). A subsequent computational study by Houk et al. showed that the rules of torquoselectivity are still upheld, but that the expected “out” product isomerized to the thermodynamically favored “in” product *in situ*.¹¹

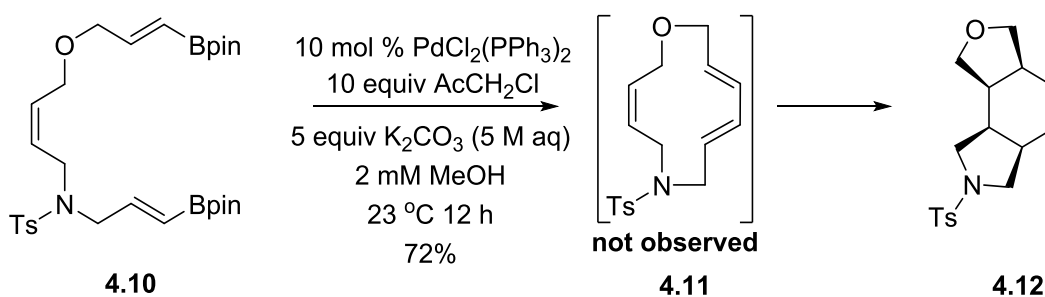
Scheme 4.5: Isolated product 4.9 upon ring-opening of cyclobutene triester 4.8



We recently developed Pd(II)-catalyzed intramolecular cross-coupling reactions of vinylboronate esters for the synthesis of macrocycles containing a 1,3-diene functionality.^{12,13} Carefully designed 1,3-diene products were sufficiently reactive to undergo electrocyclization reactions at room temperature without activating substituents. For instance, when we subjected the bis-vinylboronate **4.10** to our cross-coupling conditions at room temperature, the putative

1,3-diene intermediate **4.11** was not observed via NMR and we isolated only the trans-annular Diels-Alder (TADA) product **4.12** (Scheme 4.6). The large ring-strain in **4.11** drives the reaction thermodynamically and explains why **4.11**, the retro Diels-Alder product of **4.12**, is not observed. Thus, the strategic use of ring-strain can clearly lead to efficient reactions that avoid mixtures of products.

Scheme 4.6: Pd(II) cyclization of terminal bis-vinylboronate to give the TADA product 4.12



As an extension of this research, we reasoned that synthesis of sufficiently energetic 1,3-diene macrocycles that do not contain internal dienophiles would enable us access to interesting cyclobutene products. In particular, we have found that ring-opening of the subsequent cyclobutene rings occurs via strain-induced thermal selectivity (SITS) to give the fortuitous *Z,Z*-1,3-diene macrocycles arising from inward rotation. Herein, I describe my computational work related to this project.

COMPUTATIONAL METHODS:

For all structures, a conformational search was first performed using OPLS 2005¹⁴ (gas phase) with MacroModel 10.0^{15,16} packaged in the Maestro 9.5¹⁷ suite of software by Schrödinger, LLC. Geometries were optimized in the gas phase using the B3LYP/6-31G(d) level of theory. Frequency calculations (at 298.15 K) at the same level of theory were used to confirm the nature of all stationary points as minima or transition states and also provided values for computed free energies. Where applicable, single point calculations for energy comparisons and free energy profiles were performed using the M06/6-311++G(d,p) level of theory in the gas phase at 298.15 K. All geometry optimizations and single point calculations were performed with Gaussian 09.¹⁸

NMR simulations were performed using Tantillo's CHESHIRE suite of techniques, which have been successfully applied to calculate the chemical shifts and coupling constants of natural products.¹⁹⁻²¹ Various conformers of each structure studied were examined systematically and those lying within 2.5 kcal/mol relative to the lowest energy conformer were utilized in our predictions according to the Boltzmann weighted averages (based on relative free energies at 298.15 K). NMR single point calculations (GIAO) were performed on the B3LYP/6-31G(d) geometries at the mPW1PW91/6-311+G(d,p) level of theory in an implicit chloroform solvent continuum (CPCM, UAKS radii). Final predicted chemical shifts relative to TMS in CHCl₃ were obtained by applying linear regression parameters that have been previously determined.²²

RESULTS AND DISCUSSION:

The trans-substituted cyclobutene **4.1** was previously shown by Houk to undergo electrocyclic ring-opening via the outward ring-opening pathway.² In the original calculations, performed at the RHF level using the 3-21G basis set, the predicted energy for the outward ring-opening transition state was 40.4 kcal/mol. This value was higher than the experimental value of 30.6 ± 0.4 kcal/mol due to neglect of the correlation energy, which stabilizes the transition structures more than the reactants.^{23,24} The inward ring-opening transition state was found to be 13 kcal/mol higher in energy than the outward ring-opening transition state. The difference in energies is due to destabilizing interactions between the p-orbital of the donor substituent and the HOMO and LUMO of the cyclobutene transition structure when the donor rotates inwards.

We calculated both the outward and inward ring-opening of **4.1** to give **4.13** and **4.14**, respectively, at the M06/6-311++G(d,p)//B3LYP/6-31G(d) level of theory (Figure 4.1). The outward ring-opening product **4.13** was predicted to be 2.2 kcal/mol lower in energy than the inward ring-opening product **4.14**, and was 14.9 kcal/mol lower in energy than **4.1**. The activation energy for outward ring-opening of **4.1** via **TS4.1** was computed to be 29.4 kcal/mol and is 13.2 kcal/mol lower than the activation energy of the inward transition state **TS4.2**. The calculated activation energy for outward ring-opening of **4.1** is in excellent agreement with the experimentally obtained value of 30.6 ± 0.4 kcal/mol, confirming the validity of this method for future calculations.

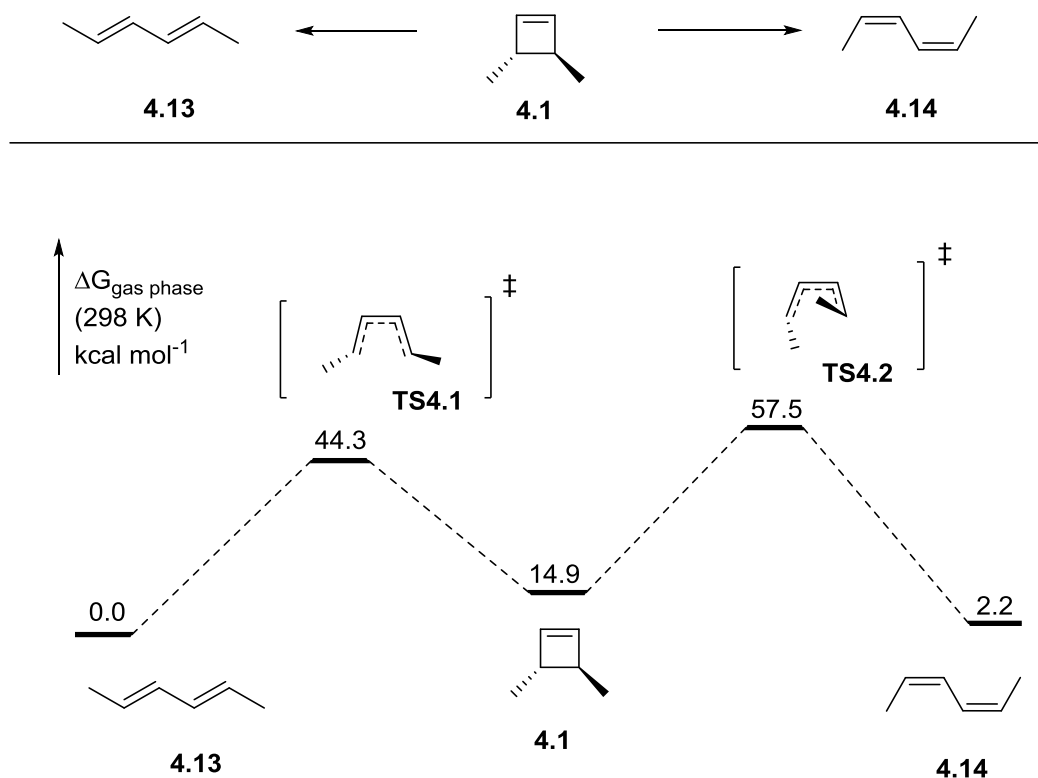


Figure 4.1: Computed free-energy surface for electrocyclic ring-opening of **4.1** to give either **4.13** or **4.14**.

We next turned to theory to gain an understanding of relative ring-strain in macrocyclic 1,3-dienes of different ring sizes and stereochemistries. Ring-strain energy was calculated as the heat of dehydrogenation of the parent acyclic α,ω diene to form the 1,3-diene ring and H_2 . We computed strain energies using DFT at the B3LYP/6-31G(d) level of theory. As a simple model, we chose to look at ring-strain energies for 9, 10 and 11-membered 1,3-cycloalkadiene rings in (*E,E*), (*E,Z*) and (*Z,Z*) stereoconfigurations.

Results of computations for nine macrocyclic 1,3-dienes **4.15-4.23** are shown in Figure 4.2. Analysis of the ring-strain energies led to several observations. First, energy increases in the

order $Z,Z < E,Z < E,E$ due primarily to increasing deformation of the 1,3-diene functionality. Second, we observed the highest ring strain energy for the 9-membered (E,E)-1,3-diene ring **4.15** (63 kcal/mol) and the lowest ring strain energies for the (Z,Z)-1,3-dienes **4.21-4.23** (15-16 kcal/mol). Finally, these results suggested that a broad range of ring-strain energies can be accessed within 9-, 10-, and 11-membered rings. At the low end of the spectrum are the less strained (E,Z)- and (Z,Z)-1,3-diene rings **4.19-4.23**. Intermediate ring-strain is found in rings **4.16-4.18**. On the highly strained end of the spectrum is the 9-membered (E,E)-1,3-diene ring **4.15**, which lies approximately 48 kcal/mol higher in energy than **4.21**.

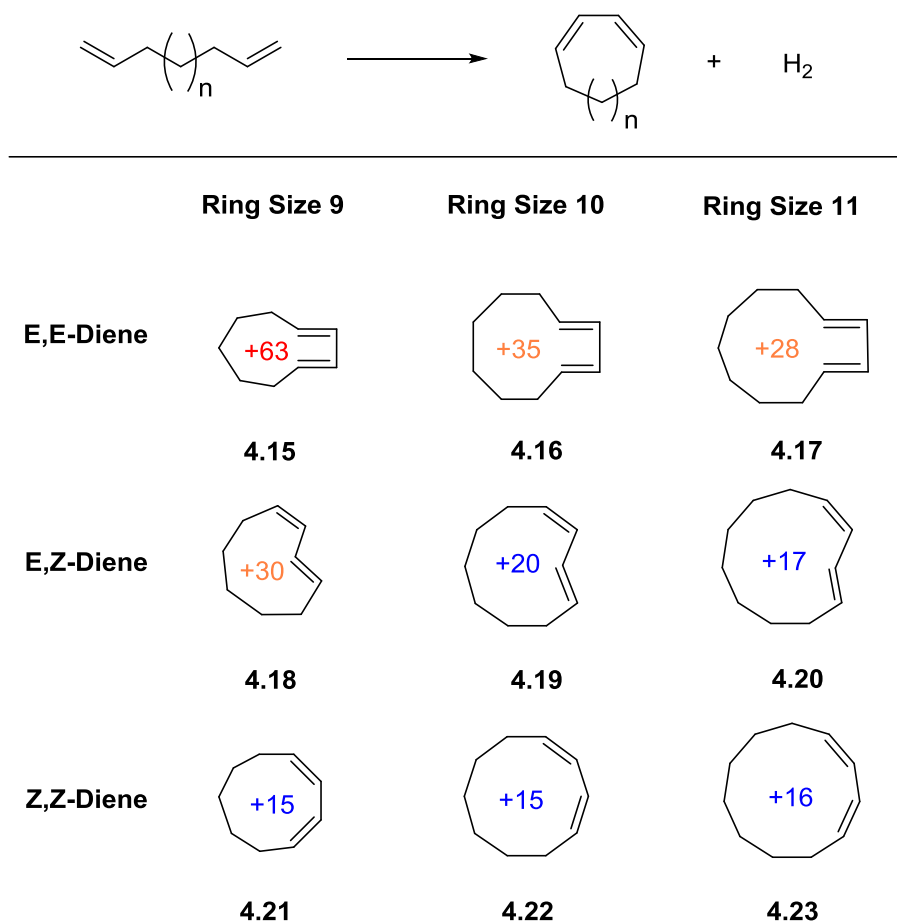
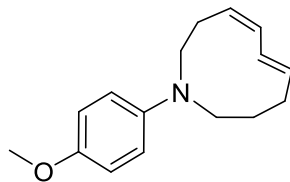


Figure 4.2: Predicted strain enthalpies (kcal/mol) of **4.15-4.23** relative to the parent acyclic diene (calculated at the B3LYP/6-31G(d) level of theory).

Based on these calculations, we decided to target a 10-membered ring for our initial studies. My colleague, Byron Boon, synthesized the following 10-membered (*E,Z*)-1,3-diene **4.24** (Figure 4.3), however, this product was found to be stable indefinitely at room temperature, suggesting that we needed to target rings with greater ring-strain (details of the synthesis, characterization and reactivity of this compound and others will be enumerated in Byron's dissertation).



4.24

Figure 4.3: Structure of 10-membered (*E,Z*)-1,3-diene **4.24**.

To target a macrocyclic 1,3-diene ring that would have higher strain energy, we aimed to synthesize the related 10-membered (*E,E*)-1,3-diene isomer **4.25** instead. When Byron attempted to synthesize **4.25** from the bisvinylboronate **4.26** using our Pd(II) cross-coupling procedure,^{12,13} he isolated what we believed to be either the *cis*- or the *trans*-bicyclic cyclobutene ring **4.27** or **4.28**, respectively (Figure 4.4).

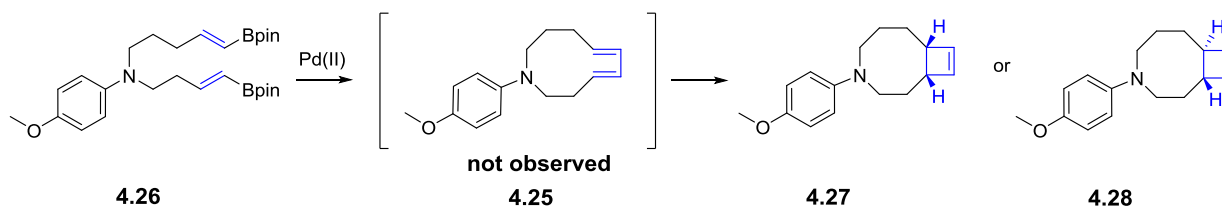


Figure 4.4: Attempted synthesis of a 10-membered (*E,Z*)-1,3-diene from a bisvinylboronate and the resulting possible cyclobutene products.

Determination of the stereochemistry of the bicyclic cyclobutene ring by NMR was complicated by conflicting literature data for the *cis*- and *trans*-coupling constants of the

bridgehead protons on cyclobutene rings containing alkyl substituents on the 3- and 4- positions. For example, in 1965, Roberts reported coupling constants for the allylic cis- and trans- protons of cyclobutene to be 1.65 Hz and 4.35 Hz, respectively;²⁵ however, in a computational study by Helgaker at the B3LYP/cc-pVXZ level of theory, cis- and trans- protons of cyclobutene were calculated to be 5.3 Hz and 2.1 Hz, respectively.²⁶ Since the observed allylic coupling constant was between 1-3 Hz, we were still unable to make an assignment of the configuration of the obtained product with confidence. Since recent computational predictions for chemical shifts²⁷ and coupling constants²¹ of organic compounds have proven valuable in elucidating stereochemical configurations of complex natural products, we decided NMR simulations of the model compounds **4.29** and **4.30** (Figure 4.5) would be useful in determining the configuration of the isolated material.



Figure 4.5: Structures of the desmethoxy model compounds **4.29** and **4.30**.

We performed conformational analyses on **4.29** and **4.30** in order to determine the energetically significant conformers for our NMR simulation. On one hand, the cis-cyclobutene **4.29** was found to have three low-energy conformers which contributed significantly to the

weighted Boltzmann average (Table 4.1). On the other hand, of the three conformers located for the trans-cyclobutene **4.30**, only one was predicted to be a significant contributor (Table 4.2).

Table 4.1: Free energies and weighted Boltzmann average contributions for conformers of the cis isomer **4.29** calculated using the B3LYP/6-31G(d) level of theory at 298.15 K.

Conformer	Rel. Free Energy (kcal/mol)	Contribution
1	“0”	~79%
2	+1.1	~12%
3	+1.3	~9%

Table 4.2: Free energies and weighted Boltzmann average contributions for conformers of the trans isomer **4.30** calculated using the B3LYP/6-31G(d) level of theory at 298.15 K.

Conformer	Rel. Free Energy (kcal/mol)	Contribution
1	“0”	~100%
2	+3.0	~0%
3	+3.6	~0%

The structures of the lowest energy conformers for **4.29** and **4.30** are shown in Figure 4.6 along with the relevant dihedral angles and coupling constants of the allylic protons. The small dihedral angle between the allylic protons of 2.0° for the cis-isomer **4.29** is consistent with a larger calculated 3J coupling constant of 4.1 Hz. The intermediate dihedral angle of 140.3° for the trans-isomer **4.30** is in agreement with the smaller calculated 3J coupling constant of 2.1 Hz. On the basis of these results, and in conjunction with our experimentally determined allylic

coupling constant of 1-3 Hz, we surmised that the compound Byron isolated was likely the trans-isomer, **4.28**. This would also be most consistent with its mechanism of formation (vide infra).

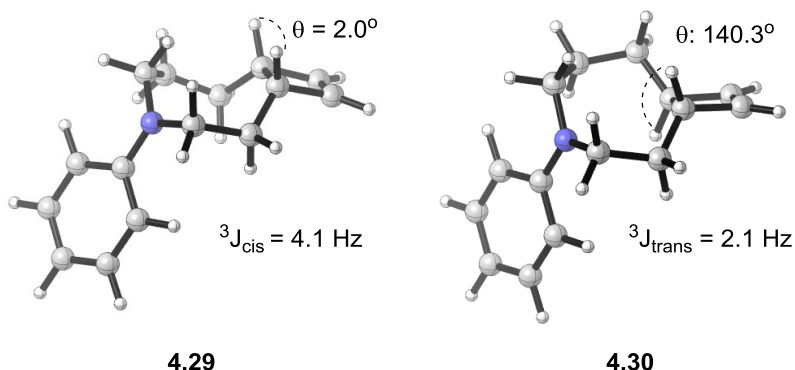


Figure 4.6: Predicted lowest energy structures, dihedral angles and relevant coupling constants for **4.29** and **4.30**.

We viewed **4.28** as the product of electrocyclic ring-closing of **4.25** and conducted further computations to support this hypothesis. To begin, we calculated relative energies of **4.29**, **4.30** and the cyclic (*E,E*)-, (*E,Z*)-, (*Z,E*)-, and (*Z,Z*)-1,3-dienes **4.31-4.34** (Figure 4.7). Upon analysis of the energies, we found an interesting result: The (*Z,Z*)-1,3-diene **4.34** was lower in energy than the (*E,E*)-1,3-diene **4.31** by 25.1 kcal/mol. This energy difference indicates a substantial thermodynamic preference for ring-opening of **4.30** to yield **4.34**. By comparison, the (*Z,E*)-1,3-diene **4.33** is only 0.8 kcal/mol lower in energy than the (*E,Z*)-1,3-diene **4.32**. These energies indicate by comparison that there is little thermodynamic preference for ring-opening of **4.29** to give either **4.32** or **4.33**.

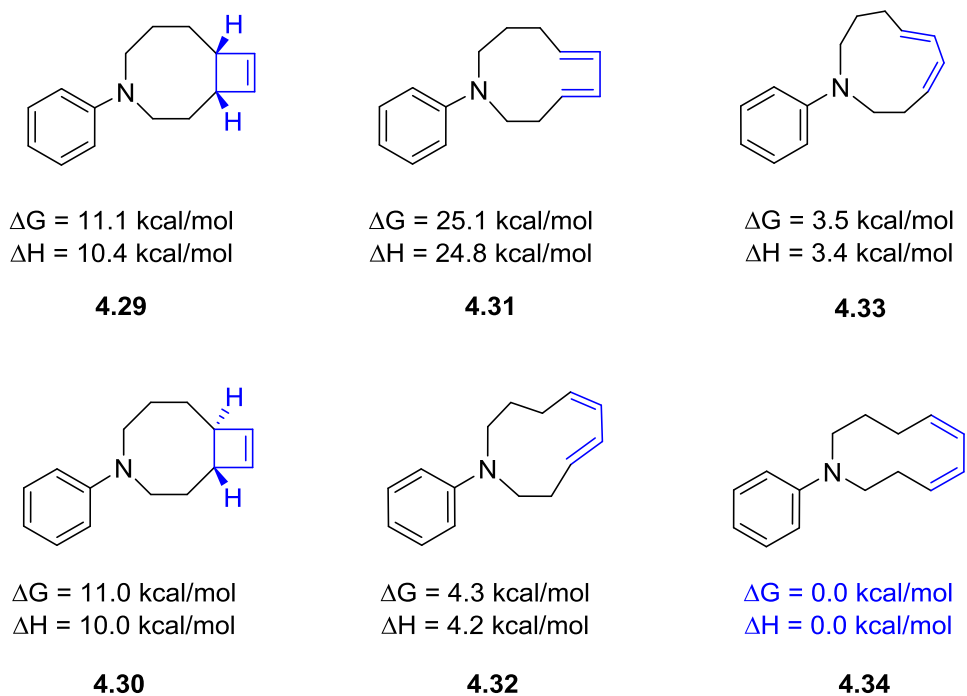


Figure 4.7: Structures and free energies for **4.29-4.34**.

Transition structures and energies were calculated for both the inward and outward ring opening of **4.30** and the full reaction coordinate diagram starting from the electrocyclic ring-closing of **4.31** is shown in Figure 4.8. Starting from **4.31**, the activation energy for electrocyclic ring-closing via **TS4.3** is low (20.4 kcal/mol), which explains why **4.25** was not observed under the reaction conditions. The trans-cyclobutene product **4.30** lies 14.1 kcal/mol lower in energy than **4.31**. Electrocyclic ring-opening of **4.30** occurs via **TS4.4** to give **4.34**. Both inward and outward ring-opening pathways for **4.30** are highly energetic with activation energies of 40.7 kcal/mol and 34.5 kcal/mol, respectively. The high activation energies for ring-opening in either direction explains why **4.28** was isolable and stable at room temperature. The results also show that the outward rotation pathway, which is predicted by torquoselectivity to be kinetically

preferred, is indeed lower in energy for the transition structure by 4.2 kcal/mol. However, given sufficient temperatures, equilibrium greatly favors the inward rotation product **4.34**.

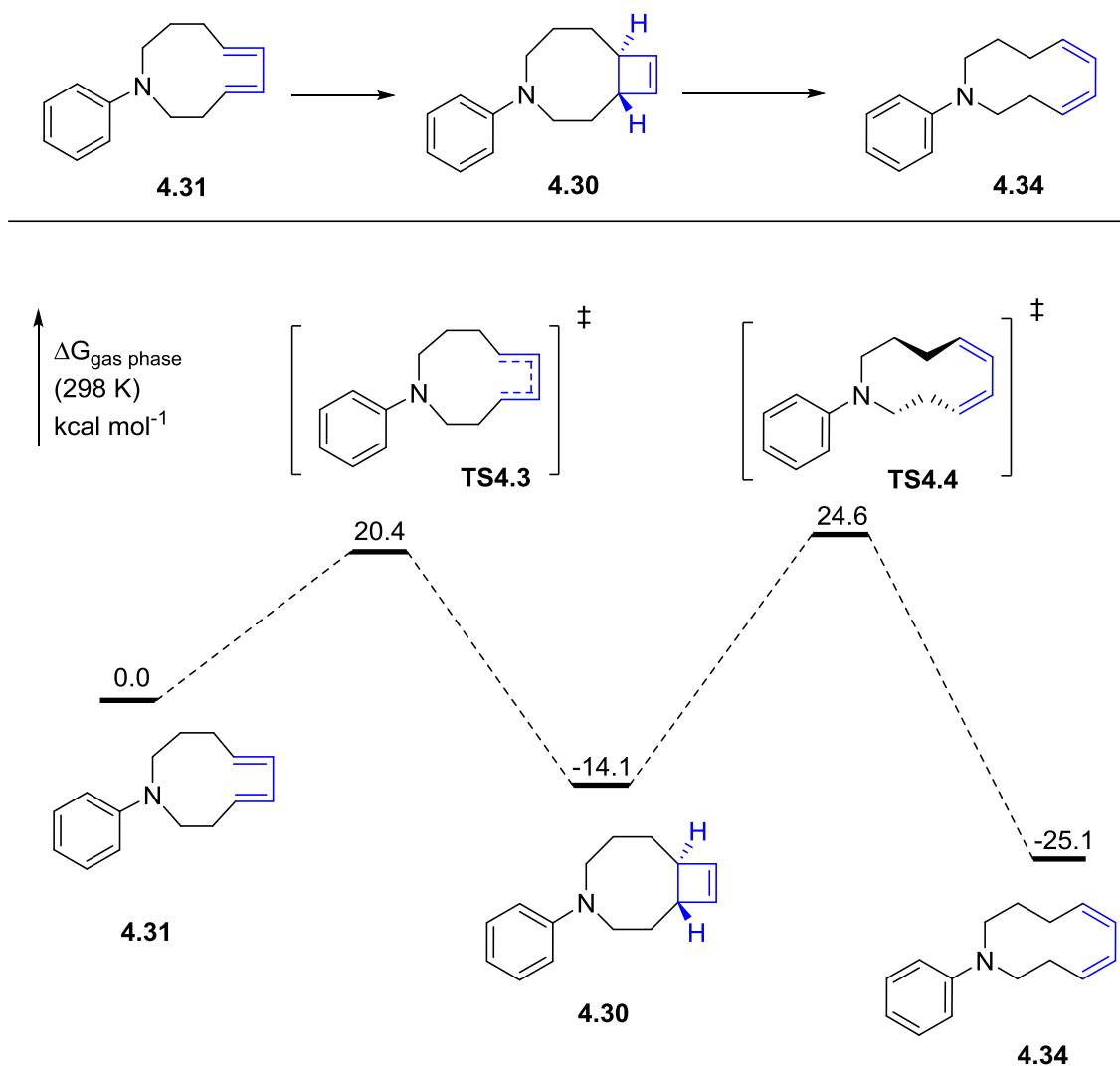


Figure 4.8: Computed free-energy surface for electrocyclic ring-closure of (*E,E*)-1,3-diene **4.31** to give the trans-cyclobutene product **4.30** and ring-opening of **4.30** to yield (*Z,Z*)-1,3-diene **4.34**.

The products and transition structures for the ring-opening of **4.30** are shown in Figure 4.9. C–C bond lengths for **4.31** and **4.34** are consistent with two conjugated double bonds. The experimental crystal structure of cyclobutene exhibits bond lengths of 1.571, 1.521, 1.521 and 1.335 Å for C₃–C₄, C₁–C₃, C₂–C₄ and C₁–C₂, respectively.²⁸ The calculated C–C bond lengths for the cyclobutene ring in **4.30** (1.583, 1.522, 1.520 and 1.340 Å for C₃–C₄, C₁–C₃, C₂–C₄ and C₁–C₂, respectively) are reasonable for a strained cyclobutene ring and elongation of the C₃–C₄ bond has been observed previously in substituted cyclobutenes.^{29,30} The outward ring-opening transition structure **TS4.3** differs markedly from the inward ring-opening structure **TS4.4**. Starting from **4.30**, ring opening to form **4.31** via **TS4.2** results in significant elongation of the cyclobutene C=C bond (1.397 Å) and shortening of the C–C bonds (1.416 and 1.415 Å) in the transition structure. By contrast, the transition structure **TS4.4** for the outward ring-opening of **4.30** represents an earlier transition state. For **TS4.4** the C=C length is 1.371 Å and the C–C bond lengths are 1.434 and 1.432 Å, respectively.

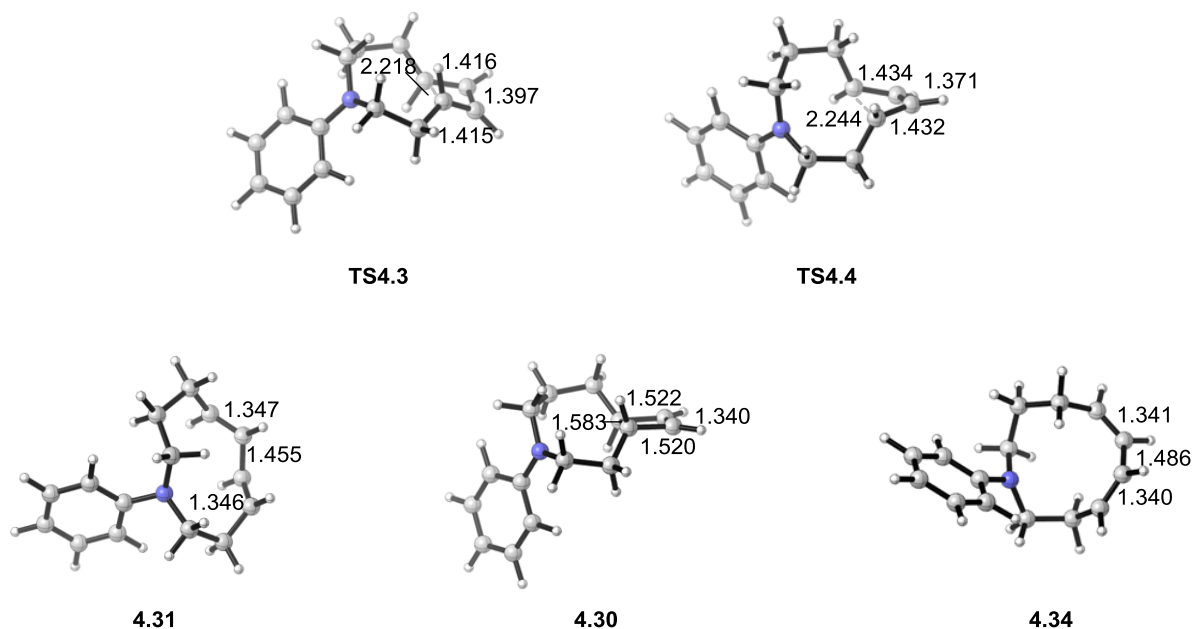


Figure 4.9: Structures and selected C–C bond lengths of **4.30**, **4.31**, **4.34**, **TS4.3** and **TS4.4**.

These computational results revealed that starting from **4.28** the inward ring-opening (*Z,Z*)-1,3-diene product **4.35** may be obtained experimentally. Byron devised a thermolysis experiment to heat **4.28** at high temperatures in decalin and obtain the inward ring-opening product **4.35**. The experiment was successful and we observed conversion of **4.28** to **4.35** exclusively by NMR.

Given the success of our computational model for predicting reactivity of 10-membered macrocyclic 1,3-dienes, we sought to find similar reactivity within the family of 9-membered rings. We observed from previous calculations that the 9-membered ring **4.15** had, by far, the largest ring strain. Attempts by Byron to synthesize a 9-membered (*E,E*)-1,3-diene, indeed, resulted in product decomposition, possibly due to the highly reactive nature of this molecule as a result of ring strain. Reasoning that ring strain could be reduced by increasing the lengths of

some of the intra-ring bonds, we investigated the use of sulfur as a component in the ring. At an average of length of 1.84 Å, S–C bonds are approximately 20% longer than the average C–C bond length (1.54 Å). Given that the 9-membered sulfur-containing bisvinylboronate **4.36** (Figure 4.10) is readily accessible, Pd(II) cross-coupling of **4.36** seemed like an excellent starting point for further investigations into SITS.

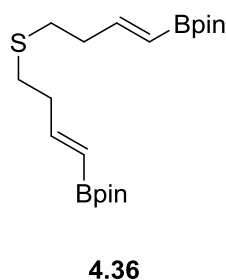


Figure 4.10: Structure of bisvinylboronate sulfide **4.36**.

We computed the reaction coordinate for the formation of the trans-cyclobutene ring **4.37** from the sulfur-containing (*E,E*)-1,3-diene **4.38** via **TS4.5** followed by inward ring-opening **TS4.6** to give the (*Z,Z*)-1,3-diene **4.39** (Figure 4.11). As in the case with the 10-membered ring **4.31**, the (*E,E*)-1,3-diene **4.38** contains significantly more ring-strain than the trans-cyclobutene or (*Z,Z*)-1,3-diene **4.39**. Trans-cyclobutene **4.37** and the inward ring-opening product **4.39** are more stable than **4.38** by 25.1 kcal/mol and 30.1 kcal/mol, respectively. Ring-closing from **4.38** to form **4.37** should be rapid at room temperature (15.2 kcal/mol). From **4.37**, outward ring-opening to form **4.38** is kinetically favored over inward ring-opening to give **4.39** by 2.4 kcal/mol. This is in agreement with the rules of torquoselectivity for a 3,4-disubstituted trans-

cyclobutene where the substituents are donors. Again, there is a substantial thermodynamic preference to form the (*Z,Z*)-1,3-diene **4.39** leading to thermodynamic selectivity favoring the inward rotation product.

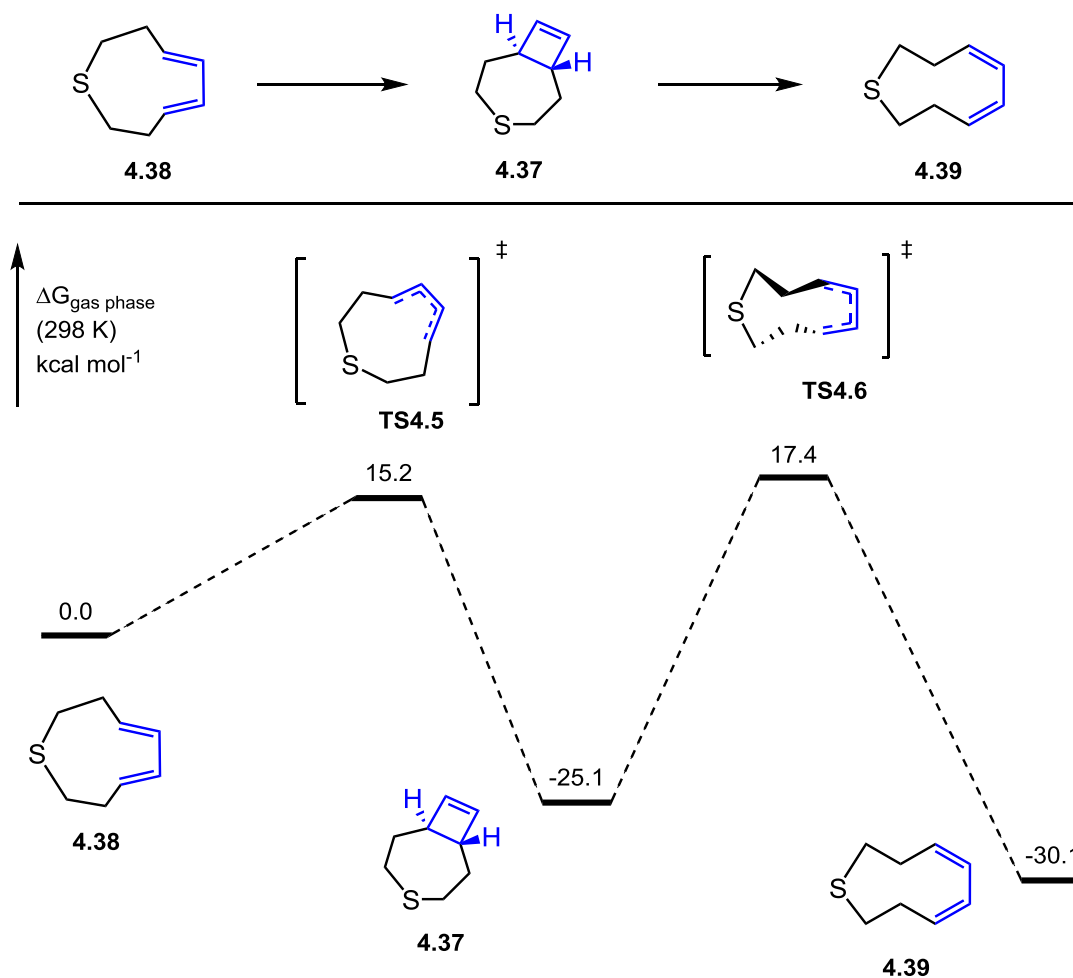


Figure 4.11: Computed free-energy surface for electrocyclic ring-closure of (*E,E*)-1,3-diene sulfide **4.38** to give the trans-cyclobutene product **4.37** and ring-opening of **4.37** to yield (*Z,Z*)-1,3-diene sulfide **4.39**.

The products and transition structures for ring-opening of the trans-cyclobutene ring **4.37** are shown in Figure 4.12. Similar to **4.31** and **4.34** discussed previously, C–C bond lengths for **4.38** (1.349, 1.459 and 1.349 Å) and **4.39** (1.342, 1.480 and 1.342 Å) are consistent with lengths for two conjugated double bonds. The C–C bond lengths for the cyclobutene carbons in **4.37** (1.573, 1.523, 1.522 and 1.342 Å) are similar to the previously discussed bond lengths for **4.30**. As before, the outward ring-opening transition structure **TS4.5** differs markedly from the inward ring-opening structure **TS4.6**. Starting from the trans-cyclobutene **4.37**, outward ring-opening to form the (*E,E*)-1,3-diene **4.38** results in significant elongation of the cyclobutene C=C bond (1.411 Å) and shortening of the C–C bonds (1.408 and 1.409 Å). In contrast, the transition structure **TS4.6** for the inward ring-opening of **4.37** represents an earlier transition state. The C=C length is 1.371 Å and the C–C bonds lengths are 1.433 and 1.433 Å, respectively.

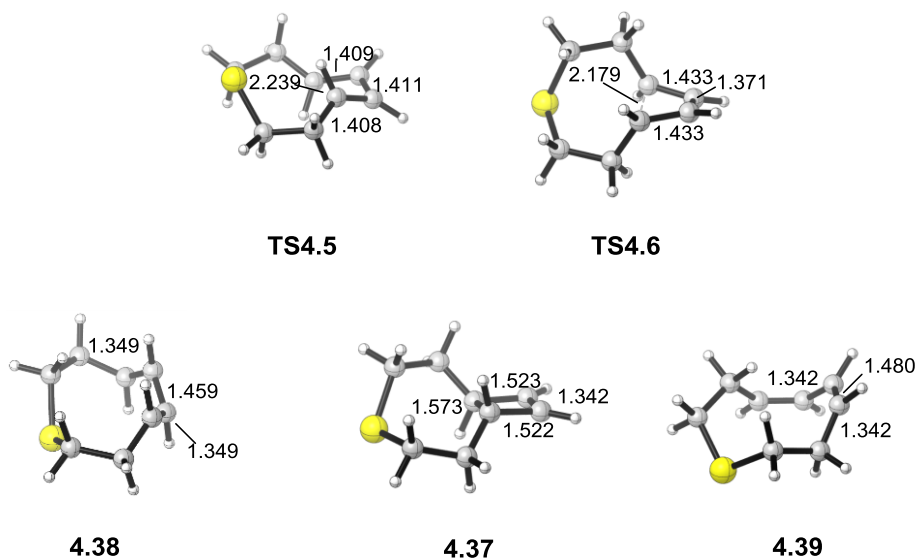


Figure 4.12: Structures and selected C–C bond lengths of **4.37**, **4.38**, **4.39**, **TS4.5** and **TS4.6**.

Given the proposed experimental conditions for the syntheses of **4.36** and **4.38**, there was concern that a sulfide-containing substrate might oxidize to the sulfone *in situ*. For this reason, we decided to calculate the ring-closing and ring-opening energies for the corresponding sulfone rings. Figure 4.13 illustrates the formation of the trans-cyclobutene ring **4.40** from the sulfone-containing (*E,E*)-1,3-diene **4.41** via **TS4.7** followed by inward ring-opening via **TS4.8** to give the (*Z,Z*)-1,3-diene **4.42**. Thermodynamic properties of the products are similar to those found for the sulfide rings; the (*E,E*)-1,3-diene **4.41** is higher in energy than the (*Z,Z*)-1,3-diene **4.42** by 32.9 kcal/mol. The activation energy for ring-closing from **4.41** to form **4.40** (14.0 kcal/mol) is lower than in the case of **4.38**. From **4.40**, outward ring-opening to form **4.41** is kinetically favored over inward ring-opening to give **4.42** by 2.1 kcal/mol. As seen in all previous cases, there is a substantial thermodynamic preference to form the (*Z,Z*)-1,3-diene **4.42** due to strain-induced thermodynamic selectivity which favors the inward rotation product upon electrocyclic ring-opening.

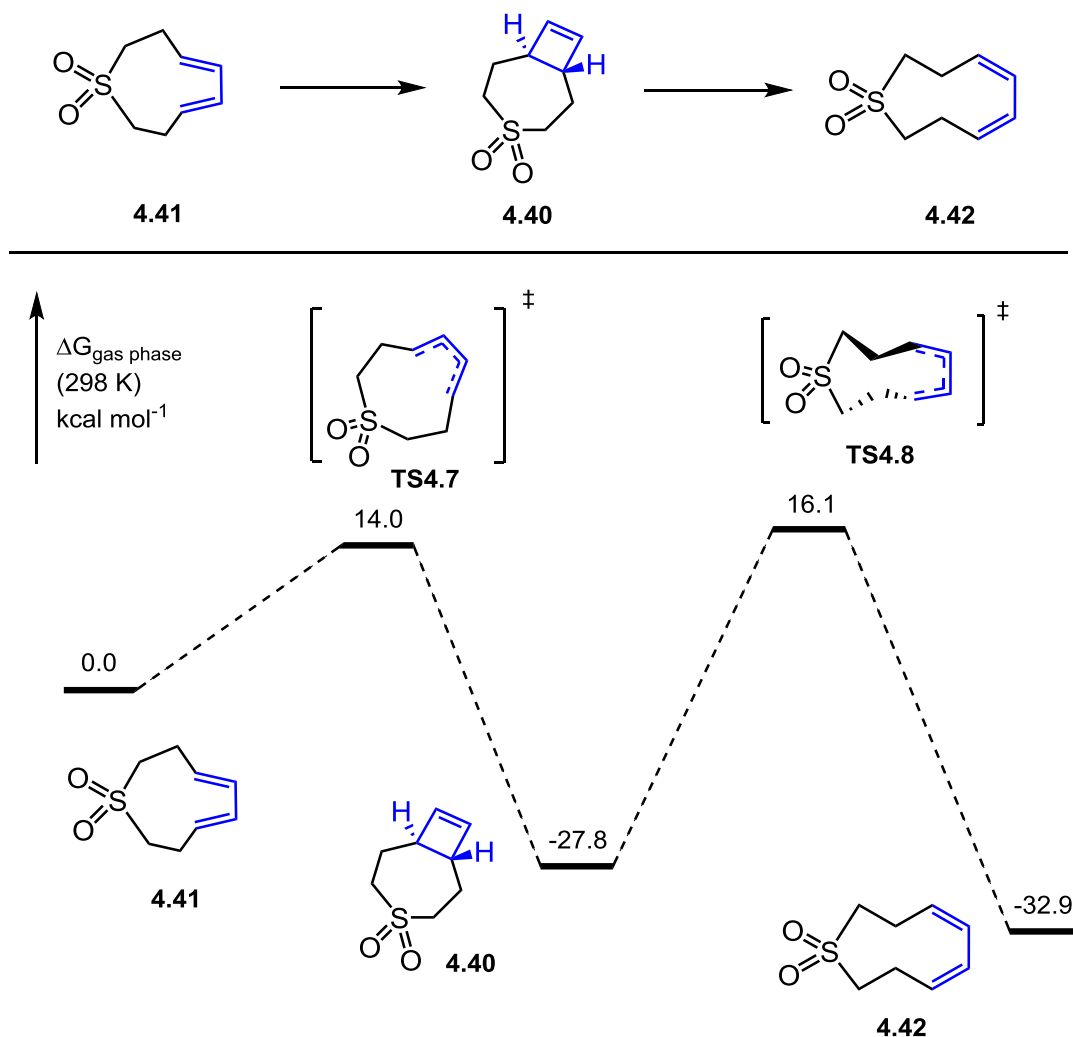


Figure 4.13: Computed free-energy surface for electrocyclic ring-closure of (*E,E*)-1,3-diene sulfone **4.41** to give the trans-cyclobutene product **4.40** and ring-opening of **4.40** to yield (*Z,Z*)-1,3-diene sulfone **4.42**.

Finally, products and transition structures for ring-opening of the trans-cyclobutene ring **4.40** are given in Figure 4.14. C–C bond lengths for **4.41** (1.349, 1.459 and 1.349 Å) and **4.42** (1.341, 1.478 and 1.341 Å) are, again, consistent with values for two conjugated double bonds and are nearly identical to the values for **4.38** and **4.39**. The C–C bond lengths for the

cyclobutene carbons in **4.40** (1.574, 1.523, 1.521 and 1.341 Å) are also nearly identical to **4.37**. Furthermore, the outward ring-opening transition structure **TS4.7** exhibits marked differences from the inward ring-opening structure **TS4.8**. Outward ring-opening from **4.40** to form the (*E,E*)-1,3-diene **4.41** results in significant elongation of the cyclobutene C=C bond (1.414 Å) and shortening of the C–C bonds (1.406 and 1.406 Å). Transition structure **TS4.8** for the inward ring-opening of **4.40** represents an earlier transition state. The C=C length is 1.369 Å and the C–C bonds lengths are 1.434 and 1.433 Å, respectively.

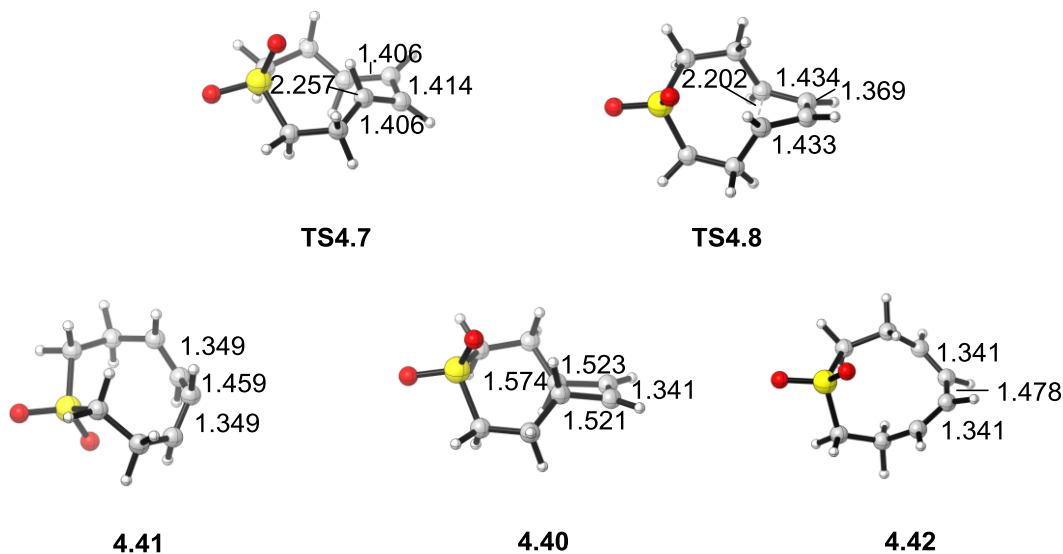


Figure 4.14: Structures and selected C–C bond lengths of **4.40**, **4.41**, **4.42**, **TS4.7** and **TS4.8**.

CONCLUSION:

In summary, we performed computations on a series of macrocyclic 1,3-dienes and bicyclic cyclobutene rings. Attempted synthesis of 10-membered (*E,E*)-1,3,-diene **4.25** resulted in the isolation of the ring-closed trans-cyclobutene product **4.28**. NMR simulations on model compounds **4.29** and **4.30** assisted in assigning the trans configuration to **4.28**. Computations on **4.30** revealed that the (*Z,Z*)-1,3-diene product of inward ring-opening **4.33** should be accessible under thermal conditions. Subsequent thermolysis of **4.28** led to formation of the inward ring-opening (*Z,Z*)-1,3-diene product **4.35** on the basis of NMR, confirming computational predictions. Further computations identified the feasibility of 9-membered rings containing either a sulfide or a sulfone linkage to undergo similar inward ring-opening electrocyclization reactions. We observed that thermodynamic selectivity is imparted on these reactions due to the large ring-strain inherent in the (*E,E*)-1,3-diene macrocycles. We term this phenomenon strain-induced thermal selectivity (SITS). Future work will involve identifying useful applications of this methodology.

REFERENCES:

- (1) Woodward, R. B.; Hoffmann, R. *J. Am. Chem. Soc.* **1965**, *87*, 395.
- (2) Kirmse, W.; Rondan, N. G.; Houk, K. N. *J. Am. Chem. Soc.* **1984**, *106*, 7989.
- (3) Rondan, N. G.; Houk, K. N. *J. Am. Chem. Soc.* **1985**, *107*, 2099.
- (4) Dolbier, W. R.; Koroniak, H.; Houk, K. N.; Sheu, C. *Acc. Chem. Res.* **1996**, *29*, 471.

- (5) Niwayama, S.; Kallel, E. A.; Spellmeyer, D. C.; Sheu, C.; Houk, K. N. *J. Org. Chem.* **1996**, *61*, 2813.
- (6) Branton, G. R.; Frey, H. M.; Skinner, R. F. *Trans. Faraday Soc.* **1966**, *62*, 1546.
- (7) Winter, R. E. K. *Tetrahedron Lett.* **1965**, *6*, 1207.
- (8) Schreiber, S. L.; Santini, C. *Tetrahedron Lett.* **1981**, *22*, 4651.
- (9) Schreiber, S. L.; Santini, C. *J. Am. Chem. Soc.* **1984**, *106*, 4038.
- (10) Xu, H.; Zhang, W.; Shu, D.; Werness, J. B.; Tang, W. *Angew. Chem. Int. Ed.* **2008**, *47*, 8933.
- (11) Um, J. M.; Xu, H.; Houk, K. N.; Tang, W. *J. Am. Chem. Soc.* **2009**, *131*, 6664.
- (12) Iafe, R. G.; Chan, D. G.; Kuo, J. L.; Boon, B. A.; Faizi, D. J.; Saga, T.; Turner, J. W.; Merlic, C. A. *Org. Lett.* **2012**, *14*, 4282.
- (13) Iafe, R. G.; Kuo, J. L.; Hochstatter, D. G.; Saga, T.; Turner, J. W.; Merlic, C. A. *Org. Lett.* **2013**, *15*, 582.
- (14) Banks, J. L.; Beard, H. S.; Cao, Y.; Cho, A. E.; Damm, W.; Farid, R.; Felts, A. K.; Halgren, T. A.; Mainz, D. T.; Maple, J. R.; Murphy, R.; Philipp, D. M.; Repasky, M. P.; Zhang, L. Y.; Berne, B. J.; Friesner, R. A.; Gallicchio, E.; Levy, R. M. *J. Comp. Chem.* **2005**, *26*, 1752.
- (15) Mohamadi, F.; Richards, N. G. J.; Guida, W. C.; Liskamp, R.; Lipton, M.; Caufield, C.; Chang, G.; Hendrickson, T.; Still, W. C. *J. Comp. Chem.* **1990**, *11*, 440.
- (16) **Schrödinger Release 2013-1**: MacroModel, 10.0, Schrödinger, LLC, New York, NY, 2013.
- (17) **Schrödinger Release 2013-1**: Maestro, 9.5, Schrödinger, LLC, New York, NY, 2013.
- (18) Gaussian 09, Revision C.01, Frisch, M. J.; Trucks, G. W.; Schlegel, H. B.; Scuseria, G. E.; Robb, M. A.; Cheeseman, J. R.; Scalmani, G.; Barone, V.; Mennucci, B.; Petersson, G. A.;

Nakatsuji, H.; Caricato, M.; Li, X.; Hratchian, H. P.; Izmaylov, A. F.; Bloino, J.; Zheng, G.; Sonnenberg, J. L.; Hada, M.; Ehara, M.; Toyota, K.; Fukuda, R.; Hasegawa, J.; Ishida, M.; Nakajima, T.; Honda, Y.; Kitao, O.; Nakai, H.; Vreven, T.; Montgomery, J. A.; Peralta, J. E.; Ogliaro, F.; Bearpark, M.; Heyd, J. J.; Brothers, E.; Kudin, K. N.; Staroverov, V. N.; Kobayashi, R.; Normand, J.; Raghavachari, K.; Rendell, A.; Burant, J. C.; Iyengar, S. S.; Tomasi, J.; Cossi, M.; Rega, N.; Millam, J. M.; Klene, M.; Knox, J. E.; Cross, J. B.; Bakken, V.; Adamo, C.; Jaramillo, J.; Gomperts, R.; Stratmann, R. E.; Yazyev, O.; Austin, A. J.; Cammi, R.; Pomelli, C.; Ochterski, J. W.; Martin, R. L.; Morokuma, K.; Zakrzewski, V. G.; Voth, G. A.; Salvador, P.; Dannenberg, J. J.; Dapprich, S.; Daniels, A. D.; Farkas; Foresman, J. B.; Ortiz, J. V.; Cioslowski, J.; Fox, D. J. Wallingford CT, 2009.

(19) Lodewyk, M. W.; Tantillo, D. J. *J. Nat. Prod.* **2011**, *74*, 1339.

(20) Quasdorf, K. W.; Hutters, A. D.; Lodewyk, M. W.; Tantillo, D. J.; Garg, N. K. *J. Am. Chem. Soc.* **2011**, *134*, 1396.

(21) Lodewyk, M. W.; Soldi, C.; Jones, P. B.; Olmstead, M. M.; Rita, J.; Shaw, J. T.; Tantillo, D. J. *J. Am. Chem. Soc.* **2012**, *134*, 18550.

(22) For additional details on linear regression parameters see the Tantillo Group's CHESHIRE website: <http://cheshirenmr.info>. Accessed Nov. 9 2013.

(23) Hess, B. A.; Schaad, L. J. *J. Am. Chem. Soc.* **1983**, *105*, 7185.

(24) Rondan, N. G.; Houk, K. N. *Tetrahedron Lett.* **1984**, *25*, 2519.

(25) Borčić, S.; Roberts, J. D. *J. Am. Chem. Soc.* **1965**, *87*, 1056.

(26) Lutnæs, O. B.; Ruden, T. A.; Helgaker, T. *Mag. Reson. Chem.* **2004**, *42*, S117.

(27) Lodewyk, M. W.; Siebert, M. R.; Tantillo, D. J. *Chem. Rev.* **2011**, *112*, 1839.

(28) Goldish, E.; Hedberg, K.; Schomaker, V. *J. Am. Chem. Soc.* **1956**, *78*, 2714.

(29) Richardson, A. D.; Hedberg, K.; Junk, C. P.; Lemal, D. M. *J. Phys. Chem. A* **2003**, *107*, 3064.

(30) Richardson, A. D.; Hedberg, K.; Lunelli, B. *J. Phys. Chem. A* **2010**, *114*, 5358.